Developing new methods for Satellite Remote Sensing of Soil Moisture

by

Neda Mohamadzadeh

B.S., University of Bijnor, 2010
M.S., Imam Khomeini International University, 2013

AN ABSTRACT OF A DISSERTATION

submitted in partial fulfillment of the requirements for the degree

DOCTOR OF PHILOSOPHY

Department of Geography and Geospatial
College of Arts and Sciences

KANSAS STATE UNIVERSITY
Manhattan, Kansas

2025

Abstract

The Optical Trapezoid Model (OPTRAM) has been widely used for high-resolution mapping of surface soil moisture (top 0-5 cm) using optical satellite data. Despite its strengths, it faces limitations in parameter calibration, particularly in defining the wet edge in areas with high moisture content, and in applying a single set of parameters across heterogeneous landscapes. Moreover, Shortwave transformed reflectance used as input in this model is affected by variables not related to soil moisture and all these limitations introduce uncertainties in the model outputs. This dissertation addresses OPTRAM's limitations through three methodological advancements aimed at improving the accuracy, and consistency of OPTRAM-derived soil moisture estimates.

First, a new variant of OPTRAM is introduced to enhance its ability to distinguish not only soil moisture but also surface water bodies such as lakes and rivers, as well as saturated pixels. Using Landsat-8 surface reflectance data across the Central Valley, California, the modified model demonstrated improved performance in differentiating land and water pixels and reduced sensitivity to user-defined parameters. Quantitative comparison showed that the new variant achieved higher consistency in soil moisture estimates, with R^2 values between parameter sets ranging from 0.67 to 0.76, compared to 0.47 to 0.52 for the original OPTRAM.

Second, a landcover-specific calibration approach (OPTRAM-LS) is proposed, in which separate parameter sets are derived for different land cover types, as opposed to a uniform calibration for the entire study region (OPTRAM-CV). Leveraging Sentinel-2 surface reflectance and the Cropland Data Layer dataset, 20-m resolution soil moisture maps were generated for the Central Valley. Comparative validation against in situ observations and SMAP-Hydro Blocks (a 30-m soil moisture dataset) showed that OPTRAM-LS significantly outperformed OPTRAM-CV, reducing the average root mean square error from 0.09 to 0.05 m^3m^{-3}.

Finally, a novel method called Microwave-Guided OPTRAM (MG-OPTRAM) has been developed to further improve soil moisture retrieval by fusing optical and microwave remote sensing data. MG-OPTRAM integrates Soil Moisture Active Passive (SMAP) observations at 9-km resolution into OPTRAM calibration, enabling us to extend the soil moisture estimations beyond SMAP's operational period (2015–present) back to 2000, and downscale SMAP data to a finer resolution (500-m) using Moderate Resolution Imaging Spectroradiometer (MODIS) observations. Application in the Central Valley demonstrated that MG-OPTRAM reliably reconstructs SMAP-like soil moisture. Validation against in situ and radar-derived soil moisture data confirmed its robustness at coarse and high resolution, although some uncertainty persists at finer resolutions due to model simplicity and subpixel heterogeneity.

Together, the three methodological advancements represent a connected and progressive refinement of the OPTRAM framework. By adopting the enhanced OPTRAM formulation, shifting from region-wide to land cover-specific calibration, and advancing to SMAP pixel-level calibration as well as filtering the soil moisture-related reflectance, MG-OPTRAM emerges as the most evolved version of the model. It integrates the strengths of the previous improvements and fulfills the dissertation's goal of developing an accurate, high-spatial-resolution soil moisture dataset spanning a long historical period.

Based on these findings, this dissertation recommends future research directions including: (1) incorporating environmental covariates such as precipitation and soil texture; (2) exploring Synthetic Aperture Radar (SAR)-based calibration potential; and (3) enhancing the model framework to better identify soil moisture-related reflectance characteristics. These improvements can further strengthen the performance and accuracy of soil moisture estimated by OPTRAM.

Developing new methods for Satellite Remote Sensing of Soil Moisture

by

Neda Mohamadzadeh

B.S., University of Bijnor, 2010
M.S., Imam Khomeini International University, 2013

A DISSERTATION

submitted in partial fulfillment of the requirements for the degree

DOCTOR OF PHILOSOPHY

Department of Geography and Geospatial
College of Arts and Sciences

KANSAS STATE UNIVERSITY
Manhattan, Kansas

2025

Approved by:

Major Professor
Marcellus Marques Caldas

Copyright

Abstract

The Optical Trapezoid Model (OPTRAM) has been widely used for high-resolution mapping of surface soil moisture (top 0-5 cm) using optical satellite data. Despite its strengths, it faces limitations in parameter calibration, particularly in defining the wet edge in areas with high moisture content, and in applying a single set of parameters across heterogeneous landscapes. Moreover, Shortwave transformed reflectance used as input in this model is affected by variables not related to soil moisture and all these limitations introduce uncertainties in the model outputs. This dissertation addresses OPTRAM's limitations through three methodological advancements aimed at improving the accuracy, and consistency of OPTRAM-derived soil moisture estimates.

First, a new variant of OPTRAM is introduced to enhance its ability to distinguish not only soil moisture but also surface water bodies such as lakes and rivers as well as saturated pixels. Using Landsat-8 surface reflectance data across the Central Valley, California, the modified model demonstrated improved performance in differentiating land and water pixels and reduced sensitivity to user-defined parameters. Quantitative comparison showed that the new variant achieved higher consistency in soil moisture estimates, with R^2 values between parameter sets ranging from 0.67 to 0.76, compared to 0.47 to 0.52 for the original OPTRAM.

Second, a landcover-specific calibration approach (OPTRAM-LS) is proposed, in which separate parameter sets are derived for different land cover types, as opposed to a uniform calibration for the entire study region (OPTRAM-CV). Leveraging Sentinel-2 surface reflectance and the Cropland Data Layer dataset, 20-m resolution soil moisture maps were generated for the Central Valley. Comparative validation against in situ observations and SMAP-hydro Blocks (a 30-m soil moisture dataset) showed that OPTRAM-LS significantly outperformed OPTRAM-CV, reducing the average root mean square error from 0.09 to 0.05 m^3m^{-3}.

Finally, a novel method called Microwave-Guided OPTRAM (MG-OPTRAM) has been developed to further improve soil moisture retrieval by fusing optical and microwave remote sensing data. MG-OPTRAM integrates Soil Moisture Active Passive (SMAP) observations at 9-km resolution into OPTRAM calibration, enabling us to extend the soil moisture estimations beyond SMAP's operational period (2015–present) back to 2000, and downscale SMAP data to a finer resolution (500-m) using Moderate Resolution Imaging Spectroradiometer (MODIS) observations. Application in the Central Valley demonstrated that MG-OPTRAM reliably reconstructs SMAP-like soil moisture. Validation against in situ and radar-derived soil moisture data confirmed its robustness at coarse and high resolution, although some uncertainty persists at finer resolutions due to model simplicity and subpixel heterogeneity.

Together, the three methodological advancements represent a connected and progressive refinement of the OPTRAM framework. By adopting the enhanced OPTRAM formulation, shifting from region-wide to land cover-specific calibration, and advancing to SMAP pixel-level calibration as well as filtering the soil moisture-related reflectance, MG-OPTRAM emerges as the most evolved version of the model. It integrates the strengths of the previous improvements and fulfills the dissertation's goal of developing an accurate, high-spatial-resolution soil moisture dataset spanning a long historical period.

Based on these findings, this dissertation recommends future research directions including: (1) incorporating environmental covariates such as precipitation and soil texture; (2) exploring Synthetic Aperture Radar (SAR)-based calibration potential; and (3) enhancing the model framework to better identify soil moisture-related reflectance characteristics. These improvements can further strengthen the performance and accuracy of soil moisture estimated by OPTRAM.

Table of Contents

List of Figures

List of Tables

Acknowledgements

Completing a PhD is an intense and transformative journey that requires immense effort, dedication, and resilience. Wrapping up this path in just three years took countless hours of study, long days and nights working on my laptop, weekends spent immersed in research, and missed breaks. It also took patience and, most importantly, the support of many people who helped me along the way.

First and foremost, I would like to thank my family. Your unwavering encouragement, patience, and belief in me, especially during the most challenging periods of my life have been my foundation. I could not have done this without your inspiration and love.

I am sincerely grateful to the College of Arts and Sciences and the Department of Geography and Geospatial Sciences at Kansas State University for financially supporting my doctoral studies through a Graduate Teaching Assistantship. I also want to thank the Natural Resource and Environmental Science (NRES) fellowship for its generous support.

To my advisor, Dr. Marcellus Caldas, thank you for believing in me from the very beginning and for giving me the opportunity to pursue this path. Your consistent encouragement, guidance, and mentorship have been instrumental to my academic growth.

I extend my heartfelt thanks to my committee members: Dr. Morteza Sadeghi, whose thoughtful guidance, generous support, and inspiring mentorship have profoundly shaped both my academic and professional development. Dr. Jida Wang and Dr. Gaurav Jha, for their valuable feedback, insightful suggestions, and steady support throughout this process.

Special thanks to Dr. Helene Avocat and Dr. Arnaud Temme, for whom I served as a Graduate Teaching Assistant over multiple semesters. Your trust and guidance helped me grow in this important responsibility.

I also want to thank Dr. Charles Martin, former department head, whose support and leadership meant a great deal to me.

I would also like to acknowledge the faculty members from whom I have learned so much during my time at Kansas State University, including Dr. Shawn Hutchinson, whose classes were so engaging and insightful that I often joined even when I was not officially enrolled, simply to keep learning. I am also thankful to Dr. Douglas Goodin and Dr. Laura Moley for the valuable knowledge and perspectives they shared.

A heartfelt thanks to Penny Crawford, your warm smile, kind words, and Christmas gifts always brightened my days and reminded me of home. You were a source of comfort and joy.

I am also grateful to Dr. Andres Patrignani for giving me the opportunity to assist in his lab during my first summer. That experience contributed significantly to my overall learning and growth as a researcher.

To all my friends in Manhattan, thank you for making this town feel like home. Your kindness, shared laughter, and companionship made this journey memorable and full of life. And to all the graduate students in the department, your friendship, and encouragement made this experience truly meaningful.

Finally, thank you to everyone who has supported me throughout this journey; your encouragement has made all the difference!

Dedication

To everyone who believed in me, even when I doubted myself.

Chapter 1 - Introduction to remote sensing of soil moisture

Soil moisture is a critical environmental variable influencing water, carbon, and energy exchanges at the surface-atmosphere interface (Robinson et al., 2008; De Queiroz et al., 2020). It plays a key role across diverse environmental processes by shaping rainfall-runoff relationships in hydrology, regulating net ecosystem exchange in ecology (Ochsner et al., 2013; Hosseini et al., 2023), and determining plant water availability in agriculture, thereby affecting plant productivity and crop yields (Wang et al., 2011). Furthermore, soil moisture has emerged as a valuable indicator for monitoring drought conditions (Wang et al., 2019) and assessing wildfire occurrence and severity (Jensen et al., 2018), stimulating growing interest in its estimation through satellite remote sensing.

Research into soil moisture estimation began in the 1960s, driven by the limitations of traditional methods like the gravimetric technique, which requires destructive, labor-intensive, and non-reproducible measurements (Zhang & Zhou, 2016). The advancement of satellite technology provided a transformative solution, enabling the acquisition of spatially distributed soil moisture data over large areas with consistent temporal frequency (Ahmed et al., 2011; Huete, 2004).

Extensive research has confirmed the strong correlation between soil moisture and remotely sensed parameters, including soil optical reflectance (Tian & Philpot, 2015; Babaeian et al., 2016; Sadeghi et al., 2017), thermal emission (Hassan-Esfahani et al., 2015), and microwave backscatter (Njoku & Entekhabi, 1996). These findings have led to the development of several remote sensing methods across different spectral domains, summarized in Table 1. Each approach offers distinct advantages and limitations depending on the application and environmental conditions (Zhang & Zhou, 2016; L. Wang & Qu, 2009).

Table 1.1. Summary of remote sensing techniques for near-surface soil moisture estimation.

Spectrum domain	Properties observed	Method	advantageous	limitations
Optical	- Soil reflectance		- Fine spatial resolution - Broad coverage - Multiple satellites available	- Limited surface penetration - Cloud contamination
Thermal infrared	- Surface temperature	- Thermal Inertia - Temperature Index Method	- Fine spatial resolution - Broad coverage	- Limited surface penetration - Cloud contamination - Affected by meteorological conditions and vegetation cover - Limited satellites available
Microwave /active or passive	- Backscatter coefficient - Brightness temperature - Dielectric properties - Soil temperature	- Backscattering models - Universal triangular relationship method	- Low atmospheric noise - Moderate surface penetration - High temporal resolution - Unlimited by clouds and/or daytime conditions	- Low spatial resolution - Affected by surface roughness and vegetation cover - Coarse temporal resolution

(Wang & Qu, 2009; Sadeghi et al., 2015; Zhang & Zhou, 2016; Ahmed et al., 2011; Huete, 2004)

1. Microwave remote sensing of soil moisture

Microwave remote sensing, which includes both active and passive techniques, has proven particularly effective for estimating soil moisture at the global scale. Unlike optical and thermal sensors, microwave instruments operate at longer wavelengths, allowing them to penetrate clouds, vegetation canopies, and the underlying soil. This capability makes microwave sensing uniquely suited for all-weather, day-and-night observations, ensuring consistent temporal coverage across a wide range of environmental conditions (Entekhabi et al., 2010).

Active microwave systems work by transmitting radar signals and analyzing the returned backscatter coefficient, which varies in response to the dielectric properties of the soil, as well as surface roughness and vegetation structure. In contrast, passive microwave sensors measure the naturally emitted radiation from the Earth's surface in terms of brightness temperature, which is also sensitive to soil moisture due to the strong relationship between water content and the soil's dielectric constant (Jensen, 2009; Sadeghi et al., 2018).

Key satellite missions such as the Soil Moisture Active Passive (SMAP) and Soil Moisture and Ocean Salinity (SMOS) provide reliable soil moisture products with near-global coverage and revisit intervals of 2–3 days. Despite their advantages, microwave-based methods are subject to several limitations. Most notably, their coarse spatial resolution, often ranging between 25 to 50 km, limits their applicability in small-scale, heterogeneous landscapes (Sadeghi et al., 2017). Additionally, SMAP's data record, which only extends back to 2015, may be too short for long-term hydrological studies or climate trend analyses.

By contrast, optical and thermal infrared sensors provide higher spatial resolution (in meters) and often longer temporal archives, offering a complementary solution for fine-scale, long-term soil moisture mapping.

2. Thermal and Optical Remote Sensing of soil moisture

Given the importance of optical and thermal satellite observations in the remote sensing of soil moisture, the Thermal-Optical Trapezoid Model (TOTRAM) was one of the earliest models developed to estimate surface soil moisture by leveraging both optical and thermal data. The model is based on interpreting the distribution of pixels within the LST-VI space, where LST refers to Land Surface Temperature and VI represents a remotely sensed vegetation index (Nemani et al., 1993; Carlson et al., 1994; Moran et al., 1994). TOTRAM has gained popularity due to its straightforward parameterization, which relies primarily on optical and thermal remote sensing observations and does not require ancillary atmospheric or surface data (Carlson, 2007).

When the study area boasts enough pixels and is free from cloud and water body interference, the distribution of LST and VI across a landscape forms characteristic triangular or trapezoidal feature space (Sandholt et al., 2002; Moran et al., 1994) (see Fig. 1.1). This LST-VI feature space is constrained by the dry and wet edges. The wet edge signifies maximum evapotranspiration and ample soil moisture, while the dry edge indicates water stress on vegetation, resulting in minimum evapotranspiration and an absence of soil moisture, indicating no available water. Analyzing the pixel distribution within the LST-VI feature space allows for the extraction of soil moisture information (Zhang & Zhou, 2016).

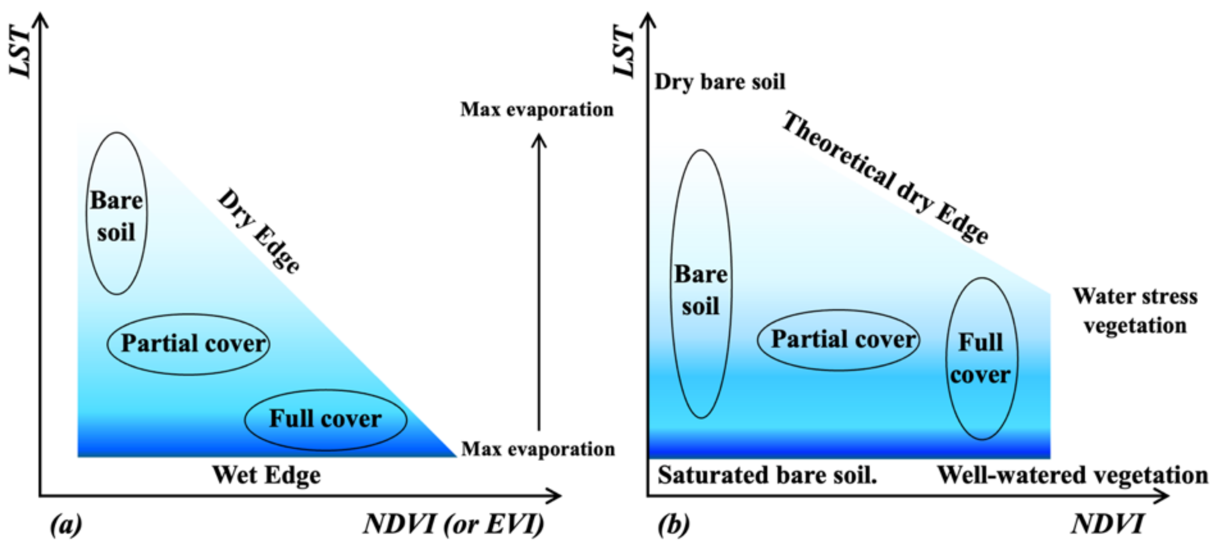

Figure 1.1. The conceptual triangle (a) and trapezoid space (b) of LST and Vegetation Indices (VI) used for soil moisture monitoring.

Despite the success of models using the thermal approach, challenges arise due to their limited applicability across various satellites, especially those with high spatiotemporal resolution and multiple spectral bands but lacking a thermal band. For instance, among the commonly used satellites for remote sensing (Table 2), Sentinel-2 satellite launched in 2015 cannot be employed for soil moisture monitoring using thermal approach, due to the absence of a thermal band. Another limitation of the thermal approach is due to the influence of atmospheric conditions, such as near-surface air temperature, relative humidity, and wind speed, on LST. This necessitates a time-consuming and computationally demanding process of individual parameterization/calibration for each observation date (Sadeghi et al., 2017; Mallick et al., 2009).

Table 1.2. Currently available satellites used for soil moisture monitoring.

Satellite	Sensor	Spatial Resolution	Temporal Resolution	advantageous	limitations
Soil Moisture Active Passive (SMAP) 2015 -present	Synthetic-Aperture Radar (SAR) / L band	9 km	2-3 days	Global Coverage, Accurate soil moisture	Coarse spatial resolution, highly influenced by surface roughness and vegetation canopy
Soil Moisture and Ocean Salinity (SMOS) 2009- present	Microwave Imaging Radiometer using Aperture Synthesis (MIRAS)	35-50 km	3 days	- Global Coverage, Low sensitive to cloud and vegetation contamination, highly sensitive to soil moisture fluctuation	Coarse spatial resolution, highly influenced by surface roughness and vegetation canopy
Sentinel 1	Synthetic-Aperture Radar (SAR)	10 m	6 days	Accurate soil moisture, High spatial and temporal resolution	Highly influenced by surface roughness and vegetation canopy
Landsat 8 2013- present Landsat 9 2021-present	Operational Land Imager (OLI), Thermal Infrared Sensor (TIRS)	- 30 m for V, NIR, and SWIR -100 m for TIR	16 days	Good spatial resolution, multi bands available	Vegetation and cloud interference
Sentinel 2 2015-present	Multi-spectral instrument (MSI)	- 10 m for V and NIR - 20 m for SWIR	5-10 days	High spatial and temporal resolution	cloud interference
Moderate-Resolution Imaging Spectroradiometer (MODIS) 1999-present		250 m – 1 km	1-2 days	Good spatial resolution	Vegetation interference, cloudy contamination, night and atmospheric effects

(Zhang & Zhou, 2016; Ahmed et al., 2011; Camps et al., 2008; Schlund & Erasmi, 2020)

3. Optical Trapezoid Model (OPTRAM)

To address the limitations associated with thermal approaches to soil moisture estimation, Sadeghi et al. (2017) introduced the Optical Trapezoid Model (OPTRAM). OPTRAM is a physically based model and relies on a recently established physical relationship between soil moisture and shortwave infrared transformed reflectance (STR). OPTRAM calculates soil moisture (θ) as:

$$\theta = \theta_d + (\theta_w - \theta_d)\frac{\mathrm{STR}-\mathrm{STR}_d}{\mathrm{STR}_w-\mathrm{STR}_d} \tag{1.1}$$

Where STR represents the SWIR transformed reflectance and STR_d and STR_w correspond to the dry and wet edges, respectively, associated with $\theta = \theta_d$ (dry soil) and $\theta = \theta_w$ (wet edge).

The relationship between STR and shortwave infrared reflectance, is defined as follows (Sadeghi et al., 2015):

$$\mathrm{STR} = \frac{(1-R_{SWIR})^2}{2R_{SWIR}} \tag{1.2}$$

Assuming a linear correlation between soil and vegetation water content, OPTRAM predicts that NDVI, calculated as Eq. 1.3, and STR will form a trapezoid shape, where drier pixels are located at a lower position and wetter pixels are located at a higher position on the data cloud (see Fig. 1.2).

$$\mathrm{NDVI} = \frac{NIR-R}{NIR+R} \tag{1.3}$$

The OPTRAM parameters (i_d, s_d, i_w, s_w) can be determined either by fitting two edge lines to enclose the densest part of the NDVI-STR data cloud or by a least-squares optimization fitting of the OPTRAM-based soil moisture to in-situ observations of soil moisture. While optimization approach yields higher accuracy, it requires dense in-situ soil moisture observations in space and time. Alternatively, the line fitting method is more practical for users as it does not need any in-situ observations, though it introduces user subjectivity. Further details on parameter estimation are found in Sadeghi et al. (2017).

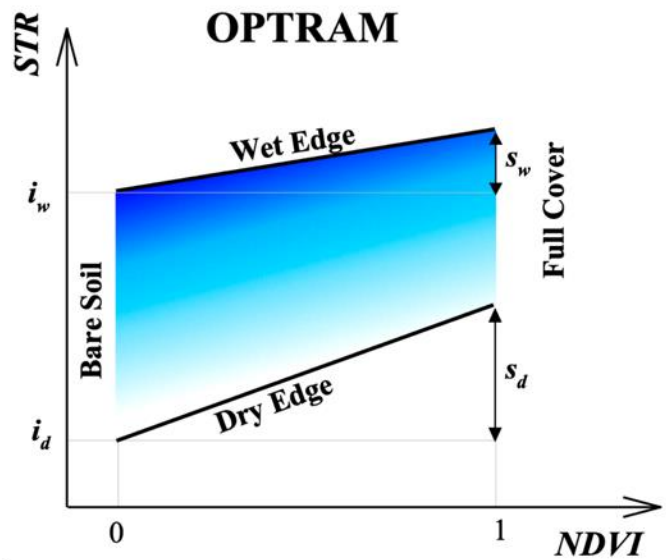

Figure 1.2. Sketch illustrating the NDVI-STR trapezoidal space defining the OPTRAM parameters, i_d, s_d, i_w, s_w [from Sadeghi et al. (2017)].

Using either of the approaches, the dry and wet edges are defined as linear equations:

$$\mathrm{STR}_d = i_d + s_d\mathrm{NDVI} \tag{1.4}$$

$$\mathrm{STR}_w = i_w + s_w\mathrm{NDVI} \tag{1.5}$$

Where STR_d and STR_w indicate STR at the dry and wet edges, respectively, i_d and s_d are the dry edge parameters, and i_w and s_w are the wet edge parameters.

Assuming soil moisture (θ) at the dry edge is nearly zero and at the wet edge is close to the saturated soil moisture (θ_s), OPTRAM proposed to mask water bodies (typically characterized by negative NDVI values) and estimate soil moisture as:

$$\theta = \begin{cases} \theta_s\left(\frac{\mathrm{STR}-\mathrm{STR}_d}{\mathrm{STR}_w-\mathrm{STR}_d}\right) & (\mathrm{STR} \leq \mathrm{STR}_w) \\ \theta_s & (\mathrm{STR} > \mathrm{STR}_w) \end{cases} \tag{1.6}$$

4. Motivations, Contributions, and Research Objectives

Unlike thermal approaches that rely on LST, OPTRAM which uses STR, can be directly applied for estimating soil moisture from satellites equipped solely with optical observations, such as Sentinel 2. Moreover, in contrast to the LST-NDVI space, which undergoes variations over time due to changes in ambient atmospheric parameters, it is assumed that the STR-NDVI space will remain nearly time-invariant. This is attributed to the fact that STR is influenced solely by surface properties and not by ambient atmospheric conditions. Consequently, it is theorized that OPTRAM would require only a single parametrization for a specific location (Sadeghi et al., 2017).

Vegetation information, provided through NDVI, is a key input to OPTRAM parameterization. NDVI is a widely used spectral vegetation index that leverages the differential reflectance of healthy vegetation, which strongly absorbs red and reflects near-infrared (Burdun et al., 2023). However, NDVI is not without limitations. It is sensitive to soil background reflectance and atmospheric conditions, such as aerosols, dust, and moisture, which can distort spectral reflectance and lead to over- or underestimation of vegetation activity. To address these shortcomings, several enhanced vegetation indices have been proposed. For instance, the Soil-Adjusted Vegetation Index (SAVI) introduces a correction factor to reduce soil brightness influence in sparsely vegetated areas. The Atmospherically Resistant Vegetation Index (ARVI) incorporates the blue band to correct for atmospheric scattering. Taking a further step, the Enhanced Vegetation Index (EVI) was developed to address both soil and atmospheric limitations simultaneously (Xue and Su, 2017).

These advancements in vegetation indices have led researchers to experiment with alternatives to NDVI within OPTRAM. For example, Babaeian et al. (2019) replaced NDVI with SAVI for estimating soil moisture in agricultural fields, particularly where vegetation transitions from bare soil to full canopy. In another large-scale study, Burdun et al. (2023) assessed OPTRAM performance using four different vegetation indices including NDVI, EVI, red-edge NDVI, and kernel NDVI across 53 northern peatlands in North America and Europe to monitor the temporal fluctuations in water table. While the correlation between water table depth and each vegetation index varied significantly across sites, the OPTRAM estimates based on all four indices showed consistently strong and similar correlations with in-situ measurements. These findings suggest that OPTRAM is robust across different vegetation index and can effectively detect soil moisture and water table dynamics across heterogeneous landscapes.

Therefore, while acknowledging the theoretical advantages of newer indices, the continued use of NDVI in OPTRAM remains justified given its consistent empirical performance and widespread availability across sensors and historical archives.

Nevertheless, even with these methodological strengths, OPTRAM is not without limitations. Despite its promise in high-resolution soil moisture mapping (Ambrosone et al., 2020; Chen et al., 2020; Pandey et al., 2024; Mananze et al., 2019; Burdun et al., 2020; Mokhtari et al., 2023; Acharya et al., 2022; Hassanpour et al., 2020; Longo-Minnolo et al., 2022), OPTRAM faces challenges, particularly in defining the wet edge in regions with high moisture content. Scattering caused by oversaturated pixels and surface water can distort the upper STR boundary, leading to inconsistent interpretations and user-dependent results. Moreover, by filtering out water bodies and capping soil moisture to the saturated point (θ_s), the model ignores actual oversaturation and surface water, introducing uncertainty.

A second limitation is the use of a single set of parameters across regions with diverse land cover types, each showing distinct surface reflectance (Huete, 2004; Mohamadzadeh & Ahmadisharaf, 2024; Shu et al., 2024), which is ignored in the model parameterization. By generating a single NDVI–STR data cloud for an entire region of interest, the current method fails to capture the true heterogeneity of the landscape and biases the results toward the dominant land cover class, imposing a constraint on the OPTRAM methodology.

To address these challenges, the second chapter of this dissertation introduces a new OPTRAM variant. Unlike the original model, this version allows soil moisture estimates to exceed porosity in areas with water presence, enabling the detection of oversaturated pixels and water bodies. This reduces sensitivity to wet edge uncertainty and user subjectivity.

In the third chapter, the model is further refined by incorporating land cover data into the parameterization. Instead of using region-wide parameters, this approach estimates OPTRAM parameters for each land cover class, acknowledging their distinct STR and NDVI characteristics. This method improves soil moisture estimation, particularly in heterogeneous regions.

Building upon these improvements, the next chapter introduces a synergistic approach that integrates microwave and optical observations. Specifically, SMAP as a well-validated microwave soil moisture product is used to calibrate OPTRAM at the scale of individual SMAP pixels. This fusion model, termed Microwave-Guided OPTRAM, combines the high spatial resolution of optical methods with the accuracy and all-weather capability of microwave observations.

This novel model not only enhances OPTRAM's soil moisture estimation but also addresses key SMAP limitations, such as coarse spatial resolution and relatively short temporal coverage, with data available since 2015. By adopting the enhanced OPTRAM formulation (from Chapter 2) and reducing calibration areas from region-wide (original OPTRAM) to land cover-specific (Chapter 3) and then to SMAP pixel level, Microwave-Guided OPTRAM represents the most evolved form of the model.

The overarching goal of this dissertation is to develop a high spatial resolution soil moisture dataset using OPTRAM. To achieve this, the research pursues the following objectives:

Objective 1: Develop a new OPTRAM variant that explicitly accounts for oversaturation by enabling the estimation of both soil moisture and surface water. Evaluate its effectiveness in reducing sensitivity to wet edge uncertainties and minimizing user dependency.

Objective 2: Improve OPTRAM's soil moisture estimation accuracy by incorporating land cover-specific parameterization, and to assess the performance of this approach relative to the standard region-wide calibration.

Objective 3: Fuse microwave (SMAP) and optical (MODIS) data within an OPTRAM framework to develop a Microwave-Guided OPTRAM model and evaluate its ability to overcome limitations of individual methods and enhance soil moisture estimation accuracy.

Chapter 2 - A New Variant of OPTRAM for Remote Sensing of Soil Moisture and Water Bodies

1. Introduction

Chapter 1 introduced the Optical Trapezoid Model (OPTRAM) as a promising optical remote sensing approach to estimate soil moisture using surface reflectance data. Despite its utility, the OPTRAM formulation is limited by filtering out water bodies, typically characterized by negative NDVI values. As a result, fully saturated and ponded surfaces are omitted from analysis, reducing the model's effectiveness in capturing oversaturated pixels, particularly in irrigated or wetland areas.

Moreover, the current formulation presents challenges in determining the wet edge in moist regions, where the upper portion of the STR data cloud becomes scattered due to the presence of oversaturated pixels and water bodies. In these cases, users may interpret the densest part of the data cloud differently, leading to inconsistencies in wet edge parameterization. Consequently, this results in variations in the final soil moisture estimates and introduces user dependency.

This chapter addresses these limitations by introducing a new variant, OPTRAM-2, that removes the saturation threshold and explicitly incorporates oversaturation into the soil moisture estimation process, when there is a pond of water on top of the soil surface. OPTRAM-2 also reduces sensitivity to wet edge uncertainty, thereby minimizing user dependency.

The goal of this chapter is to fulfill Objective 1 of this dissertation:

To develop and evaluate an OPTRAM variant capable of estimating both soil moisture and surface water, while reducing reliance on user dependency and improving robustness in regions with high moisture content, particularly the Central Valley of California.

2. Theoretical Background

OPTRAM is a physically based trapezoid model that relies on a recently established physical relationship between surface soil moisture and shortwave infrared Transformed Reflectance (STR). OPTRAM calculates soil moisture (θ) as:

$$\theta = \theta_d + (\theta_w - \theta_d)\frac{\mathrm{STR}-\mathrm{STR}_d}{\mathrm{STR}_w-\mathrm{STR}_d} \tag{2.1}$$

Where STR represents the SWIR transformed reflectance and STR_d and STR_w correspond to the dry and wet edges, respectively, associated with $\theta = \theta_d$ (dry soil) and $\theta = \theta_w$ (wet edge).

Assuming soil moisture (θ) at the dry edge is nearly zero and at the wet edge is close to the saturated soil moisture (θ_s), the original OPTRAM estimates soil moisture as (for more details, see Section 3 in Chapter 1):

$$\theta = \begin{cases} \theta_s\left(\frac{\mathrm{STR}-\mathrm{STR}_d}{\mathrm{STR}_w-\mathrm{STR}_d}\right) & (\mathrm{STR} \leq \mathrm{STR}_w) \\ \theta_s & (\mathrm{STR} > \mathrm{STR}_w) \end{cases} \tag{2.2}$$

In this formulation, OPTRAM masks water bodies (typically characterized by negative NDVI values) and forces the moisture content to the saturated point (θ_s) when STR exceeds the wet edge (STR_w). However, it is evident that the presence of a water layer over the soil surface can increase STR, whereas soil moisture cannot exceed the saturated moisture content (θ_s). This creates ambiguity in distinguishing between saturated and oversaturated land pixels.

To address this challenge, in this chapter, we proposed a modified OPTRAM formulation that allows the estimated soil moisture to exceed θ_s when a ponded water layer exists on the soil surface (see Figure 2.1). As a first step, and for consistency, we slightly modify the original OPTRAM to retain pixels with negative NDVI values and assign them a moisture content of 1, assuming they represent pure water bodies. The updated formulation is:

$$\theta = \begin{cases} \theta_s \left(\frac{\mathrm{STR}-\mathrm{STR}_d}{\mathrm{STR}_w-\mathrm{STR}_d}\right) & (\mathrm{NDVI} > 0, \mathrm{STR} \leq \mathrm{STR}_w) \\ \theta_s & (\mathrm{NDVI} > 0, \mathrm{STR} > \mathrm{STR}_w) \\ 1 & (\mathrm{NDVI} \leq 0) \end{cases} \tag{2.3}$$

We refer to Equations (2.2) and (2.3) as OPTRAM-1a and OPTRAM-1b, respectively, and collectively as OPTRAM-1. It is because Equation (2.3) is a slight modification of Equation (2.2) that includes water bodies by assigning them a soil moisture value of 1.

In contrast, the new OPTRAM variant proposed in this chapter, OPTRAM 2, allows the estimated moisture value to exceed θ_s when ponded water is present. In these cases, the model output represents not only the soil moisture content in the surface layer (depth *d*), but also the contribution from the optically detectable portion of the surface water layer (*h*), as illustrated in Figure 2.1. When *h* = 0, the retrieval corresponds to soil moisture only. When h is much greater than *d* (*h* >> *d*), the output approaches 1, indicating a deep-water layer.

Accordingly, the formulation for OPTRAM-2 is expressed as:

$$\theta = \begin{cases} \theta_s \left(\frac{\mathrm{STR}-\mathrm{STR}_d}{\mathrm{STR}_w-\mathrm{STR}_d}\right) & (\mathrm{NDVI} > 0,\ \mathrm{STR} \leq \mathrm{STR}_w) \\ \frac{\theta_s d+h}{d+h} & (\mathrm{NDVI} > 0,\ \mathrm{STR} > \mathrm{STR}_w) \\ 1 & (\mathrm{NDVI} \leq 0) \end{cases} \tag{2.4}$$

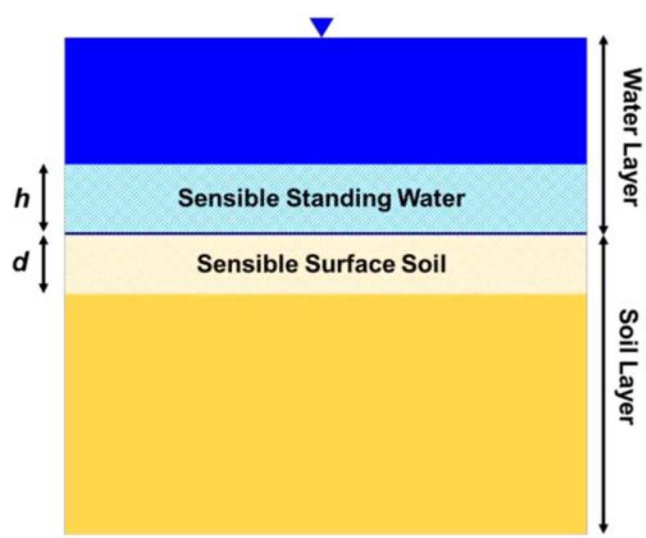

Figure 2.1. Conceptual diagram illustrating the definitions of surface layer depth (*d*) and water layer depth (*h*) used in this study.

For the practical implementation of Eq. (2.4), we assume *d* to be constant and *h* to vary as a function of STR. To establish this relationship, we adopt a linear radiative transfer model with a constant light absorption coefficient *k*, following Sadeghi et al. (2018). This relationship is expressed as:

$$\mathrm{SWIR} = \mathrm{SWIR}_w \exp(-kh) \tag{2.5}$$

where SWIR is the shortwave infrared reflectance of an oversaturated soil, SWIR_w is the reflectance of its corresponding saturated soil, and *k* is the water absorption coefficient. Eq. (2.5) shows that SWIR reflectance decreases exponentially as the water depth (*h*) increases.

To link this to STR, we use the transformation introduced by (Sadeghi et al., 2015):

$$\mathrm{STR} = \frac{(1-\mathrm{SWIR})^2}{2\mathrm{SWIR}}, \ \mathrm{SWIR} = 1 + \mathrm{STR} - \sqrt{\mathrm{STR}^2 + 2\mathrm{STR}} \tag{2.6}$$

Therefore, by combining Eqs. (2.5) and (2.6), the water layer thickness (*h*) in Eq. (2.4) can be calculated as a function of STR:

$$h = \begin{cases} 0 & (\mathrm{STR} \leq \mathrm{STR}_w) \\ -\frac{1}{k} ln\left(\frac{1+\mathrm{STR}-\sqrt{\mathrm{STR}^2+2\mathrm{STR}}}{1+\mathrm{STR}_w-\sqrt{\mathrm{STR}_w^2+2\mathrm{STR}_w}}\right) & (\mathrm{STR} > \mathrm{STR}_w) \end{cases} \tag{2.7}$$

It is important to note that OPTRAM-1 (Eqs. 2.2, 2.3) and OPTRAM-2 (Eq. 2.4) will be different only when NDVI > 0 and $\mathrm{STR} > \mathrm{STR_w}$. In this case, OPTRAM-1 output is forced to θ_s, but the OPTRAM-2 output can be larger than θ_s depending on the STR value (i.e., the higher the STR, the larger the estimated water content). This approach enables OPTRAM-2 to continue utilizing satellite observations beyond the point of soil saturation, thereby reducing the model's dependence on user-defined parameters. Further details on the calculation and interpretation of *h* can be found in Sadeghi et al. (2023).

3. Materials and Methods

To evaluate the proposed method, we studied outputs of OPTRAM-1 and OPTRAM-2 across the Central Valley (CV), California. We considered CV as a proper test case for exploring soil moisture variations as it encompasses a diverse range of landscape, from dry urban areas to fully saturated and oversaturated regions, such as rice fields and numerous water bodies, including California Delta (see Fig. 2.2). This diversity allows for a robust evaluation of the new OPTRAM variant`s sensitivity to wet edge parameters, particularly in regions with varying moisture conditions. The following datasets were used for this analysis.

3.1. Landsat 8

To derive the input variables NDVI and STR for Eqs. (2.2, 2.3, and 2.4), we used imagery from the Landsat 8 (L8) satellite, which offers high spatial resolution (30 m). The dataset includes atmospherically corrected surface reflectance produced by Operational Land Imager (OLI) and Thermal Infrared Sensor (TIRS) onboard Landsat 8 (Earth Resources Observation and Science (EROS) Center, 2020). Observations from the red band (L8 band 4, 636-673 nm) and NIR band (L8 band 5, 851-879 nm) were used to calculate NDVI (Eq. 1.3), while the SWIR band (L8 band 7, 2107-2294 nm) was used to calculate STR (Eq. 1.2).

3.2. Cropland Data Layer (CDL)

To obtain landcover information, we utilized the Cropland Data Layer (CDL) dataset, generated annually for the continental United States. This dataset was created using satellite observation with extensive agricultural ground truth data (Boryan et al., 2011). Fig. 2.2 shows the CDL landcover classification across the CV used in this study. According to this classification, CV contains over 20 distinct landcover types, including rice fields concentrated in the north and the California delta and wetlands located in the west.

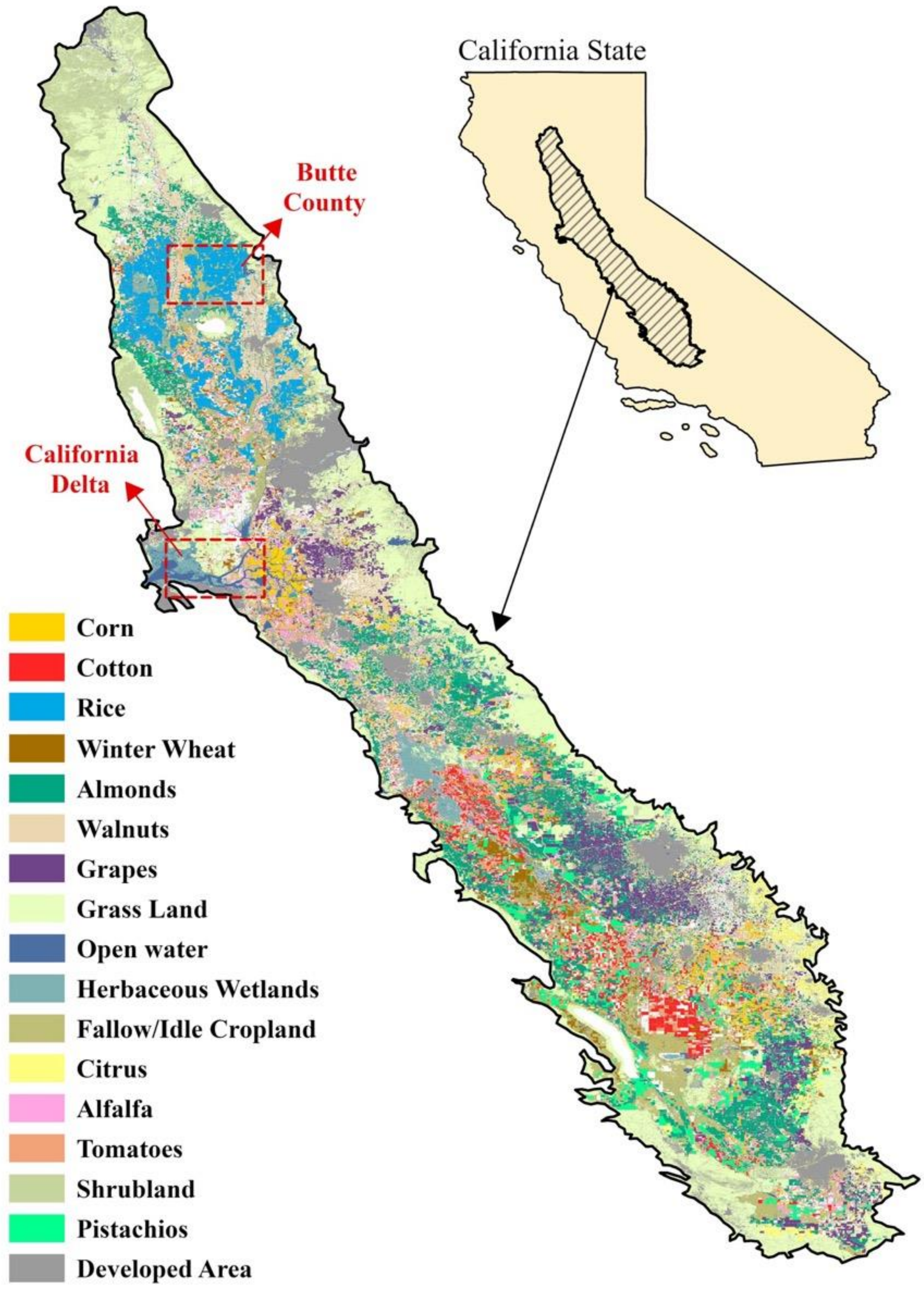

Figure 2.2. Central Valley landcover map based on the Cropland Data Layer (CDL) dataset. Red rectangles mark the locations of Butte County and the California delta, which are used to compare the resulting soil moisture maps based on OPTRAM-1a, OPTRAM-1b and OPTRAM-2 in Figures 2.5 to 2.8.

3.3. Global Surface Water Dataset

For validation of both the original OPTRAM and the new OPTRAM variant, we used the Global Surface Water Dataset. This dataset provides monthly maps of surface water locations and their temporal dynamics from 1984 to 2021, offering valuable insights into long-term water presence and variability. Each pixel in this monthly dataset is classified as either water or non-water, with a spatial resolution of 30 meters (see Fig. 2.3) (Pekel et al., 2016).

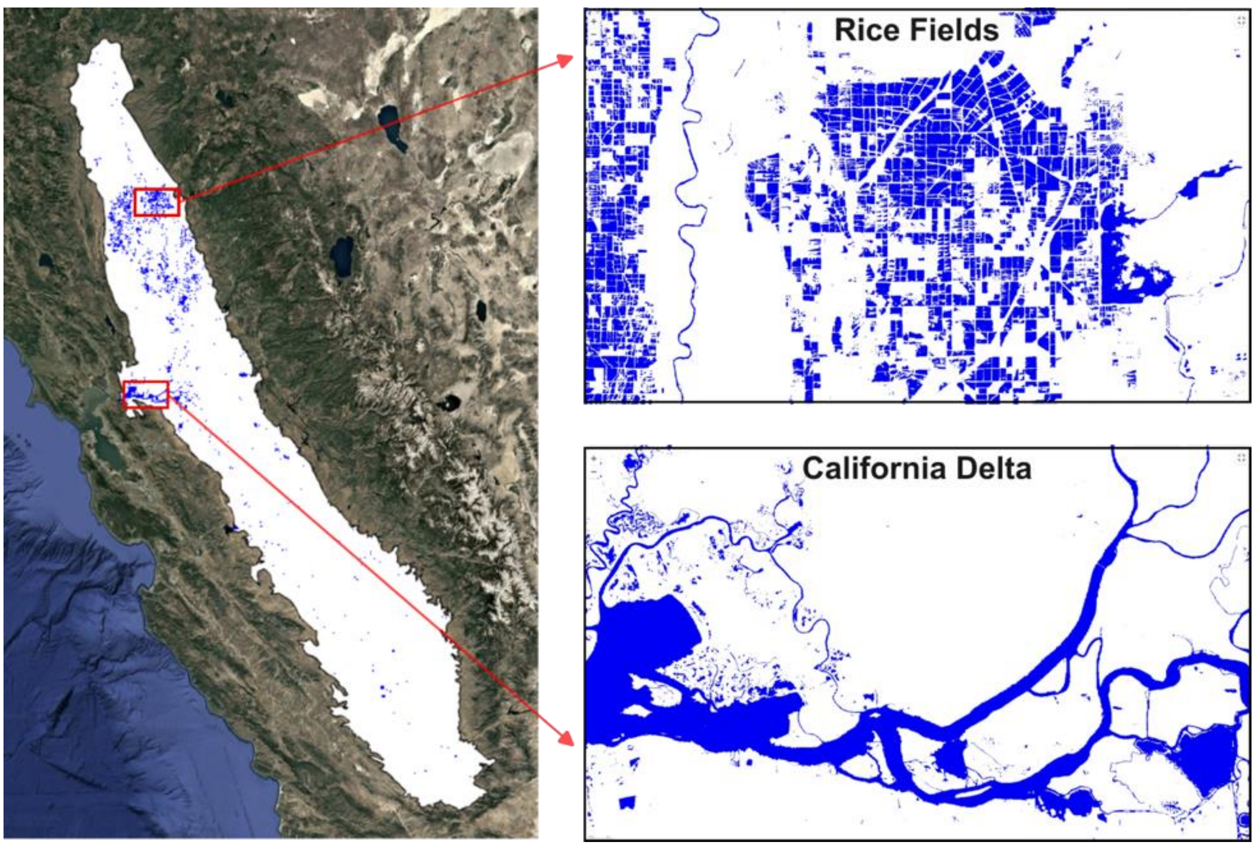

Figure 2.3. Surface water map in Central Valley California, May 2021, derived from the Surface Water dataset (left). The inset maps show detailed views of oversaturated rice fields during the irrigation season (top right) and water bodies in California delta (bottom right). The Central Valley represents an ideal case study for testing the new OPTRAM variant.

3.4. Data Analysis

We coded Eqs. (2.2), (2.3), and (2.4) in the Google Earth Engine (GEE) platform, where all datasets were readily available. To provide input for θ_s, a map of this soil property was obtained at 250-m resolution using the surface soil bulk density (ρ_b) map from Hengl (2018) available on GEE. The saturated soil moisture content was calculated using $\theta_s = 1 - \rho_b/\rho_p$, where the soil particle density (ρ_p) was assumed to be 2.65 g cm^{-3}. The water absorption coefficient k was then estimated from θ_s based on the empirical relationship presented in Eq. (2.5) of Sadeghi et al., 2023. The soil sensing depth d was assumed to be 0.001 meters, following Norouzi et al. (2021). Based on these values, the water depth (h) was calculated using Eq. (2.7).

To obtain model parameters (i_d, s_d, i_w, s_w), we aimed to plot NDVI-STR for the entire CV. However, CV contains billions of 30-m pixels, making it impossible to plot every single pixel due to the GEE computational limit (for free accounts). Therefore, an aggregation of the individual pixel values in space and time was necessary.

Recognizing that this aggregation process can introduce user subjectivity into OPTRAM parameter selection, we designed an experiment to assess this potential variability. Specifically, we simulated four different scenarios, in each we apply a distinct averaging strategy for NDVI and STR values. Scenario #1 averaging data monthly over 30×30 pixels, scenario #2 averaging data monthly over 50×50 pixels, scenario #3 averaging data yearly over 30×30 pixels, scenario #4 averaging data yearly over 50×50 pixels. In this analysis, we considered all available L8 images in 2022. The "averaging yearly" refers to the mean NDVI and STR values calculated across all observations for each pixel throughout the year, while "averaging monthly" refers to calculating the mean for each month of the year and combining data for all 12 months to form the NDVI-STR scatter plot.

The primary goal of this analysis was to understand the sensitivity of the OPTRAM outputs to the wet edge parameters (i_w, and s_w) in both OPTRAM-1 and OPTRAM-2 variants. To isolate the effect of wet-edge fitting, the dry edge parameters (i_d, and s_d) were held constant across all scenarios. Then in each simulated scenario, we manually fit the wet edge to the densest part of the NDV-STR data cloud, following the visual fitting method proposed by Sadeghi et al. (2017). As expected, this process produced different wet-edge parameter sets (i_w, and s_w) for each scenario.

Using these user-specific calibrated parameters, soil moisture content was estimated at a 30-meter resolution for both OPTRAM-1 and OPTRAM-2 approaches. For spatial analysis, we compared the soil maps generated under each scenario against the Global Surface Water dataset to assess how effectively each approach identified water bodies and oversaturated pixels.

Finally, to explore the impact of user-driven parameter selection, we evaluated the correlations between soil moisture estimates derived by each scenario across both approaches.

4. Results and Discussion

Fig. 2.4 illustrates the NDVI-STR space formed by the four scenarios described earlier. Following Sadeghi et al. (2017), only the positive NDVI range, corresponding to land pixels, was used to estimate the OPTRAM parameters. As shown, the scenarios derived notably different wet edge parameters (i_w and s_w), mainly due to their different averaging time and space windows. Another contributing factor to this variability is the subjective interpretation of the densest region of the data cloud, which introduces additional uncertainty. This is more pronounced at finer spatial resolution, where oversaturated pixels lead to greater data scattering. With these differences in mind, we now examine the soil moisture maps that could potentially generated by each scenario using both OPTRAM-1 and OPTRAM-2.

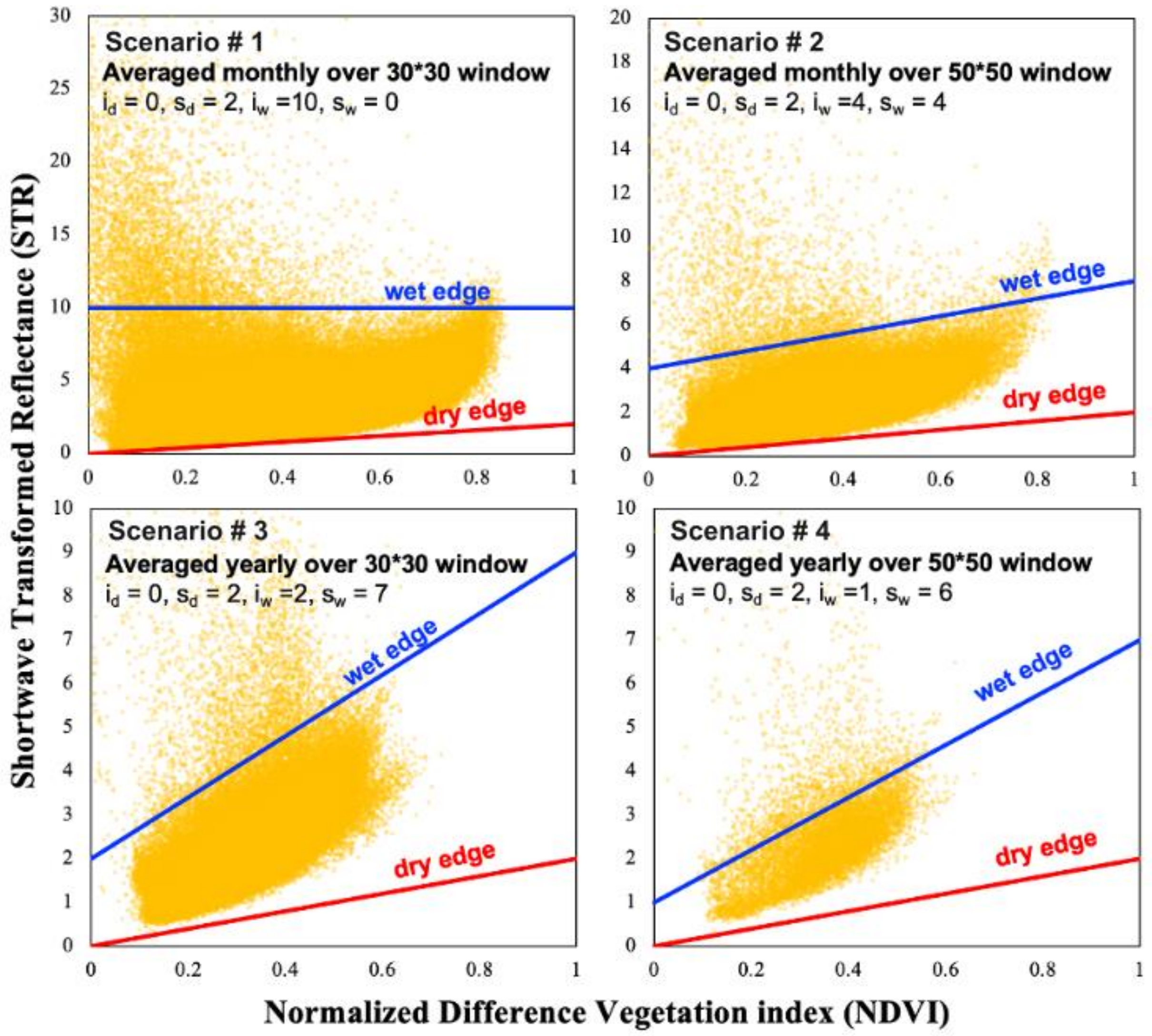

Figure 2.4. The NDVI-STR space including Landsat-8 pixels in Central Valley over 2022 averaged on different temporal and spatial scales as expected by different imaginary OPTRAM scenarios.

Fig. 2.5 presents sample soil moisture maps generated by different scenarios applying OPTRAM-1a (left side) and OPTRAM-1b (right side) in the California Delta (see Fig. 2.2). A comparison of these maps reveals key differences in model behavior. Notably, significant discrepancies appear across scenarios; for example, scenario# 1's map indicates dry conditions near the delta, while scenario# 4's map for the same time and location suggests wet conditions. This highlights the high sensitivity of OPTRAM-1a to wet edge parameterization.

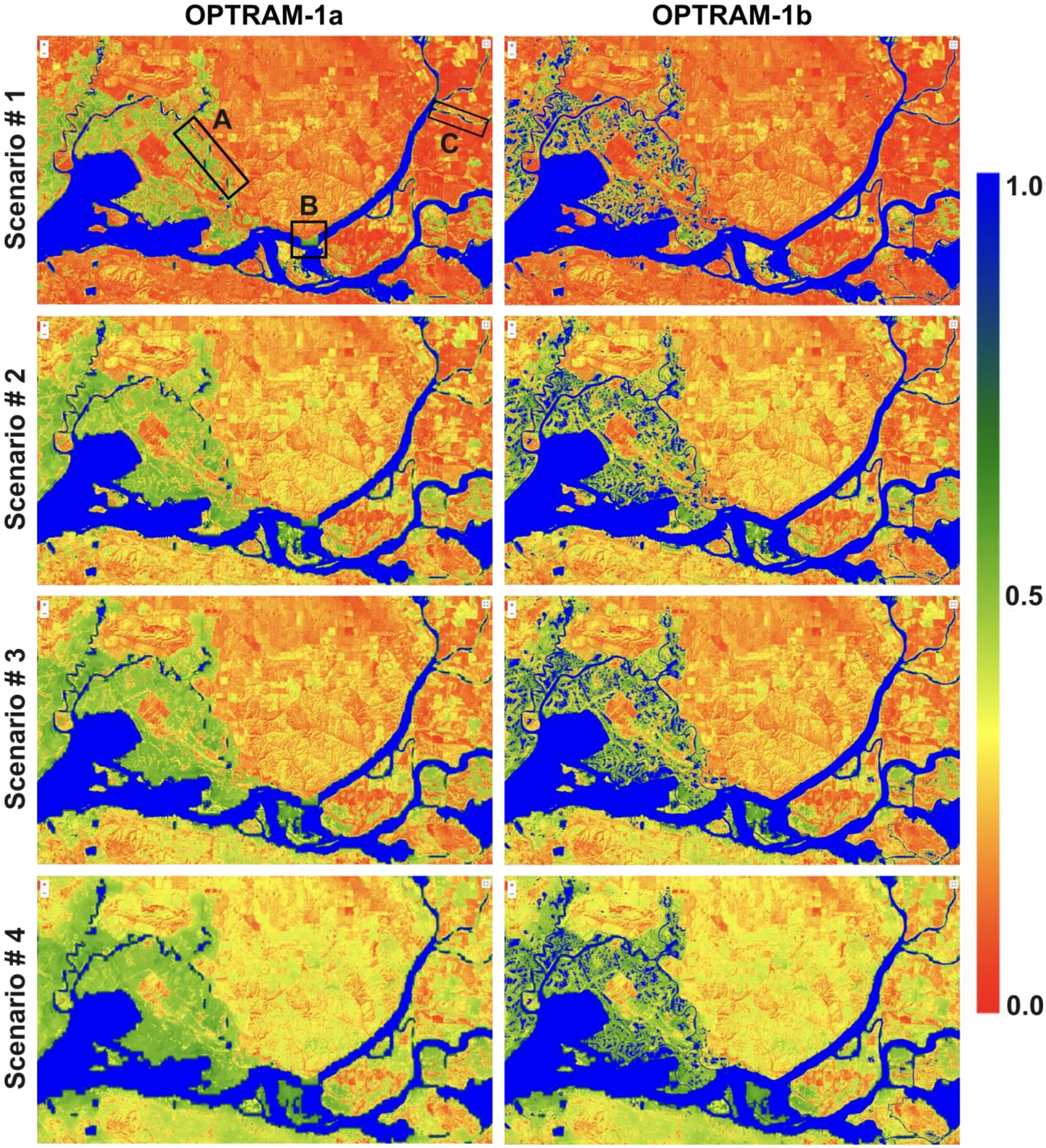

Figure 2.5. Resulting soil moisture maps based on OPTRAM-1a (Eq. 2.2) and OPTRAM-1b (Eq. 2.3) using parameters determined by scenarios #1, #2, #3 and #4 shown in Fig. 2.4. These maps show monthly average soil moisture at 30-m resolution in February 2022 in the California Delta.

In addition, OPTRAM-1a shows limited ability to accurately map river networks. For instance, in scenario#1's OPTRAM-1a output, portions of rivers in areas A, B, and C are misclassified as land (shown in light green). In these areas, STR value exceeds STR_w, and hence, OPTRAM-1a yields $\theta = \theta_s$. Therefore, the land-water separation in OPTRAM-1a is governed by the resolution and accuracy of the θ_s map, which is not high enough in these spots.

In contrast, OPTRAM-1b, through a simple modification that forces $\theta = 1$ for NDVI < 0, significantly improved the results in capturing water bodies. This is mainly because many water pixels show a negative NDVI, especially over the permanent water bodies. In other words, NDVI itself, which is already an OPTRAM input, can be used to primarily detect water bodies.

Although OPTRAM-1b shows great potential to detect water bodies compared to OPTRAM-1a, limitations remain. Several pixels classified as land in OPTRAM-1b are either water bodies or oversaturated areas not adequately captured by the model. This issue becomes evident when comparing the soil moisture maps to reference water body datasets, as shown in Fig. 2.6.

Fig. 2.6 presents a true-color image of the California Delta region alongside three reference datasets: (1) CDL land cover classification, (2) a binary land-water map derived from the Normalized Difference Water Index calculated as $\text{NDWI} = (\text{Green} - \text{NIR})/(\text{Green} + \text{NIR})$, which is widely used for delineation of water bodies (Özelkan, 2020), and (3) a binary land-water map from the Global Surface Water Dataset (see Fig. 2.6).

As shown, the CDL identifies a substantial portion of the California Delta as wetlands, supporting the accuracy of OPTRAM-1a and OPTRAM-1b in detecting saturated pixels, which appear in green in the soil moisture maps. However, both water body reference datasets reveal considerably more water pixels than those detected by OPTRAM-1a and OPTRAM-1b (Fig. 2.5), indicating a notable limitation of these models in capturing oversaturated areas.

This issue is exacerbated when the wet edge is poorly defined. For instance, scenario#4's OPTRAM-1a output demonstrates both inadequate water body delineation and a noticeable loss in spatial resolution. This stems from the saturation of many pixels near water bodies (STR > STRw), causing the model to default to $\theta = \theta_s$ which is mapped at a coarser resolution (250 meters) than STR (30 meters). As a result, both the accuracy and spatial resolution of OPTRAM-1a and OPTRAM-1b are compromised under such conditions.

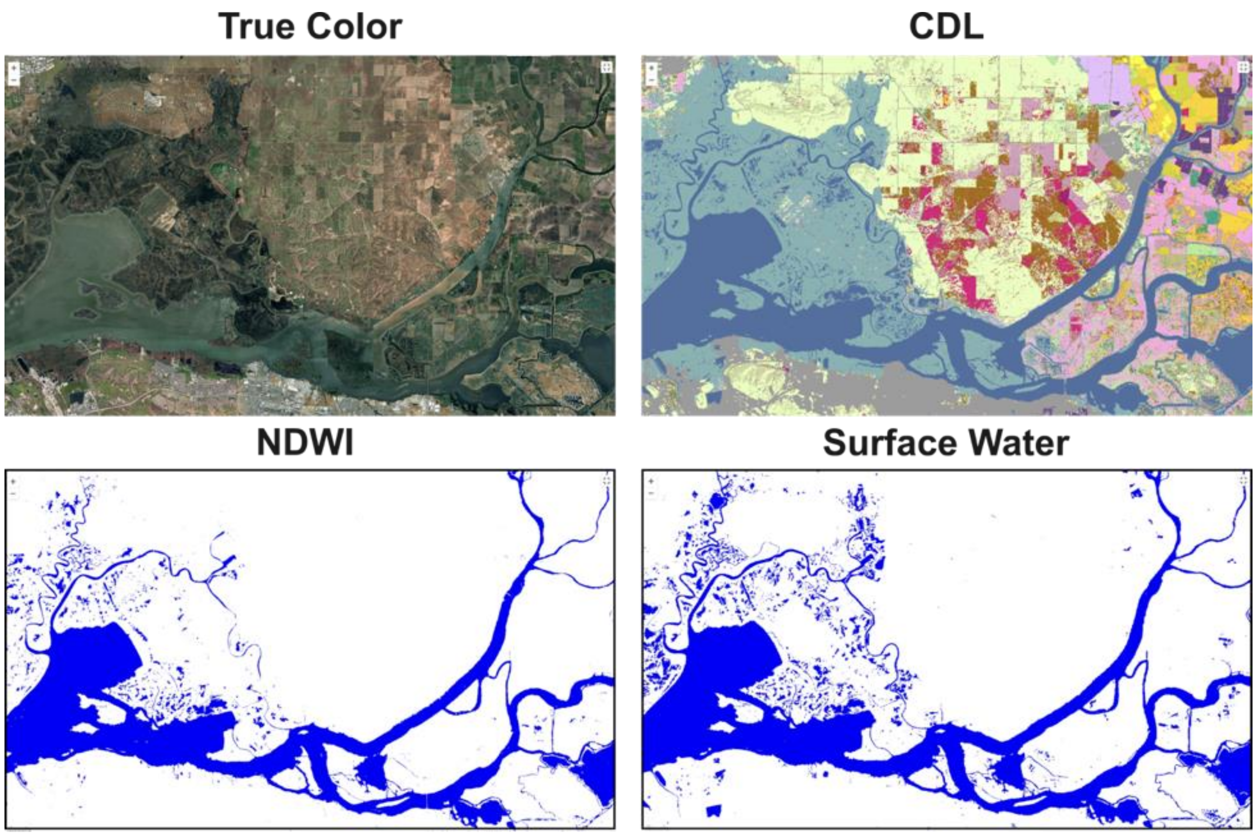

Figure 2.6. True-color image (top left), NDWI-based binary water map (middle left), CDL landcover classification (top right), and Global Surface Water dataset (bottom right), illustrating the distribution of water bodies in the California Delta in February 2022.

Fig. 2.7 shows the corresponding OPTRAM-2 soil moisture maps for the California delta. When compared with the reference water body datasets in Fig. 2.6, it is evident that all scenarios employing OPTRAM-2 were able to reasonably capture oversaturated pixels and permanent water bodies. In addition, the soil moisture patterns appear more consistent across different scenarios in OPTRAM-2 than in OPTRAM-1. This improvement highlights a key advantage of OPTRAM-2, addressing one of the primary limitations identified in OPTRAM-1.

For further evaluation, we compared soil moisture maps produced by two different scenarios in a separate region of Central Valley, as shown in Figure 2.8. The figure focuses on rice fields in Butte County and includes True-Color imagery, CDL land cover, reference water body maps, and soil moisture maps from scenarios #2 and #4 generated using OPTRAM-1a, OPTRAM-1b, and OPTRAM-2. The maps correspond to May 2021, a time when rice fields are typically flooded and oversaturated. As illustrated, the water pixels identified by OPTRAM-2 from both scenarios align closely with the reference water body map, whereas OPTRAM-1a and OPTRAM-1b show significant discrepancies. This comparison further underscores the effectiveness of the OPTRAM-2 in accurately mapping both unsaturated soil moisture and flooded areas simultaneously.

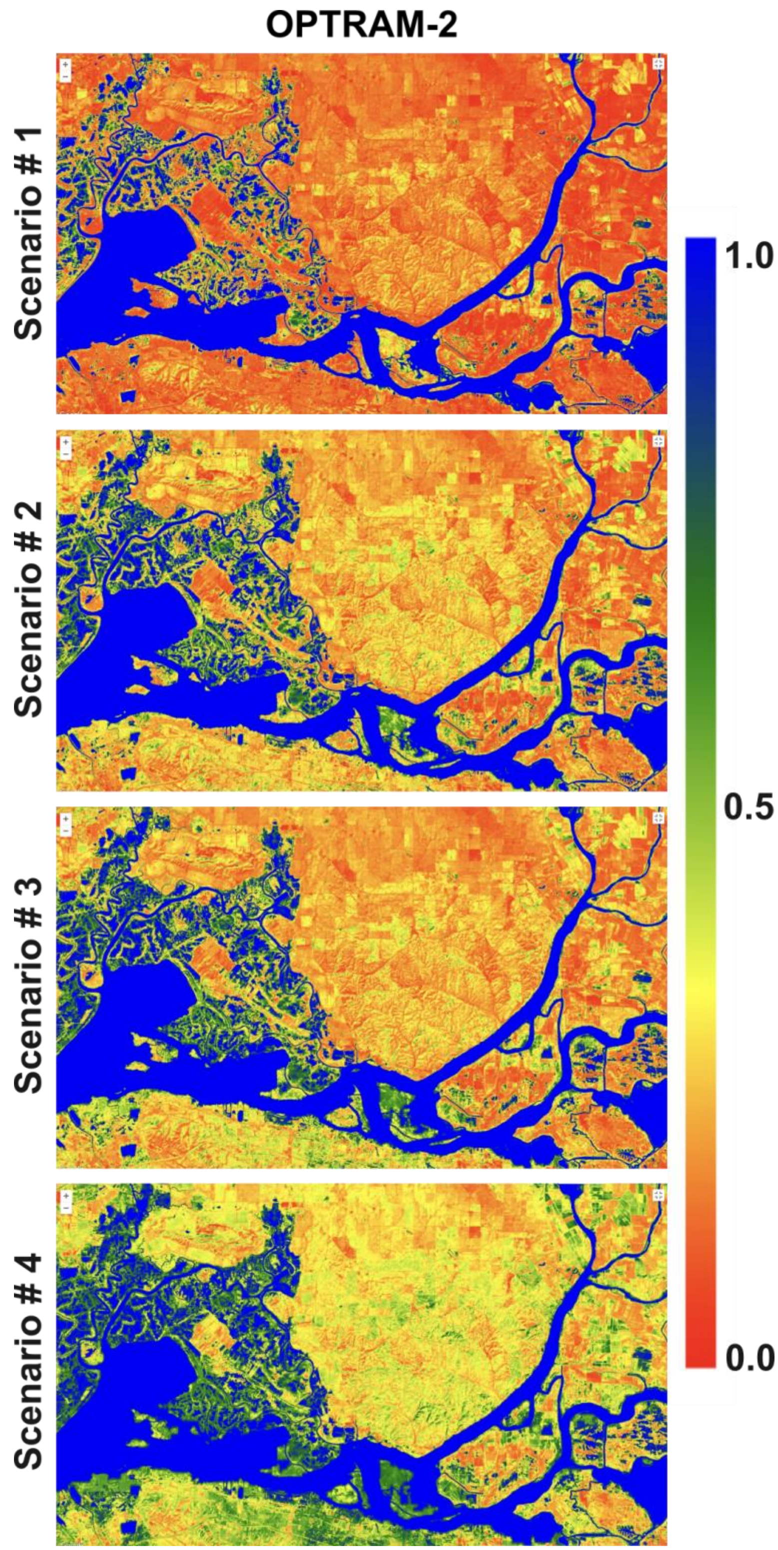

Figure 2.7. Resulting soil moisture maps based on OPTRAM-2 (Eq. 2.4) and parameters determined by scenarios #1, #2, and #4 are shown in Fig. 2.4. These maps show monthly average soil moisture at 30-m resolution in February 2022 in part of the California Delta.

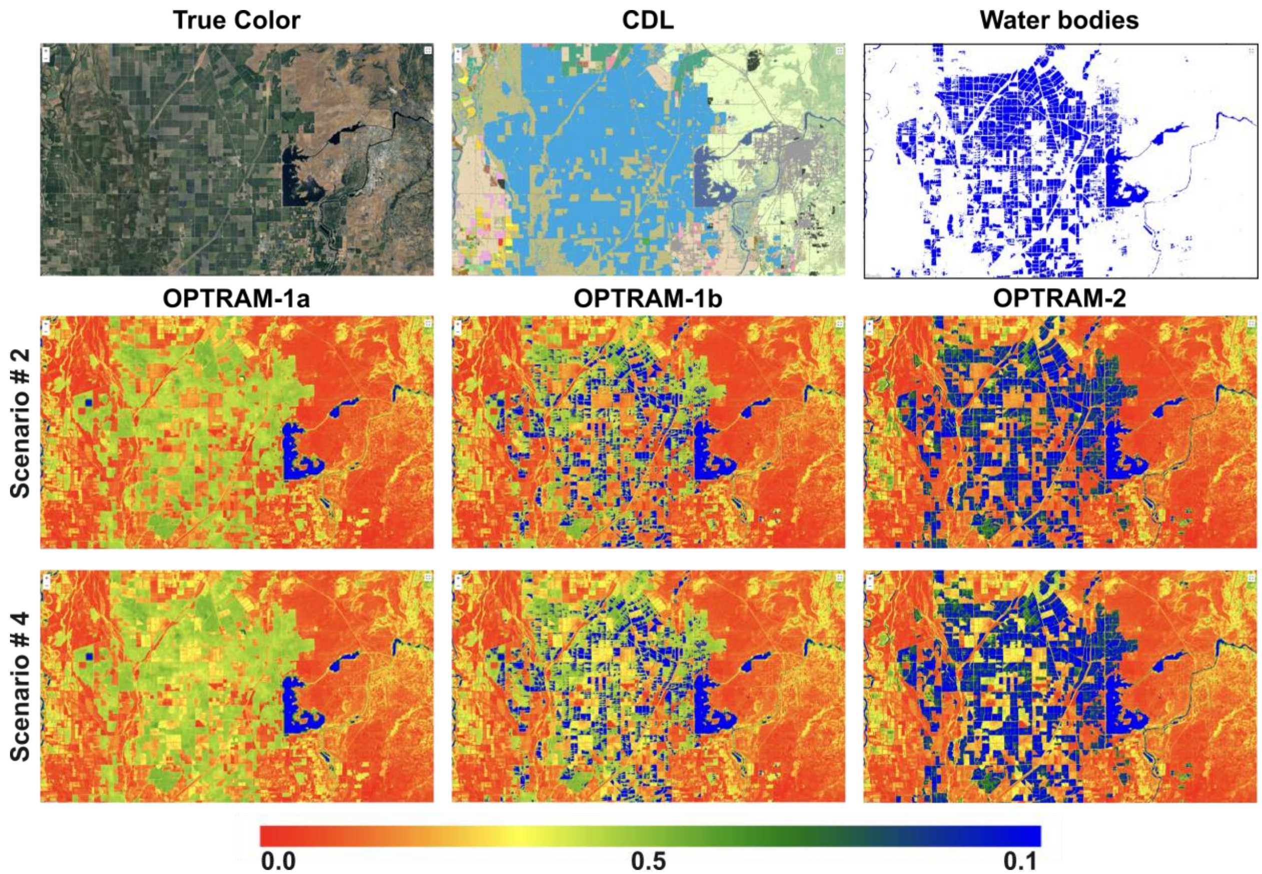

Figure 2.8. True-Color, CDL map, water body map, and scenario #2's and scenario #4's soil moisture maps based on OPTRAM-1a, OPTRAM-1b, and OPTRAM-2 over some rice fields within Butte County, California, May 2021. These maps show monthly average data at 30-m resolution.

Now that we have established that OPTRAM-2 more accurately captures oversaturated pixels and water bodies compared to OPTRAM-1, we further examined the user-dependency of these models. To do so, we analyzed the correlations between the soil moisture estimates from scenarios #1 and #4 based on OPTRAM-1a, OPTRAM-1b and OPTRAM-2. The results, presented in Fig. 2.9, show that OPTRAM-1a is the most user-dependent, while OPTRAM-2 is the least. As illustrated, the soil moisture outputs generated by different scenarios are more strongly and linearly correlated when using OPTRAM-2 compared to OPTRAM-1. Specifically, soil moisture estimates from scenarios #1 and #4 show a clear linear relationship in OPTRAM-2, whereas the correlation in OPTRAM-1 is highly nonlinear.

If the estimates from scenario #1 are more representative of the true soil moisture, even a poor wet edge parameterization by scenario #4 still leads to useful results with OPTRAM-2. This is because, in many applications, the temporal variation of soil moisture is more critical than its absolute value, and two linearly correlated datasets can be rescaled by matching their cumulative distribution functions (Madelon et al., 2022). In contrast, the nonlinear relationship observed in OPTRAM-1 makes scenario #4's soil moisture estimates much less reliable and difficult to correct.

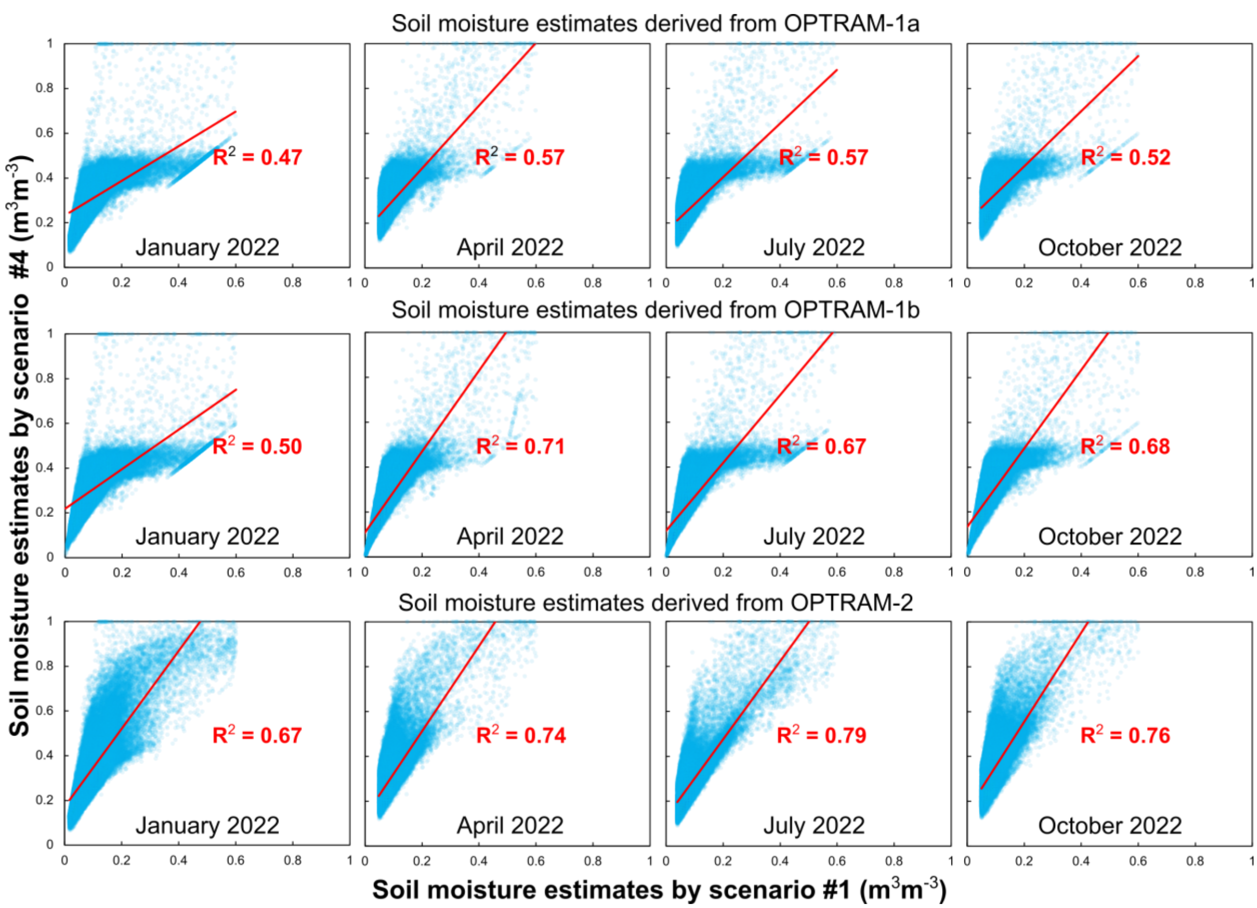

Figure 2.9. Correlations between soil moisture outputs from scenarios #1 and #4 based on OPTRAM-1a (top row), OPTRAM-1b (middle row), and OPTRAM-2 (bottom row). These data are for January, April, July, and October 2022 for the entire Central Valley after averaging over a 30×30-pixel spatial window.

5. Conclusions

The Optical Trapezoid Model (OPTRAM) was originally developed to estimate surface soil moisture using optical remote sensing data. However, its original formulation excluded water bodies, typically identified by negative NDVI values, and forced moisture content values to the saturated point, thereby limiting its ability to detect oversaturated pixels and surface water features.

In this chapter, a new variant, OPTRAM-2, was proposed to overcome these limitations. OPTRAM-2 extends the original framework by allowing the estimated water content to exceed the saturation point when ponded water exists on the soil surface. This modification enables the model to represent both soil moisture and surface water features, such as shallow ponds and lakes. Additionally, OPTRAM-2 reduces sensitivity to wet edge parameterization, an element often subject to user interpretation, thereby minimizing user dependency and improving consistency in soil moisture estimation across applications.

It is important to note that water content values greater than the saturated soil moisture threshold in OPTRAM-2 should not be interpreted as "soil moisture" in the classical sense, as soil moisture cannot exceed the soil's porosity. Instead, these values represent the combined water content of the soil and any standing surface water, as illustrated in Figure 2.1.

For applications focused exclusively on soil moisture mapping, we recommend using the modified version of the original OPTRAM formulation, Equation 2.3, which retains negative NDVI pixels and assigns them a water content value of 1.0. This adjustment not only improves the delineation of surface water bodies but also enhances the robustness of soil moisture estimation by further reducing user dependency. Accordingly, in the following chapters, any reference to the "original OPTRAM" refers to this modified version (Eq. 2.3), unless stated otherwise.

Chapter 3 - Landcover-Specific Calibration of OPTRAM for Soil Moisture Monitoring in the Central Valley, California

1. Introduction

Chapter 1 introduced the Optical Trapezoid Model (OPTRAM) as a promising optical remote sensing approach to estimate soil moisture using surface reflectance data. While OPTRAM has been successfully applied in various contexts to produce high-resolution soil moisture maps (Ambrosone et al., 2020; Chen et al., 2020; Pandey et al., 2024; Mananze et al., 2019; Burden et al., 2020a; Mokhtari et al., 2023), a key challenge remains in accurately defining the dry and wet edges that govern the model's performance (Sadeghi et al., 2023). This problem is more pronounced in diverse regions with distinct values of STR and NDVI associated with various landcover types.

The spectral reflectance captured by remote sensing instruments is highly dependent on land cover characteristics such as vegetation type, surface roughness, and canopy structure (Huete, 2004; Mohamadzadeh & Ahmadisharaf, 2024; Shu et al., 2024). In the current OPTRAM implementation, a single set of model parameters is typically applied across the entire region of interest. This approach introduces bias in heterogeneous environments by reflecting the dominant land cover class, potentially distorting the soil moisture estimates in less-represented classes. As a result, the current practice can lead to significant uncertainty and reduced reliability of OPTRAM outputs in mixed land cover settings, such as the Central Valley of California.

To address this limitation, this chapter introduces a land cover-specific calibration strategy for OPTRAM, herein referred to as OPTRAM-LS. This method explicitly incorporates land cover information into the model parameterization process, allowing the dry and wet edge parameters to be calibrated separately for each land cover class. By leveraging the distinct spectral properties of each land cover type, OPTRAM-LS aims to improve the fidelity of soil moisture estimates, particularly in complex and agriculturally diverse landscapes.

The goal of this chapter is to fulfill Objective 2 of this dissertation:

To improve OPTRAM's soil moisture estimation accuracy by incorporating land cover-specific parameterization, and to assess the performance of this approach relative to the standard region-wide calibration.

2. Theoretical Background

Sadeghi et al (2017) derived OPTRAM based on a recently established physical relationship between surface soil moisture and SWIR reflectance. OPTRAM calculates soil moisture θ as:

$$\theta = \theta_d + (\theta_w - \theta_d)\frac{\mathrm{STR}-\mathrm{STR}_d}{\mathrm{STR}_w-\mathrm{STR}_d} \tag{3.1}$$

where STR represents the SWIR transformed reflectance and STR_d and STR_w are STR at the dry edge ($\theta = \theta_d$) and wet edge ($\theta = \theta_w$), respectively (Sadeghi et al., 2015):

Assuming a linear correlation between soil and vegetation water content, it is anticipated that the NDVI and STR will form a trapezoidal data cloud, where drier pixels are located at a lower position and wetter pixels are located at a higher position on the data cloud. Fitting two lines to the lower and upper edges of the densest part of the data cloud, the dry and wet edges are formulated as follows:

$$\mathrm{STR}_d = i_d + s_d\mathrm{NDVI} \tag{3.2}$$

$$\mathrm{STR}_w = i_w + s_w\mathrm{NDVI} \tag{3.3}$$

Where i_d and s_d are the intercept and the slope of the dry edge, respectively, and i_w and s_w are the intercept and slope of the wet edge, respectively.

Accordingly, OPTRAM assigns a soil moisture value to each pixel considering its proximity to the dry and wet edges of the data cloud. By combining Eqs. (3.1) to (3.3) and assuming $\theta_d = 0$ and $\theta_w = \theta_s$, where θ_s is the soil porosity, soil moisture for each pixel can be estimated as a function of STR and NDVI as follows:

$$\theta = \theta_s \left[\frac{i_d + s_d\,\mathrm{NDVI} - \mathrm{STR}}{i_d - i_w + (s_d - s_w)\mathrm{NDVI}}\right] \tag{3.4}$$

Considering Eqs. (3.2) and (3.3), OPTRAM assumes that pixels with identical NDVI values yield identical STR_d and STR_w values, regardless of the vegetation type. However, the new approach acknowledges that OPTRAM parameters (i_d, s_d, i_w, s_w) are not constant over the study area because STR_d and STR_w can vary not only with NDVI but also with vegetation type. This leads to diverse OPTRAM parameters at a constant NDVI for various landcover types.

This is intuitively understandable that two different vegetation types might have the same greenness at a certain vegetation density. However, they can still have substantially different reflectance due to their distinct canopy structure. This variability implies that s_d and s_w may significantly vary with landcover types.

This landcover-specific variability is also the case for NDVI = 0, where soil reflectance may vary not only with soil moisture, but also with soil texture and roughness (Huete, 2004). Here, we assume that distinct landcover types most likely contain distinct soil types as well. That is why different landcover types often show substantially different soil reflectance when bare. Consequently, we propose different i_d and i_w values for different landcover types assuming they contain different soil types.

3. Materials and methods

This study focused on California's Central Valley (CV), widely known as an agricultural hub, producing nearly 80 crops such as almonds, cotton, grapes, alfalfa, lettuce, walnuts, and tomatoes (Sleeter, 2008). Beyond its agricultural significance, the CV accommodated nearly 7 million residents by 2010 (Soulard & Wilson, 2015). With a diverse mosaic of agricultural and urban landcover types, we considered this region an appropriate test case for exploring the effects of landcover variability on OPTRAM performance. The following datasets were used in this analysis.

3.1. Sentinel-2

For the input variables NDVI and STR in Eq. (3.4), we used the Multispectral ESA Sentinel-2 (S2) satellite to benefit from its high spatial resolution (10 m for visible, 20 m for SWIR) and temporal resolution (5 to 10 days) (Wang & Atkinson, 2018). We applied atmospheric correction to ensure accurate surface reflectance and used cloud-free S2 images acquired between 2015 and 2019. Clouds were masked using the Quality Assessment (QA) band to generate a precise bitmask. Observations at the red band (S2 band 4, 665 nm) and NIR band (S2 band 8, 842 nm) were used to calculate NDVI, $(NIR - red)/(NIR + red)$, and the SWIR band (S2 band 12, 2190 nm) was used to calculate STR (Eq. 1.2).

3.2. Cropland Data Layer (CDL)

To obtain landcover information, we utilized the Cropland Data Layer (CDL) dataset, generated annually for the continental United States. This dataset was created based on satellite observation and extensive agricultural ground truth data (Boryan et al., 2011). Fig. 3.1 shows the CDL landcover classification over the CV used in this study. According to this classification, CV encompasses over 20 distinct landcover types, with 12 predominant ones covering approximately 80 percent of the area.

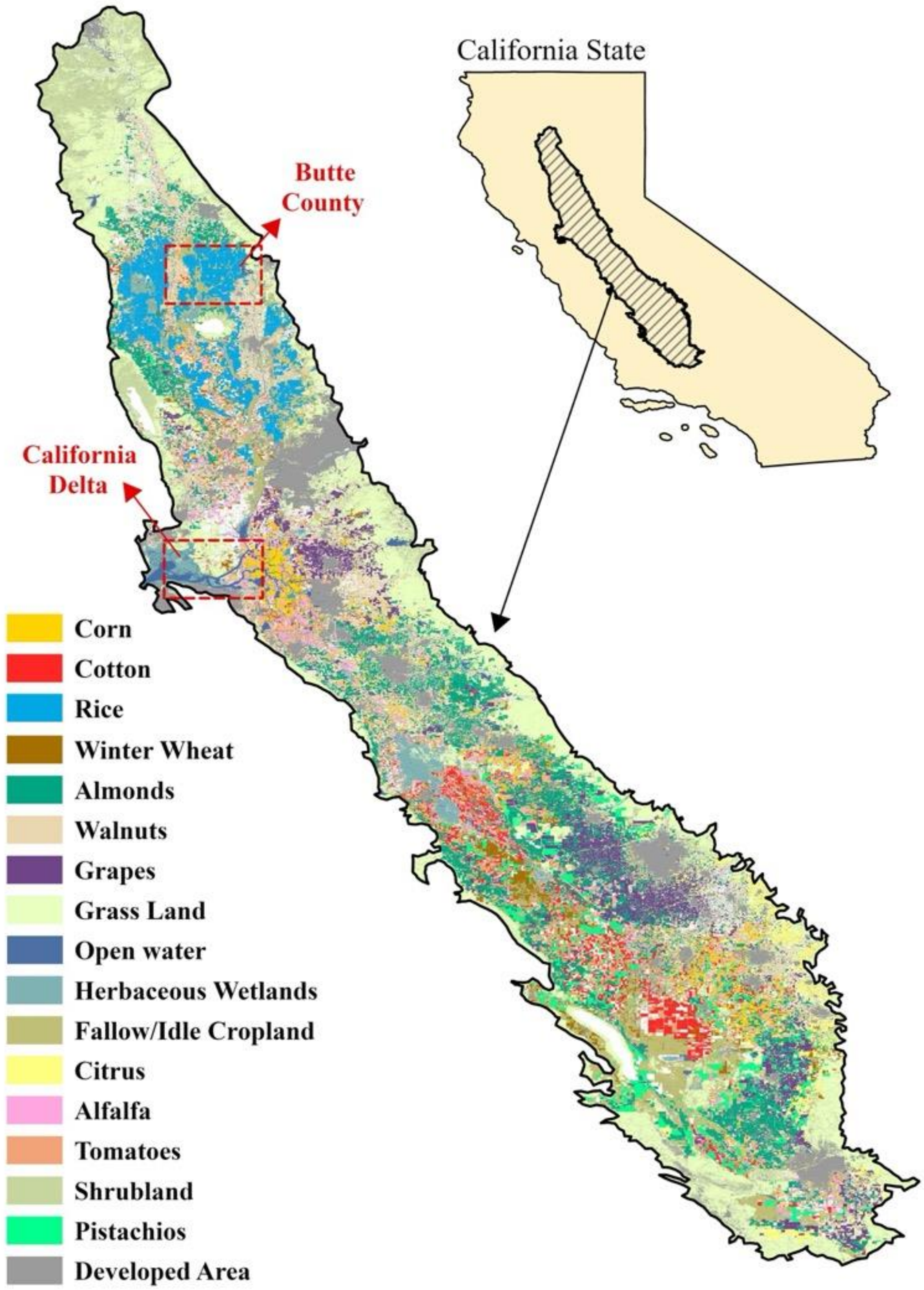

Figure 3.1. Central Valley landcover map based on the Cropland Data Layer (CDL) dataset. Red rectangles mark the locations of Butte County and the California delta, which are used to compare the spatial resolution of soil moisture maps retrieved from OPTRAM-LS to SMAP-HB (reference) in Figure 3.6.

3.3. SMAP- HydroBlocks (SMAP-HB)

To evaluate OPTRAM's performance, we initially considered in situ soil moisture measurements. However, the scarcity of available data in the CV substantially limited our ability to calibrate and validate OPTRAM. To address this challenge, we used the SMAP-HB soil moisture dataset, which is well-validated using extensive in situ observation in the US (Vergopolan et al., 2020, 2021). SMAP-HB maps soil moisture at 30-meter spatial resolution by integrating original SMAP data, land surface model simulations, and in situ soil moisture observations. SMAP-HB spatial coverage over the CV enabled us to calibrate our models for any part of the area.

3.4. In situ soil moisture data

For further validation of OPTRAM, we used in situ soil moisture data from the AmeriFlux and National Oceanic and Atmospheric Administration (NOAA) networks (NOAA, 2024). Given California's sparse soil moisture network, we incorporated stations from across the state rather than focusing solely on the CV for validation. Soil moisture data are available for only 16 out of 35 AmeriFlux stations in California. Although data availability varied across these sites, spanning from 2001 to 2022, our analysis was focused on the period covered by the SMAP-HB data (2015-2019). Consequently, we excluded specific sites with temporal coverage outside this timeframe, e.g., the US-Snd site, which had data available only from 2007 to 2014 (Goulden, 2018). Similarly, stations with a temporal coverage of less than 24 months, such as US-CZ2 and US-CZ3, were not considered (Goulden, 2018). As a result, our acquisition of AmeriFlux soil water content data led to a narrowed dataset consisting of 4 sites, namely, US-Bi1 (Bouldin Island Alfalfa), US-Snf (Sherman Barn), US-Ton (Tonzi Ranch), US-Var (Vaira Ranch- Ione). Table 2.1 provides an overview of the information about the sites used in this study.

Table 3.1. Overview of AmeriFlux network sites providing soil water content data in California and used in this study.

Site ID	Name	Lat	Long
US-Bi1	Bouldin Island Alfalfa	38.0992	-121.4993
US-Snf	Sherman Barn	38.0402	-121.7272
US-Ton	Tonzi Ranch	38.4309	-120.9660
US-Var	Vaira Ranch- Ione	38.4133	-120.9508

The NOAA network comprises sensors installed at varying depths, ranging from 5 to 100 cm, across California. These sensors cover different periods, spanning from 2005 to 2023. NOAA sites providing soil moisture data in California are namely as follows; bve (Bridgeville), czc (Cazadero), hbg (Healdsburg), hbk (Hornbrook), hld (Hopland), lsn (Lake Sonoma), mdt (Middletown), ptv (Potter Valley), pvc (Potter Valley Central), pvw (Potter Valley West), rod (Rio Nido), rve (Redwood Valley East), rvn (Redwood Valley North), rvw (Redwood Valley West), str (Santa Rosa), and wls (Willits). We preferably used 5-cm data to evaluate OPTRAM-based soil moisture estimates. In cases where this depth was unavailable (e.g., bve and hbg sites), 10-cm data were used in our analysis. Table 2.2 provides an overview of the NOAA sites used in this study.

Table 3.2. Overview of NOAA Sites Providing Soil Water Content Data in California and used in this study.

Site ID	Name	Lat	Long	Soil Moisture depth (cm)
bve	Bridgeville, CA	40.473869	-123.792820	10 / 15
czc	Cazadero, CA	38.610700	-123.215200	5 / 10 / 15 / 20 / 50 / 100
hbg	Healdsburg, CA	38.653000	-122.873200	10/ 15 / 50
hbk	Hornbrook	41.9	-122.57	10 / 15
hld	Hopland, CA	39.003000	-123.120900	10 / 15 / 50
lsn	Lake Sonoma, CA	38.718700	-123.053700	10 / 15 / 50
mdt	Middletown, CA	38.745630	-122.711200	5 / 10 / 15 / 20 / 30
ptv	Potter Valley, CA	39.335700	-123.138300	10 / 15 / 50
pvc	Potter Valley - Central	39.32	-123.1	5 / 10 / 15 / 20 / 50 / 100
pvw	Potter Valley - West	39.32	-123.18	5 / 10 / 15 / 20 / 50 / 100
rod	Rio Nido, CA	38.507300	-122.956500	10 / 15 / 50
rve	Redwood Valley - East	39.31	-123.19	5 / 10 / 15 / 20 / 50 / 100
rvn	Redwood Valley - North	39.34	-123.23	5 / 10 / 15 / 20 / 50 / 100
rvw	Redwood Valley - West	39.3	-123.26	5 / 10 / 15 / 20 / 50 / 100
str	Santa Rosa, CA	38.515400	-122.802200	5 / 10 / 15 / 20 / 50 / 100
wls	Willits, CA	39.346300	-123.316600	10 / 15 / 50

3.5. Data Analysis

We coded Eq. (3.4) in the Google Earth Engine (GEE) platform, where S2 and CDL data were already available. We also uploaded monthly-averaged SMAP-HB data to GEE. OPTRAM parameters (i_d, s_d, i_w, and s_w) were obtained by least-squares fitting of Eq. (3.4) to S2 NDVI and STR and SMAP-HB soil moisture data. We obtained one set of parameters for the entire CV for evaluating a CV-wide calibrated OPTRAM (OPTRAM-CV) and one for each landcover type for exploring a landcover-specific calibrated OPTRAM (OPTRAM-LS).

Using these calibrated parameters, moisture content was estimated for both OPTRAM-CV and OPTRAM-LS approaches at the original resolution for each image in the S-2 collection. However, to derive the monthly mean values, we needed to account for multiple images per month, covering billions of 10-meter pixels across the CV. Due to the computational limit of GEE for free accounts, aggregating high-resolution soil moisture estimates at a monthly scale was not feasible. To resolve this issue, we computed the monthly mean soil moisture values by applying a mean reducer at a 30-m scale over the region. The resulting soil moisture estimates were validated using in situ and SMAP-HB data.

4. Results and discussions

Although SMAHP-HB dataset has been validated at four extensively monitored experimental watersheds in the US (Vergopolan et al., 2020), it is validated in this study once again. To do so, the monthly surface soil moisture estimates derived from SMAP-HB were evaluated against soil moisture measurements acquired from AmeriFlux and NOAA stations (see tables 2.1 and 2.2) across California (See Fig. 3.2).

Fig. 3.2 compares SMAP-HB high-resolution soil moisture data against available in-situ observations. As observed, SMAP-HB is well correlated with in-situ observations, with a mean R^2

of 0.6 and an RMSE of 0.08 m^3 m^{-3}, which is larger than the community-accepted level of error (0.04 m^3 m^{-3}) (Entekhabi et al., 2014). The observed deviations could be due to uncertainties in the SMAP-HB inputs such as topography, land cover, soil properties, and meteorological data, the lack of representation of human activities, such as irrigation, reservoir operation, groundwater pumping, and several other reasons discussed by Vergopolan et al. (2020, 2021). Moreover, stations may not be located at the actual irrigation points within croplands, leading to potential discrepancies between soil moisture measurements and vegetation response, introducing uncertainties in estimations. Nonetheless, SMAP-HB is generally in good agreement with in-situ observations. This is especially true in terms of the temporal dynamics of soil moisture at individual site (shown later). This agreement made us confident to use SMAP-HB as a reliable high-resolution soil moisture dataset for evaluating OPTRAM in California.

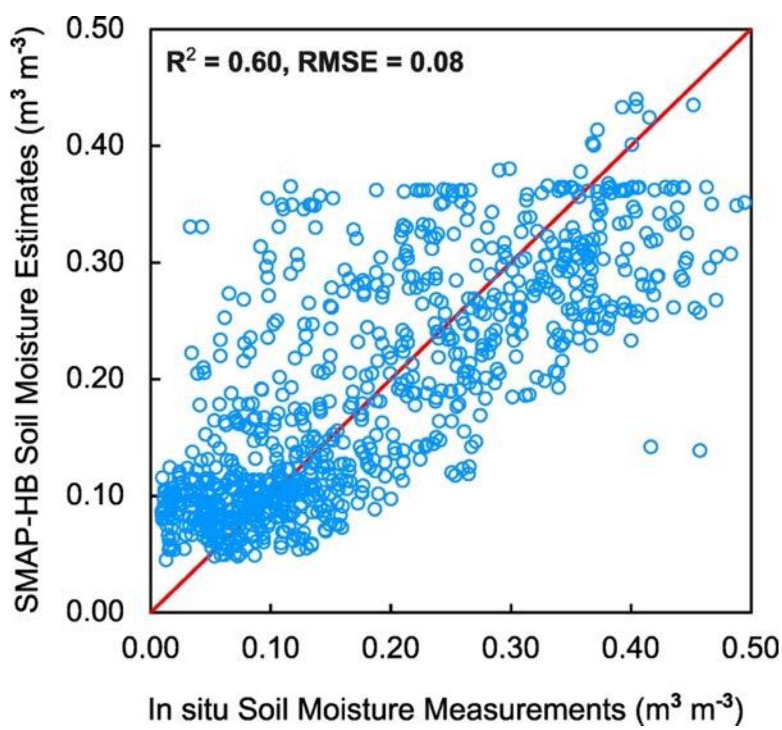

Figure 3.2. SMAP-HB soil moisture estimates compared to in situ soil moisture data from the NOAA and AmeriFlux Networks, 2015-2019.

Table 3.3 lists the calibrated parameters for OPTRAM-CV (entire CV) and OPTRAM-LS (individual landcover types). As seen, the dry and wet edges for the entire CV are largely distant from each other, mainly due to the high spatial variability of STR over the CV (e.g., high STR values in oversaturated rice fields versus low STR values in dry zones of the CV). However, the landcover-specific edges are much closer in most landcover types. While the dry edge shows a marginal variability, the wet edge varies significantly in different landcover classes. To better visualize this variability, Fig. 3.3 shows the STR-NDVI trapezoidal space in three example CV areas, including rice fields, grasslands, and the entire CV. As observed, the trapezoidal space is substantially different for different areas. This emphasizes the importance of a landcover-specific calibration of OPTRAM, as proposed here, and the extent to which one might expect different results from OPTRAM-CV and OPTRAM-LS. For example, satellite observation of STR = 5 in a grassland over the CV would be interpreted as nearly dry soil moisture by OPTRAM-CV but near-saturated soil moisture by OPTRAM-LS (see the first row of Fig. 3.4).

Table 3.3. OPTRAM calibrated parameters for various landcover types in the Central Valley, California.

Model	Area/ Land cover	Dry edge		Wet edge	
		id	sd	iw	sw
OPTRAM	Entire area	0	0	12.21	0
OPTRAM-LS	Developed area	0.61	0	7.7	0
	Rice field	0	0	16.7	2.07
	Grassland	0.59	0	4.17	3.52
	Almonds	0	5.52	5.03	2.37
	Shrubland	0.79	0	7.06	0
	Pistachios	0	0	8.27	0
	Cotton	0	0	3.29	21.9
	Grapes	0	0	0	21.75
	Walnuts	0	0	1.09	18.28
	Fallow/ Idle cropland	0	0	9.07	0.39
	Alfalfa	0.21	3.73	4.34	2.8
	Winter wheat	0	3.38	4.59	3.18

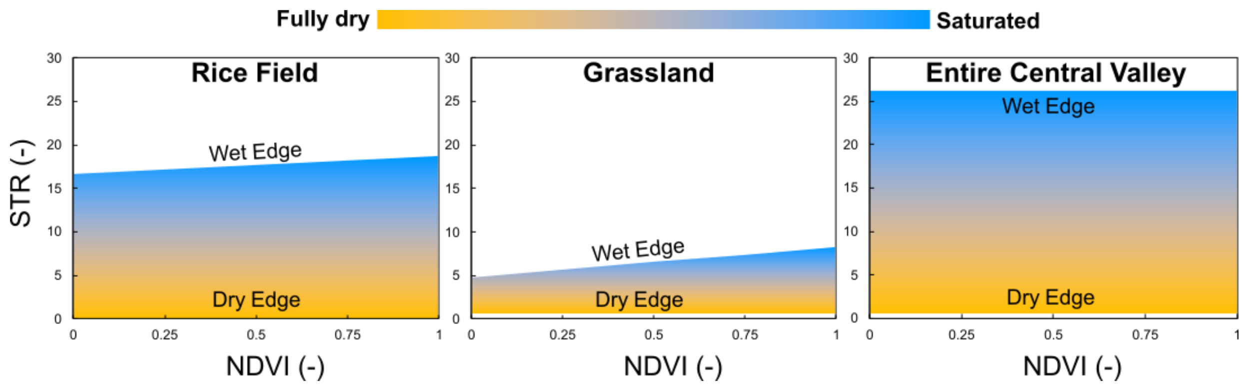

Figure 3.3. Variability of OPTRAM parameters (dry and wet edges) in three example areas of the Central Valley: rice fields, grasslands, and the entire Central Valley.

Fig. 3.4 presents the OPTRAM-CV and OPTRAM-LS soil moisture estimates compared to SMAP-HB as reference. As observed, OPTRAM-LS is significantly more accurate than OPTRAM-CV. Across all landcover types, RMSE is notably lower in OPTRAM-LS. For instance, in grassland, a major landcover constituting over 20% of the CV, and in winter wheat, another prevalent landcover type in CV, OPTRAM-LS brings the RMSE to the community-accepted level of error (0.04 $m^3 m^{-3}$), while the error in OPTRAM-CV is more than twice this level (0.09 $m^3 m^{-3}$). Except for the rice fields, walnuts, and pistachios, OPTRAM-LS provides reasonable soil moisture estimates, with about 0.04 to 0.05 ($m^3 m^{-3}$) deviations from SMAP-HB.

This figure also indicates a generally higher correlation (in terms of R^2) between OPTRAM-LS and SMAP-HB than between OPTRAM-CV and SMAP-HB. This enhanced correlation is evident across most landcover types, namely, almond, cotton, grapes, fallow idle cropland, alfalfa, winter wheat, and rice fields. It is important to note that OPTRAM-CV shows an almost zero correlation with SMAP-HB in cotton and grape landcovers, which constitute a small portion of CV. However, a meaningful correlation appears when this model is calibrated for these landcovers specifically. This emphasizes the nonlinear nature of OPTRAM, Eq. (3.4), where different sets of model parameters do not necessarily yield linearly correlated soil moisture outputs. Having that said, there are other landcover types where changing the model parameters led to a linear change in the OPTRAM soil moisture estimates, resulting in the same R^2 between OPTRAM and SMAP-HB (e.g., shrublands, developed areas). Nonetheless, OPTRAM-LS decreased the bias in these landcovers, as shown by the decreased RMSEs.

We can also see that despite the significant improvement of OPTRAM through the landcover-specific calibration, this model still shows relatively large deviations from SMAP-HB in some landcover types. This deviation can be largely due to the much simpler nature of OPTRAM compared to SMAP-HB, as the former tries to estimate soil moisture solely from optical images, but the latter integrates SMAP brightness temperature, and physically modeled soil moisture which uses meteorological data, soil properties, topography, and land cover as input.

The largest deviation between OPTRAM and SMAP-HB is found in the rice fields. This deviation could be due to not OPTRAM errors, but SMAP-HB errors. As observed, SMAP-HB shows only one soil moisture peak in the wet season, while OPTRAM exhibits two peaks, one in the wet season and another in April and May. The OPTRAM time series here is closer to our expectations for the rice fields in California. Farmers in Butte, Glenn, Colusa, Sutter, and Yuba counties often start to saturate their fields with flood irrigation at the beginning of May and drain around the beginning of September. Although SMAP-HB has limitations in representing the high-resolution spatial distribution of human-managed processes (e.g., irrigation, reservoir water release), it captures part of the effect through lower-resolution SMAP soil data. That is why SMAP-HB showed some increase in soil moisture in the rice fields around May, but not the full soil saturation. OPTRAM, however, captured the full soil saturation because it could be clearly seen in the S2 SWIR images.

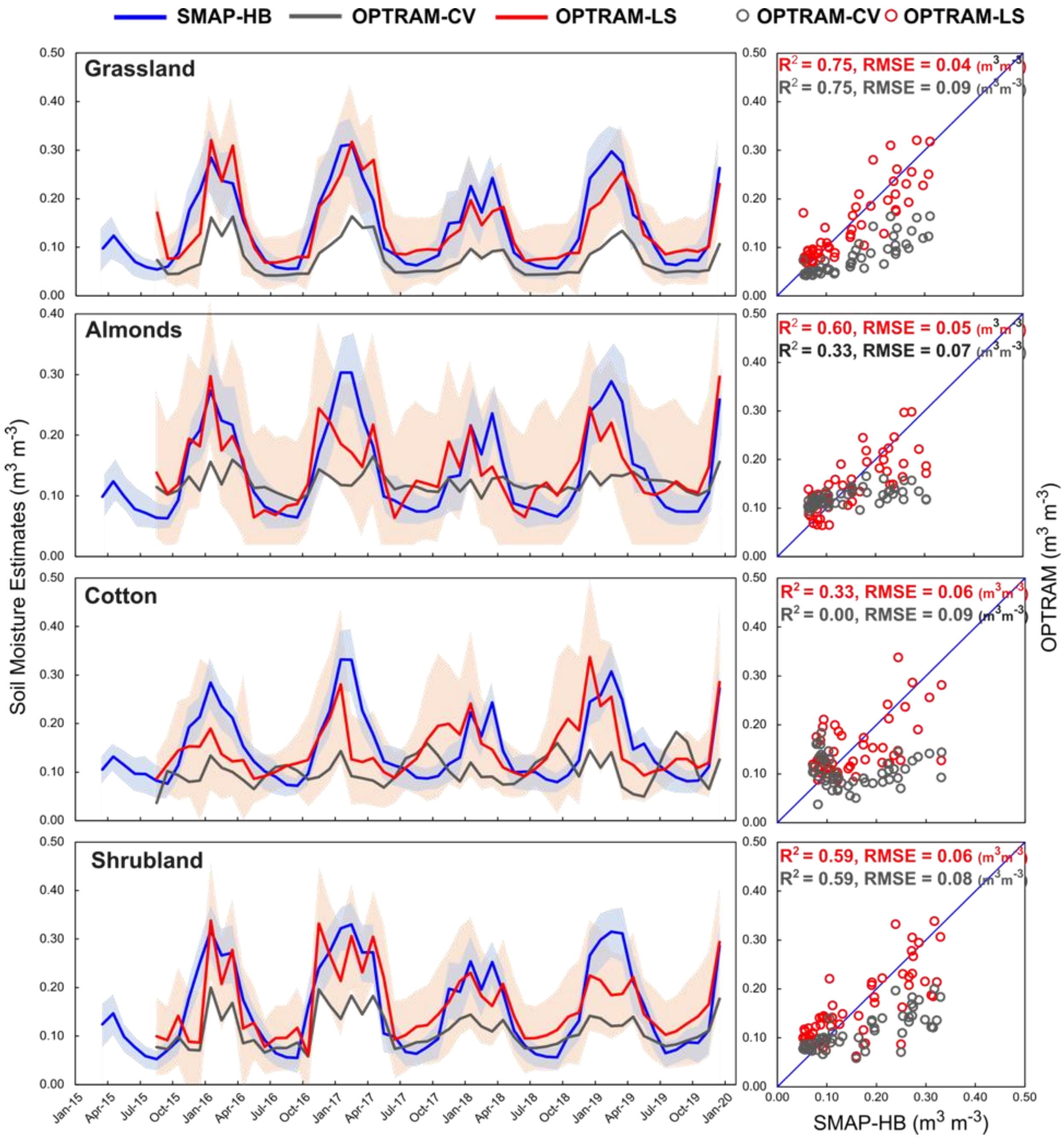

Figure 3.4. Soil moisture estimates by SMAP-HB (reference), OPTRAM-CV and OPTRAM-LS from 2015 to 2019 for various landcover types over the Central Valley, California. The solid lines represent the monthly mean values, and the shaded areas indicate the variability in estimates.

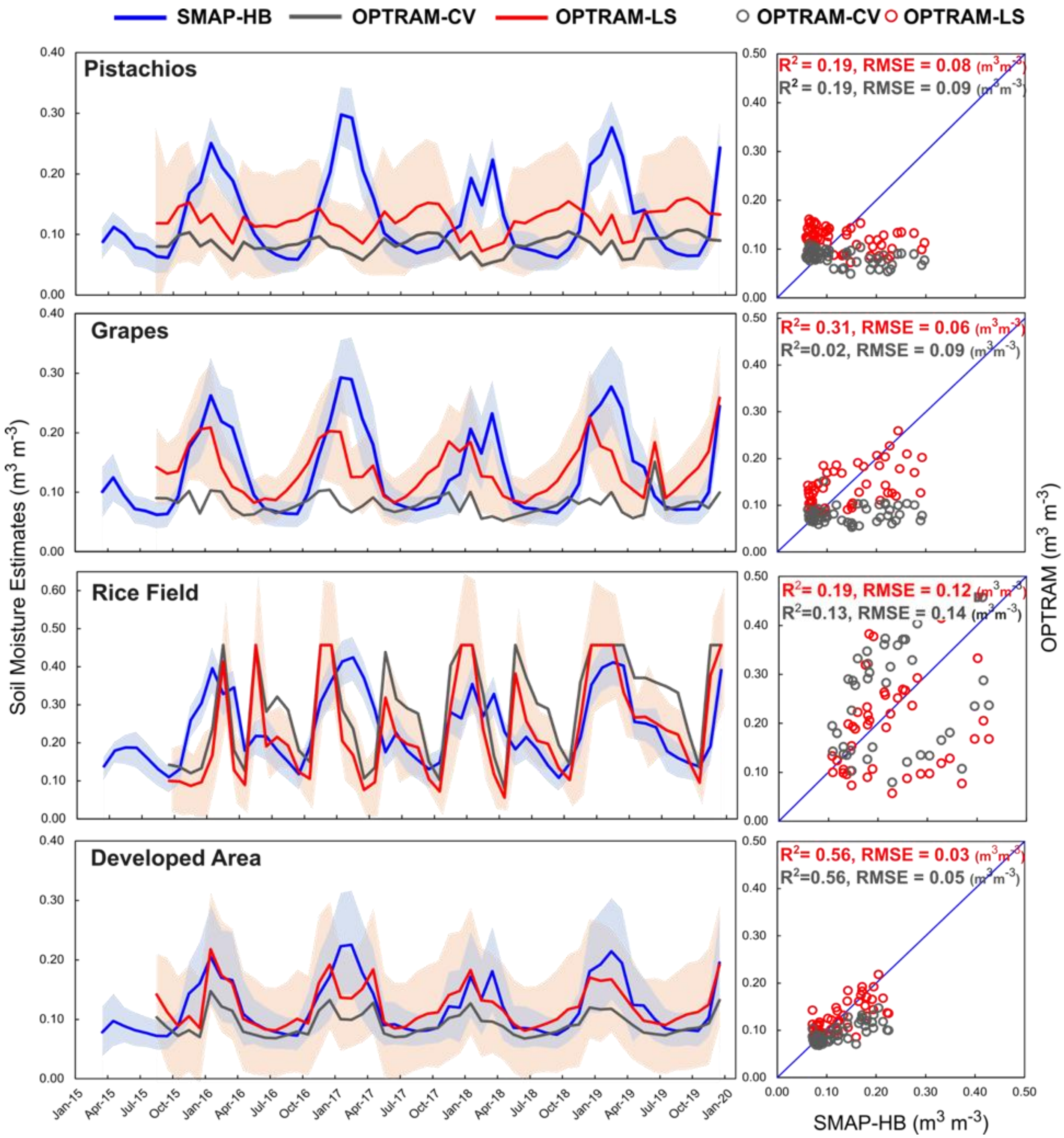

Figure 3.4 (Continued). Soil moisture estimates by SMAP-HB (reference), OPTRAM-CV and OPTRAM-LS from 2015 to 2019 for various landcover types over the Central Valley, California. The solid lines represent the monthly mean values, and the shaded areas indicate the variability in estimates.

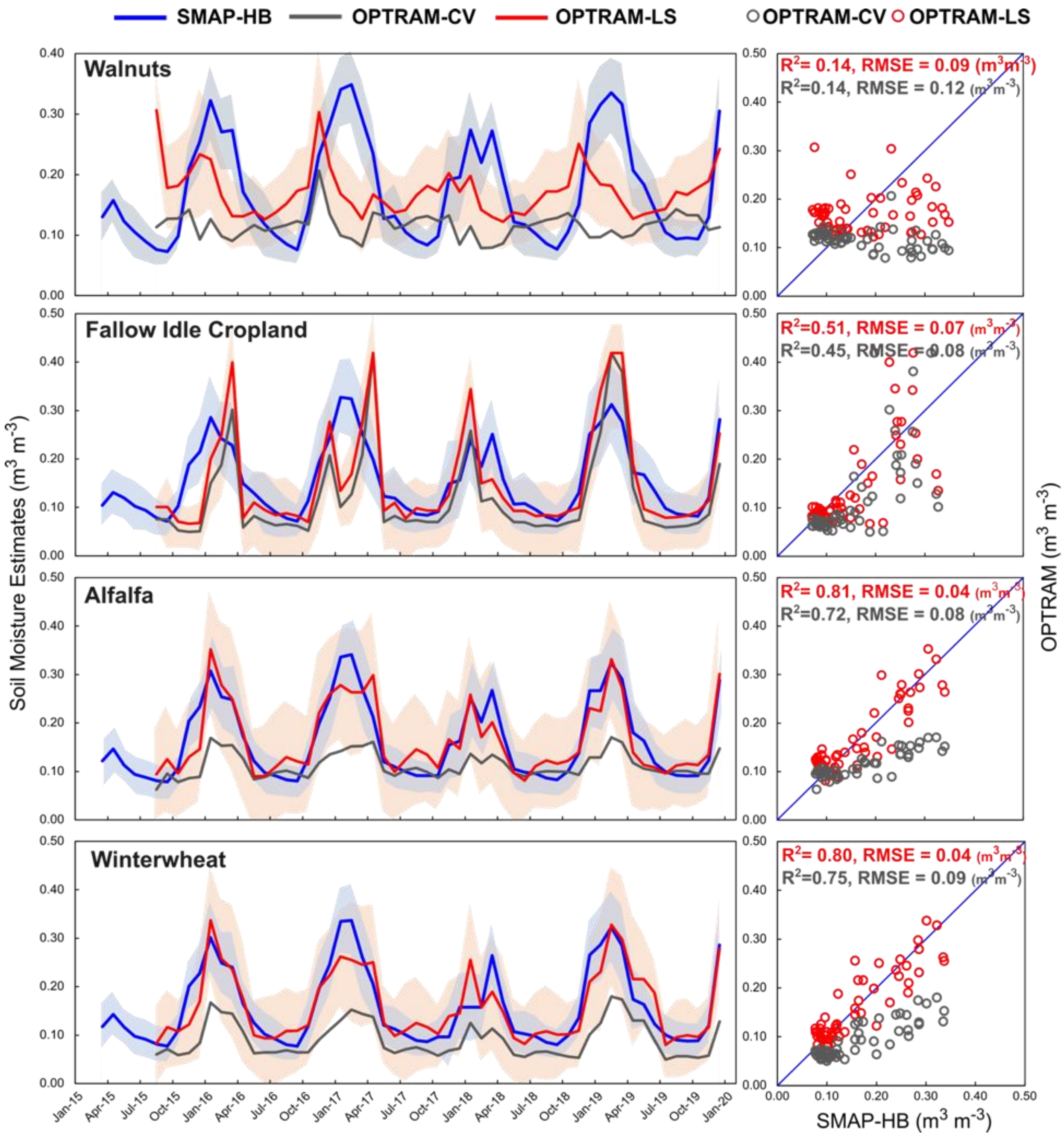

Figure 3.4 (Continued). Soil moisture estimates by SMAP-HB (reference), OPTRAM-CV and OPTRAM-LS from 2015 to 2019 for various landcover types over the Central Valley, California. The solid lines represent the monthly mean values, and the shaded areas indicate the variability in estimates.

Fig. 3.5 presents some sample soil moisture maps in the CV based on OPTRAM and SMAP-HB. As observed, significantly different spatial distributions are shown by these two models. In this figure, the most notable observation is that SMAP-HB soil moisture is much smoother than that of OPTRAM. By integrating higher spatial resolution satellite observations, OPTRAM could better capture the fine-scale imprint between different agricultural fields than SMAP-HB. Although both methods have a nominal spatial resolution of 30 m, SMAP-HB's capability to capture such fine-scale differences is hampered by the SMAP satellite's large-scale footprint. It yields a narrow range of soil moisture for large clusters, where a high spatial variability is generally expected due to the land surface heterogeneity (see Fig. 3.1).

The contrast in the spatial resolution is more clearly highlighted when comparing the soil moisture maps in May, especially in the Sacramento-San Joaquin Delta and rice fields of northern California. In these areas, OPTRAM detects many saturated and oversaturated pixels, which are common due to abundant surface water in these areas. As mentioned earlier, these high soil moisture values in the rice fields are due to flood irrigation, which is a common practice in California from May to August. In contrast, SMAP-HB shows a smooth mid-level soil moisture for the entire area and no saturated pixels. This observation agrees with the patterns shown in Fig. 3.4, where SMAP-HB presents only one soil moisture peak in the wet season, but OPTRAM exhibits one more soil moisture peak in May.

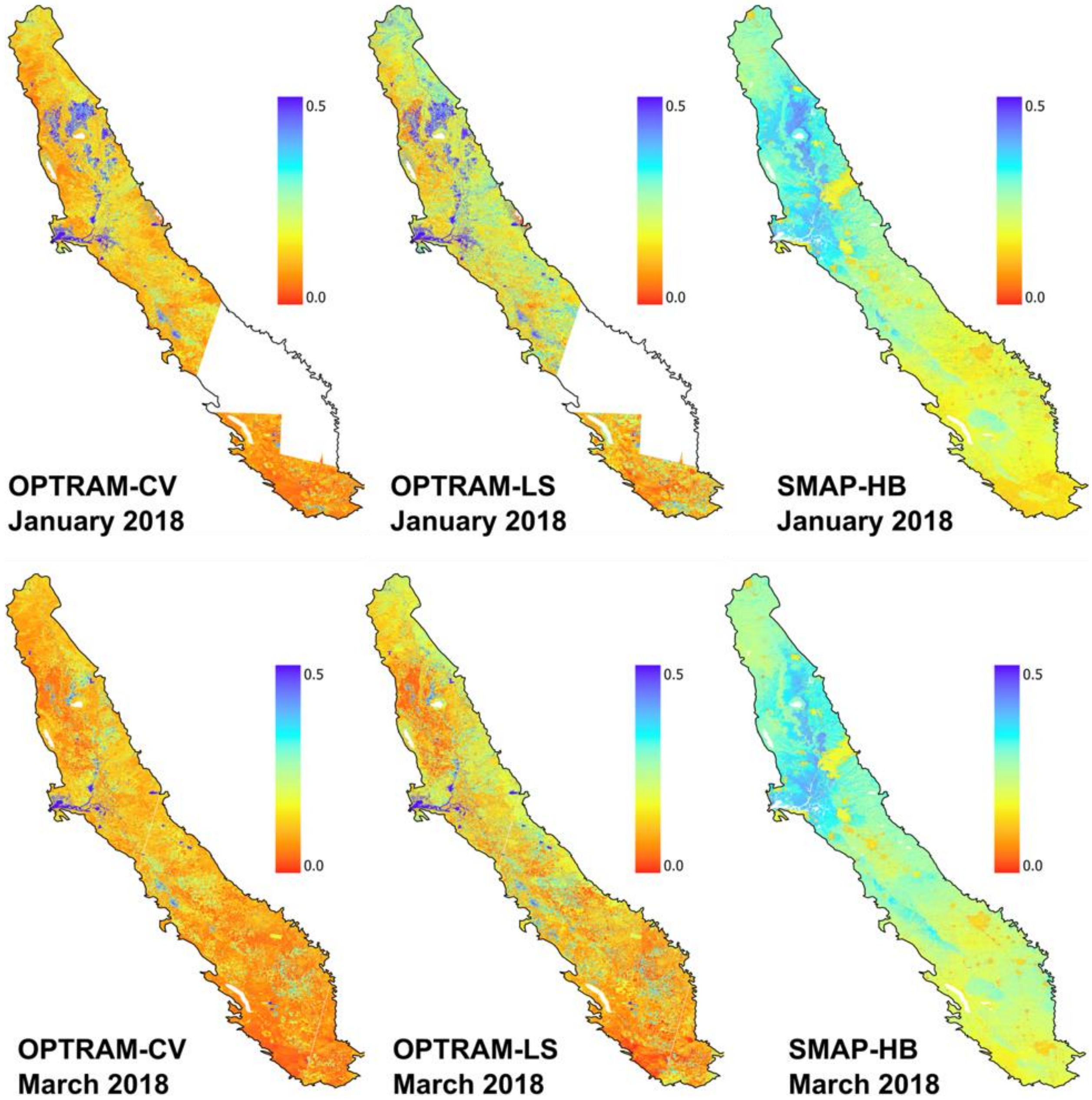

Figure 3.5. The spatial distribution of monthly OPTRAM, OPTRAM-LS, and SMAP-HB retrievals of surface soil moisture (m^3m^{-3}) over Central Valley, California, in January, and March of 2018.

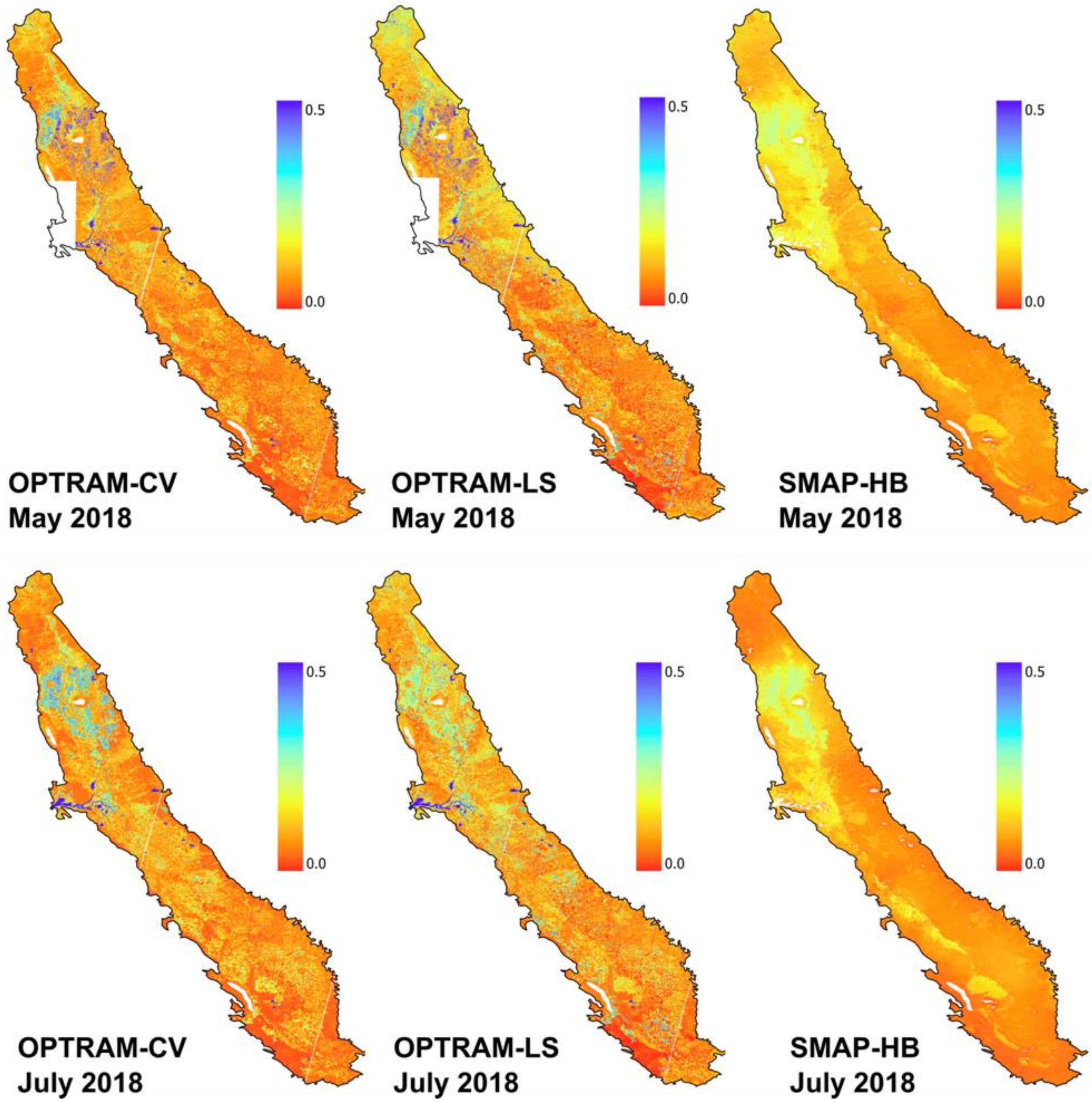

Figure 3.5 (Continued). The spatial distribution of monthly OPTRAM, OPTRAM-LS, and SMAP-HB retrievals of surface soil moisture (m^3m^{-3}) over Central Valley, California, in May, and July of 2018.

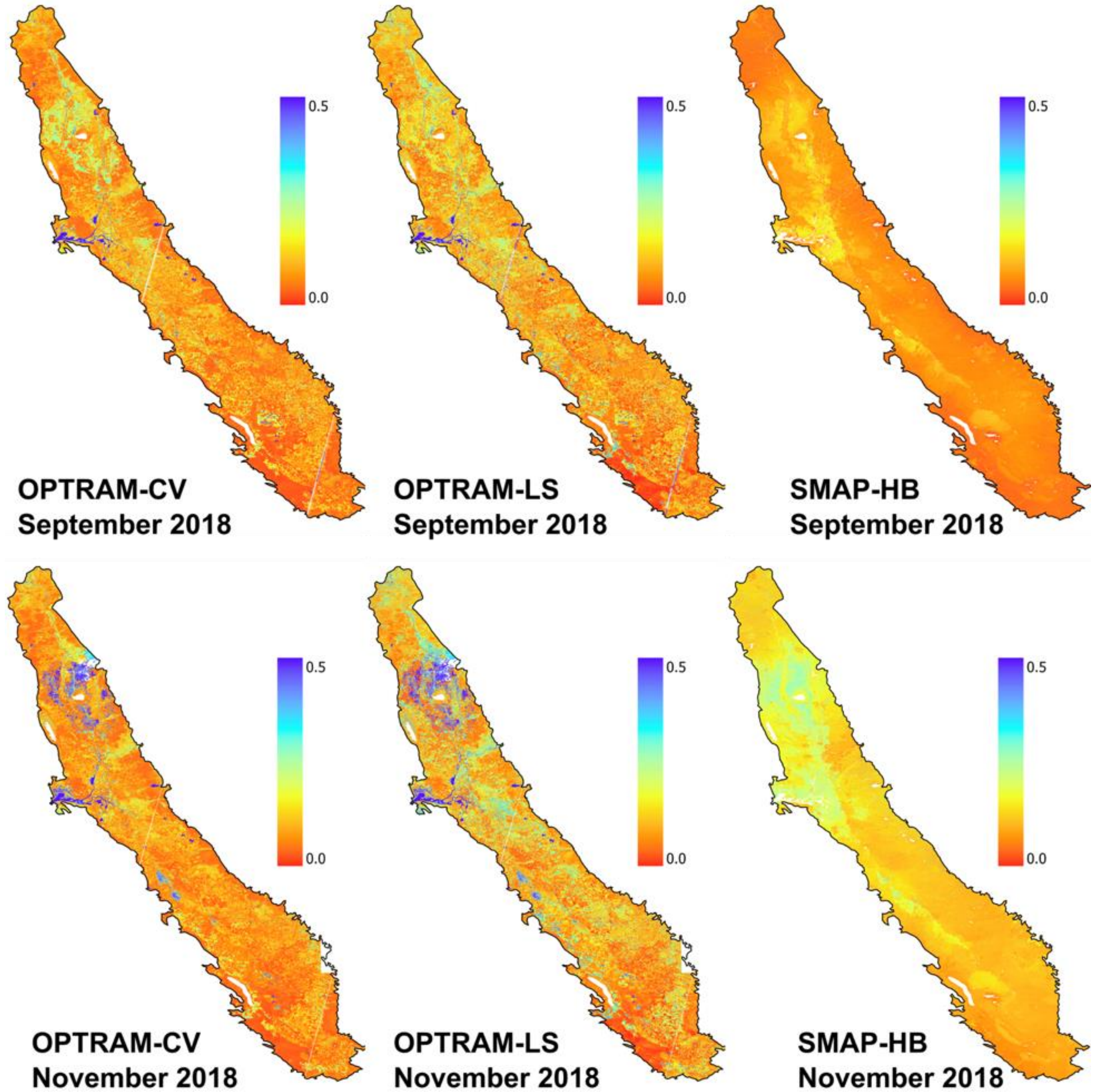

Figure 3.5 (Continued). The spatial distribution of monthly OPTRAM, OPTRAM-LS, and SMAP-HB retrievals of surface soil moisture (m^3m^{-3}) over Central Valley, California, in September, and November of 2018.

To better illustrate this fact, Fig. 3.6 shows further sample soil moisture maps over the Delta area and some rice fields within Butte County. The true-color images of these areas are also included which shed light on the expected actual spatial resolution of soil moisture. As observed, the spatial variability of OPTRAM is well aligned with the true-color image. All the individual fields, surface water pathways, and permanent water bodies are clearly seen in OPTRAM, but are barely distinguishable in SMAP-HB. This demonstrates that OPTRAM is more accurate in capturing the spatial variability of soil moisture.

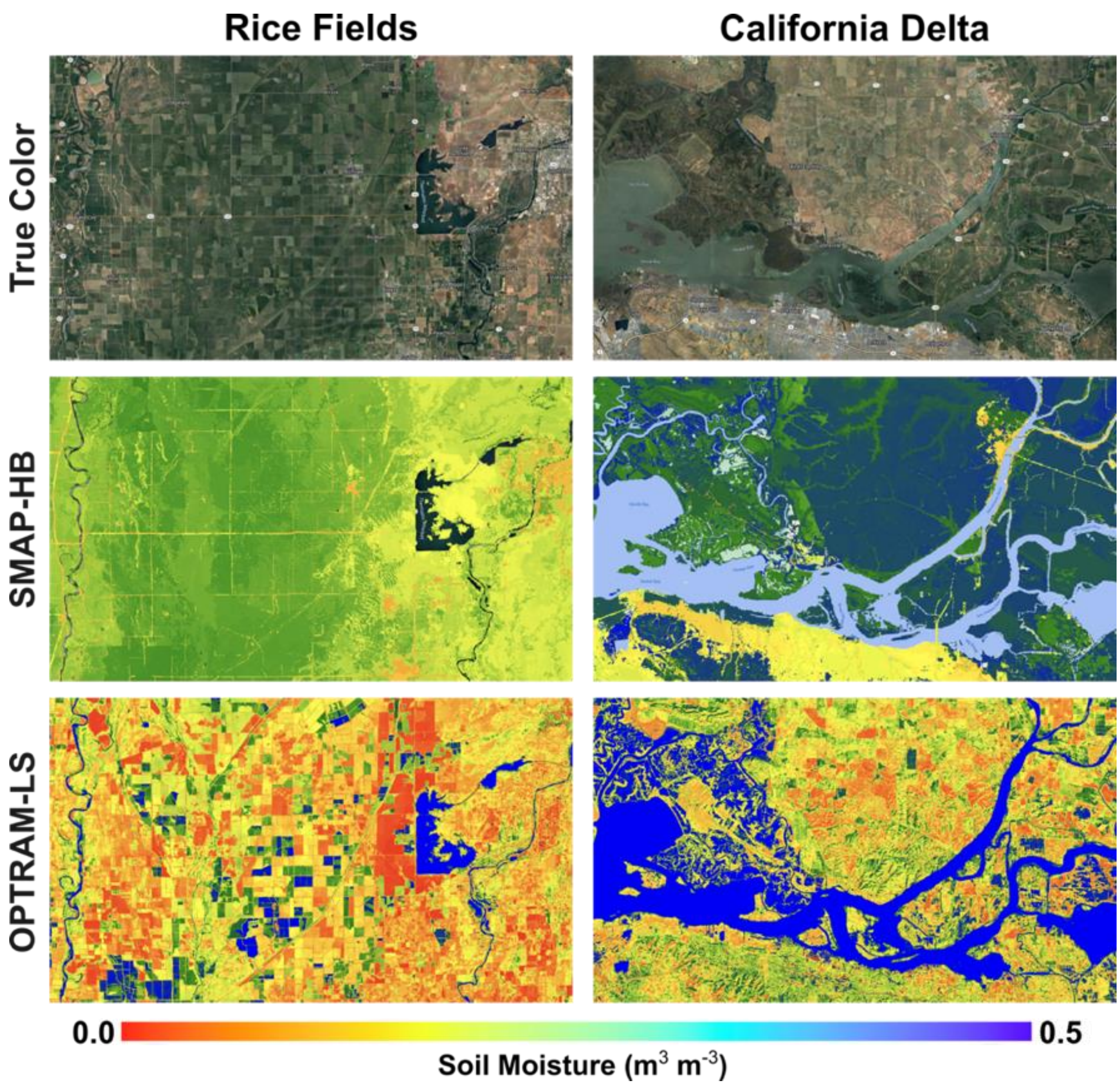

Figure 3.6. True-color image, SMAP-HB and OPTRAM-LS retrieval of surface soil moisture over the rice fields of Butte County (May 2019) and the California Delta (February 2019).

Another observation in Fig. 3.5 is that OPTRAM-CV is generally biased toward drier soil moisture values compared to SMAP-HB. As expected, OPTRAM-LS reduces this bias, because it was calibrated for each landcover class directly based on SMAP-HB data. Fig. 3.7 takes a closer look at the dry bias in OPTRAM-CV in some sample areas, including grape vineyards within Fresno and Madera counties (January 2019), grasslands within Tehama County (April 2019), and shrublands in northern CV (April 2019). As observed, OPTRAM-LS and SMAP-HB consistently estimate wetter soils than OPTRAM-CV in these areas. This dry bias in OPTRAM-CV can be explained by the model parameters, which are not representative when averaged out for the entire CV. As shown in Fig. 3.3, the CV-wide calibration of OPTRAM leads to a much higher wet edge than expected for most landcovers, causing the observed dry bias. Fig. 3.7 emphasizes the importance of a landcover-specific calibration of OPTRAM to achieve reasonable soil moisture maps based on this optical remote sensing approach.

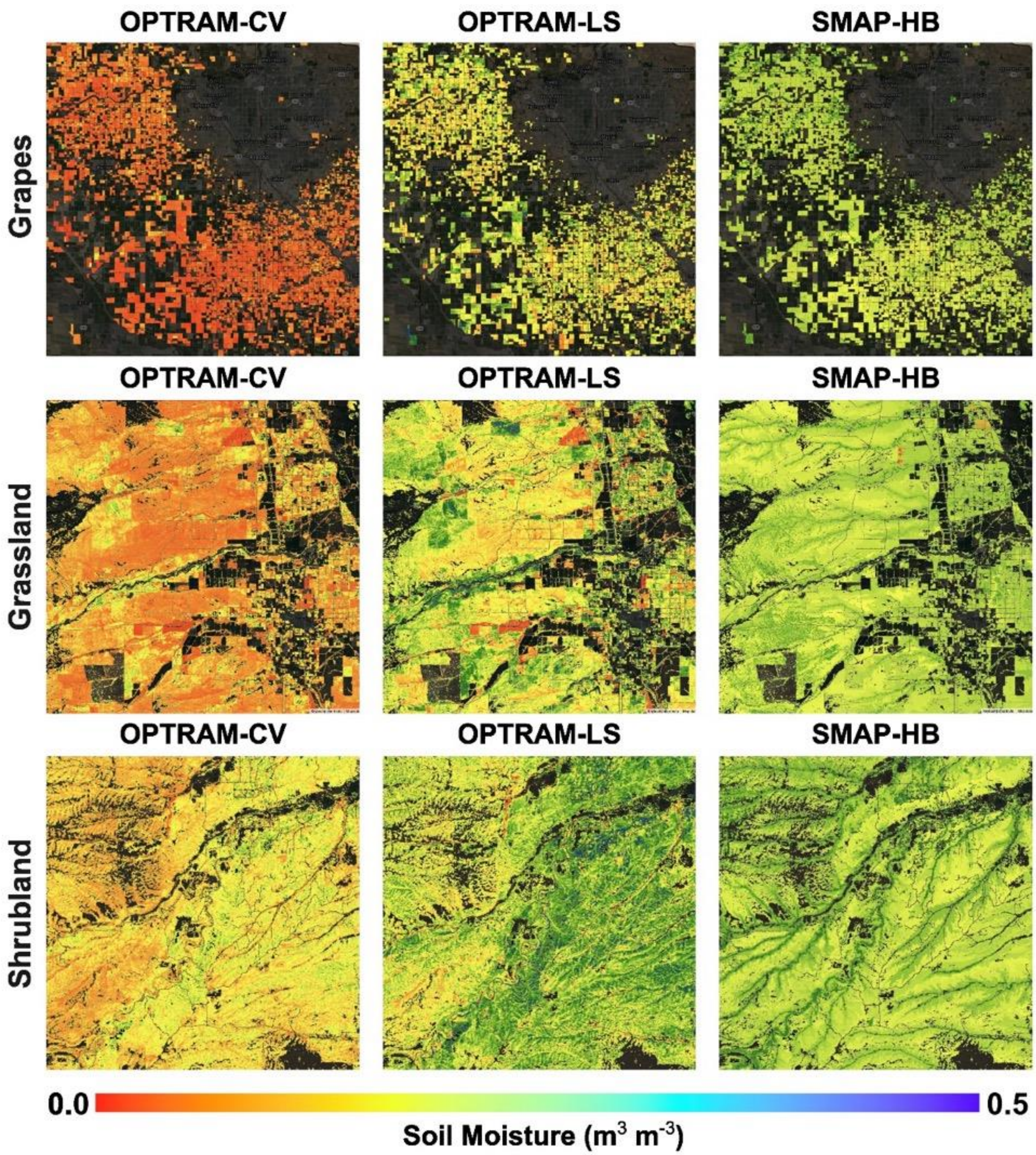

Figure 3.7. OPTRAM, OPTRAM-LS and SMAP-HB estimates of surface soil moisture for some sample landcovers within the Central Valley, including grapes in January 2019 and grassland and shrubland in April 2019.

In Fig. 3.8, remotely sensed soil moisture values from SMAP-HB, OPTRAM, and OPTRAM-LS are compared with in-situ soil moisture measurements from the NOAA and AmeriFlux Networks. As observed, SMAP-HB estimations exhibit a high correlation with the soil moisture measurements in all sites, with an R^2 greater than 0.8. Furthermore, its RMSE ranges between 0.04 to 0.09 m^3 m^{-3}, which is considered a reasonable accuracy for remote sensing applications and large-scale mapping of soil moisture (Entekhabi et al., 2014).

The comparison between OPTRAM-CV and OPTRAM-LS to the soil moisture measurements shows that in some sites, namely czc, hbg, and pvc, OPTRAM-LS outperforms OPTRAM-CV by exhibiting a higher correlation with in-situ measurements as well as a lower RMSE. However, in some other sites, namely bve, rod, rve, and wls, OPTRAM-CV performs better than OPTRAM-LS. Overall, the difference between OPTRAM-CV and OPTRAM-LS is marginal in this case.

One possible explanation lies in the spatial calibration structure of OPTRAM-LS. Although OPTRAM-LS refines the model by calibrating parameters for each land cover type, it still assumes that all pixels within a given landcover class behave similarly. However, significant intra-class variability exists due to regional differences in soil texture, vegetation condition, and climate. For instance, as previously discussed, the northern portion of the Central Valley tends to be wetter than the southern portion. Therefore, applying a uniform set of parameters across a land cover class, without accounting for geographic location, may fail to accurately represent the actual conditions at specific sites. While OPTRAM-LS improves upon the region-wide calibration of OPTRAM-CV, these findings suggest that further refinement, such as calibration at finer spatial scales (e.g., sub-regional or pixel level), may yield better performance.

Additionally, although OPTRAM assumes that STR is a reliable proxy for soil moisture, STR values can also be influenced by other factors unrelated to soil moisture such as land/ canopy dynamics. These influences may introduce uncertainties when using STR for soil moisture estimation.

Finally, the strong performance of SMAP-HB highlights the potential benefits of integrating additional independent variables into the OPTRAM framework. Incorporating complementary data sources, such as precipitation, or coarse-resolution satellite-based soil moisture products like SMAP, could help mitigate some of the current limitations of the optical-only approach and enhance the model's reliability for operational soil moisture monitoring.

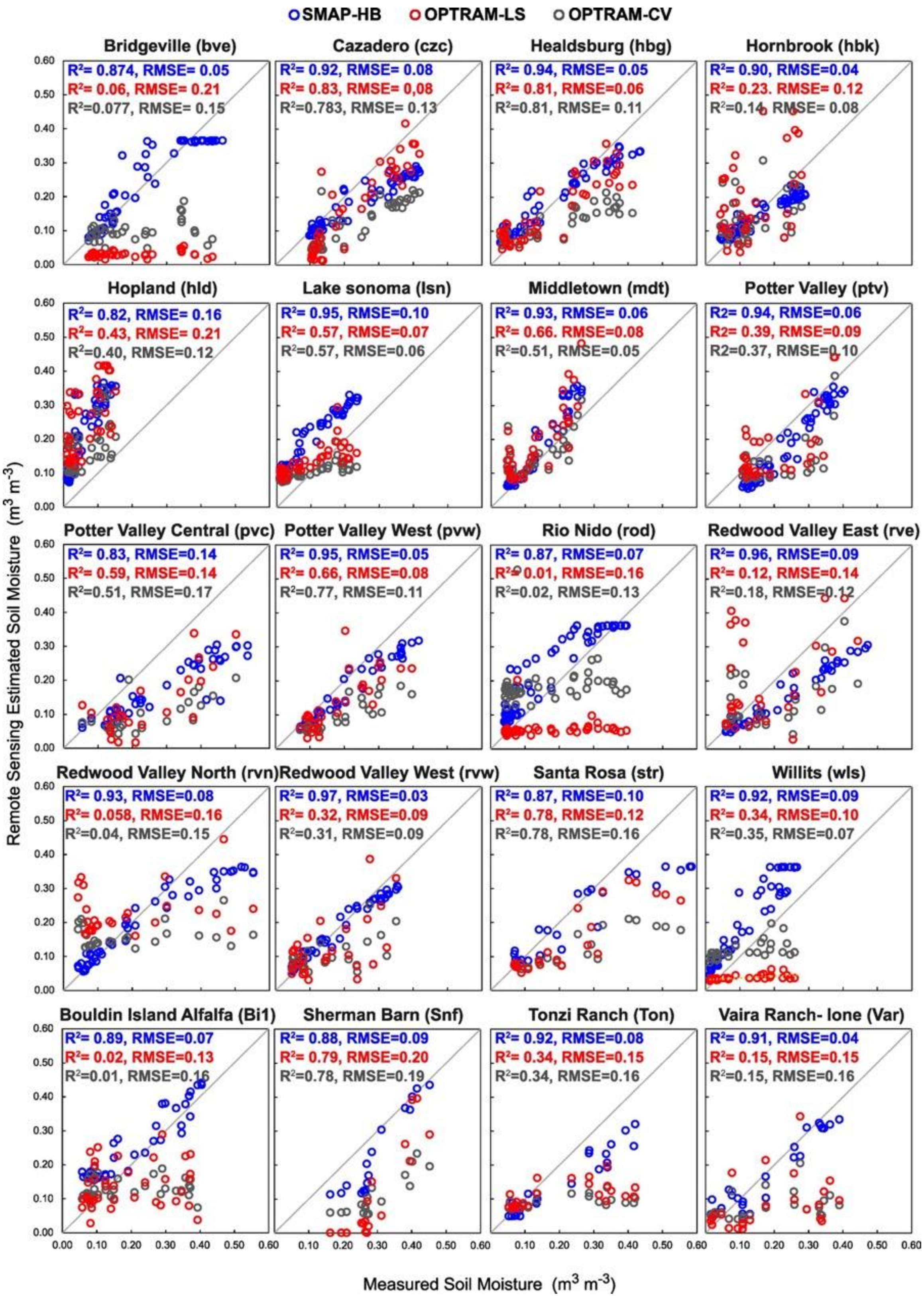

Figure 3.8. Remote sensing estimated soil moisture (SMAP-HB, OPTRAM-LS, OPTRAM-CV) compared to in-situ soil moisture data from the NOAA and AmeriFlux Networks.

5. Conclusion

This chapter addressed the second objective of this dissertation by utilizing Sentinel-2 optical reflectance data to evaluate two calibration strategies for OPTRAM across California's Central Valley (CV): a region-wide calibration (OPTRAM-CV) and a land cover-specific calibration (OPTRAM-LS). The aim was to assess whether incorporating land cover-specific parameterization could enhance the accuracy of OPTRAM-derived soil moisture estimates. The SMAP-HB dataset, a well-validated, satellite-derived soil moisture product, was used as the reference for performance evaluation.

The results demonstrated that OPTRAM-LS significantly improved soil moisture estimation over the CV compared to OPTRAM-CV. In general, OPTRAM-CV exhibited a systematic dry bias relative to SMAP-HB, largely due to calibration parameters that did not reflect the spectral characteristics of individual land cover types. Notably, the region-wide calibration tended to overestimate the wet edge for many land cover classes, leading to a consistent underestimation of soil moisture. By contrast, OPTRAM-LS reduced this bias by tailoring model parameters to each land cover category, thereby offering a more accurate representation of soil moisture across heterogeneous landscapes.

However, while OPTRAM-LS outperformed OPTRAM-CV at most in-situ validation sites, the OPTRAM-CV calibration yielded slightly better performance at some locations. These mixed results suggest that although land cover-specific calibration is an important step forward, it does not fully account for the spatial heterogeneity within individual land cover types. Variability in soil texture, vegetation health, and microclimatic conditions, particularly between the northern and southern regions of the CV, can explain these uncertainties. As such, this chapter highlights the potential value of more localized calibration strategies, including sub-land cover or pixel-level approaches, for future refinement.

This analysis also reaffirmed that SMAP-HB provides temporally reliable and accurate estimates of soil moisture when validated against in-situ data. Nonetheless, SMAP-HB lacks the high spatial resolution needed to detect fine-scale variations in soil moisture associated with local irrigation practices. For example, OPTRAM more effectively captured saturation in rice fields in May, a period when flood irrigation is a common practice there, which was not captured in SMAP-HB. Thus, while SMAP-HB offers robust temporal consistency and high accuracy at larger scales, OPTRAM, driven by high-resolution Sentinel-2 imagery, serves as a computationally efficient and spatially detailed alternative for mapping monthly-scale soil moisture variation.

Finally, this chapter underscores the need to consider additional factors that influence STR reflectance but are not directly related to soil moisture, such as vegetation dynamics or canopy structure. Accounting for these variables in the OPTRAM framework may further enhance model accuracy. In conclusion, how to integrate additional data sources (e.g., SMAP soil moisture), reduce calibration boundaries to the pixel level, and refine the treatment of non-moisture-related STR influences will be further addressed in the following chapter (Mohamadzadeh et al., 2025).

Chapter 4 - Microwave-Guided OPTRAM: A Novel Approach to Remote Sensing of Soil Moisture by Fusing SMAP and MODIS Satellite Observations

1. Introduction

Chapter 1 introduced OPTRAM as a promising method for estimating soil moisture from optical surface reflectance data. In Chapter 3, the calibration of OPTRAM using land cover-specific parameterization across California's Central Valley (CV) was shown to substantially improve estimation accuracy compared to a uniform, region-wide calibration. These findings highlighted not only the importance of accounting for land cover variability but also suggested the need to reduce calibration boundaries to finer spatial units (e.g., pixel-level) and to integrate additional datasets such as microwave observations from SMAP to further enhance OPTRAM's ability to isolate soil moisture signals from confounding variables.

To explore these opportunities, this chapter presents a novel model called Microwave-Guided OPTRAM (MG-OPTRAM). This approach represents a fusion of optical and microwave remote sensing data, designed to combine the spatial richness of optical surface reflectance (e.g., MODIS) with the physical soil moisture sensitivity of passive microwave observations (e.g., SMAP). MG-OPTRAM was developed to directly address the third objective of this dissertation:

To fuse microwave (SMAP) and optical (MODIS) data within an OPTRAM framework and evaluate whether this integration overcomes the limitations of individual methods and enhances soil moisture estimation accuracy.

MG-OPTRAM was initially conceived as an enhanced version of OPTRAM; however, it also emerged as a new methodology for downscaling SMAP data using optical satellite observations, for example, from the Moderate Resolution Imaging Spectroradiometer (MODIS). While downscaling SMAP using MODIS has been extensively explored (e.g., Colliander et al., 2017; Zhao et al., 2018; Fang et al., 2018; Wen et al., 2019; Mohseni et al., 2024), MG-OPTRAM introduces a fundamentally different approach. Most existing algorithms rely on land surface temperature (LST) to disaggregate soil moisture, whereas MG-OPTRAM is based on optical surface reflectance. Unlike LST, surface reflectance is not strongly influenced by transient weather conditions, allowing for a stable, one-time calibration. As a result, MG-OPTRAM can also be used to reconstruct SMAP-like soil moisture datasets for periods before the SMAP mission (2015–present), leveraging the temporal consistency of its model parameters.

A similar effort was recently undertaken by Zhong et al. (2024), who also employed optical data within the OPTRAM framework to downscale SMAP observations. However, a key distinction of our approach lies in how SMAP data is utilized. While Zhong et al. (2024) derived OPTRAM parameters solely from optical data, our method directly calibrates OPTRAM using SMAP observations at their original (coarse) resolution and subsequently applies the calibrated model at the finer MODIS resolution. We assume that this direct calibration with SMAP establishes a stronger link between SMAP and OPTRAM and may help mitigate potential biases in the downscaled soil moisture estimates.

In this chapter, we first introduce the MG-OPTRAM algorithm, detail its theoretical formulation, and validate it against the SMAP dataset. Then we apply MG-OPTRAM to (1) reconstructing SMAP-like soil moisture data for the pre-2015 period at SMAP's original resolution, and (2) downscaling current SMAP data to the finer MODIS resolution (500 m) over a long period.

2. Theoretical background

Sadeghi et al. (2017) proposed OPTRAM based on the relationship between surface soil moisture and SWIR reflectance. OPTRAM estimates soil moisture θ as follows:

$$\theta = \theta_d + (\theta_w - \theta_d)\frac{\mathrm{STR}-\mathrm{STR}_d}{\mathrm{STR}_w-\mathrm{STR}_d} \tag{4.1}$$

Where STR is the SWIR transformed reflectance, and STR_d and STR_w are STR at the dry edge ($\theta = \theta_d$) and wet edge ($\theta = \theta_w$), respectively. The relationship between STR and SWIR reflectance, R_{SWIR}, comes from the Kubelka and Munk (1931) transformation (Sadeghi et al., 2015):

$$\mathrm{STR} = \frac{(1-R_{SWIR})^2}{2R_{SWIR}} \tag{4.2}$$

Previous observations indicated that NDVI and STR form a trapezoidal data cloud. In this data cloud, drier pixels are located at a lower position and wetter pixels are located at a higher position. Fitting two lines to the lower and upper edges of the data cloud, the dry and wet edges are formulated as follows:

$$\mathrm{STR}_d = i_d + s_d\mathrm{NDVI} \tag{4.3}$$

$$\mathrm{STR}_w = i_w + s_w\mathrm{NDVI} \tag{4.4}$$

Where i_d and s_d are the intercept and the slope of the dry edge, respectively, and i_w and s_w are the intercept and slope of the wet edge, respectively.

Accordingly, OPTRAM assigns a soil moisture value to each pixel, considering its proximity to the dry and wet edges of the data cloud. By combining Eqs. (4.1) to (4.4) and assuming $\theta_d = 0$ and $\theta_w = \theta_s$, where θ_s is the soil porosity, soil moisture for each pixel can be estimated as a function of STR and NDVI as follows:

$$\theta = \theta_s \left[\frac{\text{STR}-i_d-s_d\ \text{NDVI}}{i_w-i_d+(s_w-s_d)\text{NDVI}}\right] \quad (4.5)$$

OPTRAM has one physically significant parameter (θ_s) and four fitting (calibration) parameters (i_d, s_d, i_w, s_w). In their original development, Sadeghi et al. (2017) assumed the fitting parameters are spatially constant over their entire study areas (Walnut Gulch watershed in Arizona and Little Washita watershed in Oklahoma). Accordingly, they estimated these constants for each watershed by fitting Eqs. (4.3) and (4.4) to the edges of the STR-NDVI data cloud. They suggested that this fitting can be simply done via a visual inspection of the STR-NDVI data cloud.

In MG-OPTRAM, we keep the original approach (i.e., visual inspection) to determine parameters i_d, s_d, i_w, and s_w. However, we expand the model relying on the fact that STR observations can be affected not only by soil moisture, but also by other variables such as land/canopy dynamics and clouds and shadows. Therefore, we partition the actual STR signals into two parts of soil-moisture-related STR (STR_{sm}) and non-soil-moisture-related STR (STR_{nsm}):

$$\text{STR} = \text{STR}_{sm} + \text{STR}_{nsm} \quad (4.6)$$

Therefore, in the newly proposed MG-OPTRAM, we attempt to use STR_{sm} instead of STR. To that end, we use SMAP as a reference and first find a theoretical STR_{sm} relying on SMAP and OPTRAM simultaneously, yielding:

$$\text{STR}_{sm} = i_d + s_d\ \text{NDVI} + \left(\frac{\theta_{SMAP}}{\theta_s}\right)[i_w - i_d + (s_w - s_d)\text{NDVI}] \quad (4.7)$$

Eq. (4.7) can provide a set of STR_{sm} data during the calibration period, where SMAP data are available. Then, we would need a set of available predictor variables $(x_1, x_2, \dots, x_N)$ to predict STR_{sm} when SMAP is not available. To that end, we rewrite Eq. (4.6) as follows:

$$\text{STR}_{sm} = \text{STR} - \text{STR}_{nsm}(x_1, x_2, \dots, x_N) \quad (4.8)$$

Where STR_{nsm} is a function of predictor variables $x_1, x_2, \ldots, x_N$. Assuming that the temporal changes of STR_{nsm} can be related to the land/canopy dynamics and clouds and shadows, for the sake of simplicity, we use only two available predictors from MODIS data; NDVI and $M = \sin\left[2\pi(t - t_0)/T\right]$:

$$\mathrm{STR}_{sm} = \mathrm{STR} - (c_0 + c_1\mathrm{NDVI} + c_2 M) \tag{4.9}$$

Where t is the time, T is the annual cycle (365 days), and t_0 is a constant matching the phase of M to the SMAP seasonality.

Now using STR_{sm} instead of STR in Eq. (4.5) yields the MG-OPTRAM formulation as:

$$\theta = \theta_s \left[\frac{\mathrm{STR} - (i_d + c_0) - (s_d + c_1)\ \mathrm{NDVI} - c_2 M}{i_w - i_d + (s_w - s_d)\mathrm{NDVI}}\right] \tag{4.10}$$

Note that Eq. (4.10) is reduced to Eq. (4.5) for $c_0 = c_1 = c_2 = 0$. In other words, OPTRAM, Eq. (4.5), is a special case of the MG-OPTRAM, Eq. (4.10). Therefore, we expect that MG-OPTRAM will always perform better than OPTRAM.

3. Materials and Methods

In this chapter, we focused on the Central Valley (CV), California, a region characterized by diverse landcover types. For obtaining landcover information, we utilized the Cropland Data Layer (CDL) dataset, which provides annual land cover classification for the continental United States (Boryan et al., 2011) (see Fig. 4.1). We considered CV as a proper test case for exploring soil moisture variations due to its inclusion of a range of dry areas such as urban landscape to fully saturated regions like rice fields. The following datasets were used in this analysis.

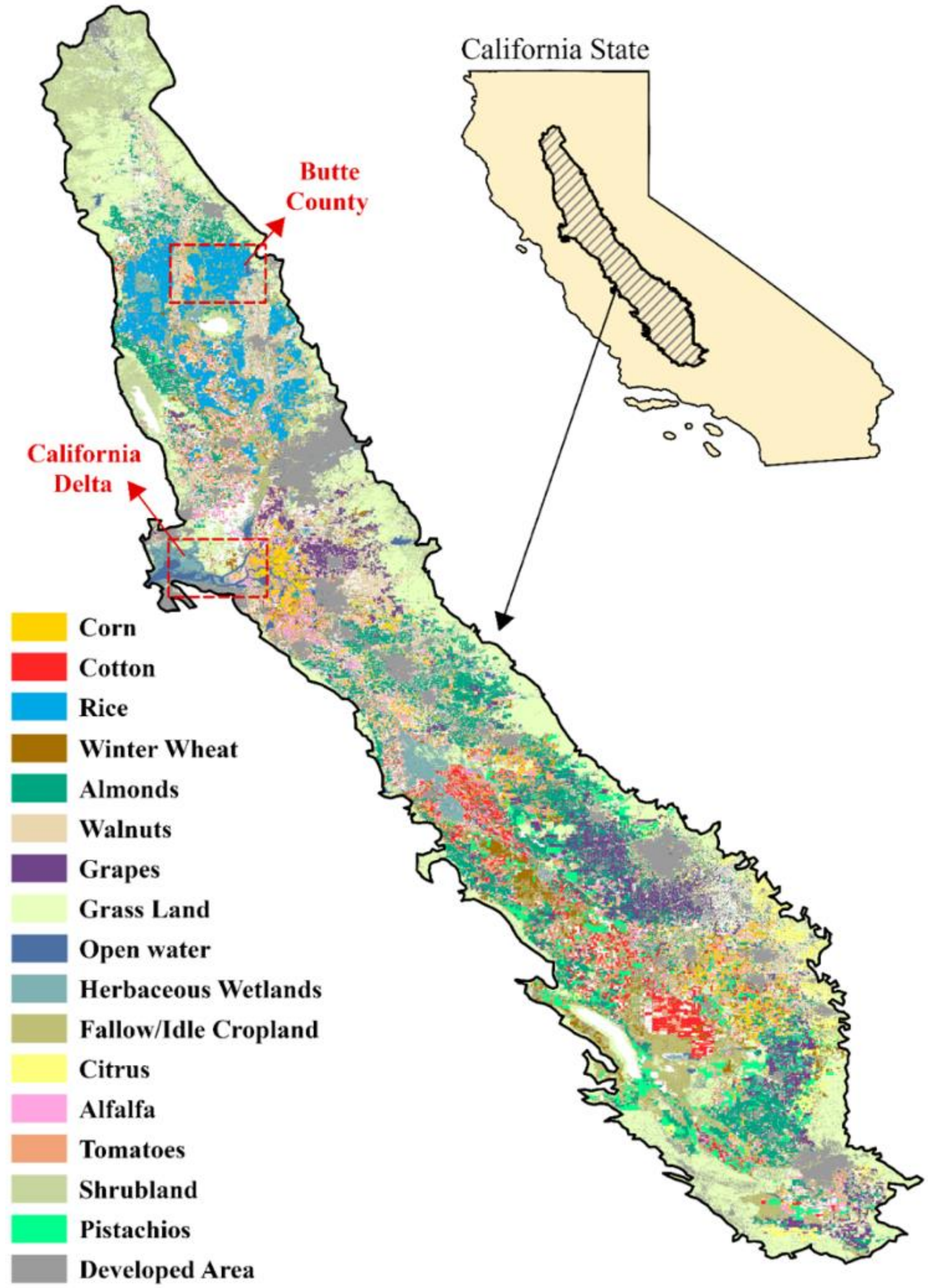

Figure 4.1. Landcover map based on the Cropland Data Layer (CDL) dataset over the Central Valley, California. Red rectangles mark the locations of Butte County and the California Delta, used to compare the spatial resolution of soil moisture maps retrieved from MG-OPTRAM to SMAP.

3.1. SMAP Data

To calibrate the MG-OPTRAM parameters (c_0, c_1, c_2), we used surface soil moisture estimates from the NASA SMAP satellite. Operational since April 2015, SMAP provides soil moisture retrievals every 2-3 days by downscaling vertical polarization brightness temperature to a 9-km grid cell. This dataset is one of the most accurate soil moisture datasets currently available with a root mean square error (RMSE) of less than 0.04 m^3m^{-3} (Entekhabi et al., 2014).

3.2. MODIS Data

For the input variables NDVI and STR, we used the MODIS satellite 8-day composite. This product is atmospherically corrected, and for each pixel, the highest-quality observation from all acquisitions within the 8 days is presented. MODIS has a spatial resolution of 500 m for visible, and shortwave infrared (SWIR) bands (Vermote, 2021). For the calibration process and validation at the SMAP scale, MODIS data were resampled to 9-km resolution. Otherwise, we used MODIS data at its original resolution to map high-resolution soil moisture data. NDVI was calculated using surface reflectance from the red band (band 1, 620 nm) and NIR band (band 2, 841 nm). The SWIR band (band 7, 2105 nm) was used to calculate STR based on Eq. (1.2).

3.3. Sentinel-1 Data

Due to the scarcity of in-situ soil moisture data in California, we also used the S1-DPA soil moisture product to validate the MG-OPTRAM high-resolution soil moisture estimates (Fan et al., 2025). This data product retrieved soil moisture from Sentinel-1 synthetic aperture radar data using a dual-polarization algorithm. This dataset is globally available at 1-km resolution from 2016 to 2022 with an unbiased root mean squared error (ubRMSE) of 0.077 m^3m^{-3}.

3.4. In-situ Data

To validate MG-OPTRAM performance, we used in-situ soil moisture data from the AmeriFlux stations (www.ameriflux.lbl.gov) and the National Oceanic and Atmospheric Administration (NOAA) stations of the National Soil Moisture Network (www.nationalsoilmoisture.com). Due to the sparse soil moisture network across the CV, we used all stations across the state with at least 2 years of data records. To that end, we applied MG-OPTRAM to the individual pixels containing the stations outside the CV.

It is known that SMAP provides estimates of surface soil moisture with a sensing depth of 2-5 cm (Entekhabi et al., 2014). We assumed MG-OPTRAM's sensing depth could be close to that of SMAP. Therefore, we primarily used 5-cm in-situ data to evaluate MG-OPTRAM soil moisture. We used 10-cm data where 5-cm data was not available.

3.5. Data Analyses

We conducted all data analyses using Google Earth Engine (GEE) for acquiring SMAP, MODIS, and other datasets used. We used MODIS data to form the STR-NDVI data cloud to estimate OPTRAM parameters using the visual inspection approach of Sadeghi et al. (2017), yielding one set of parameters (i_d, s_d, i_w, s_w) for the entire CV (see Fig. 4.2). We used soil textural data for mapping θ_s from soil bulk density (Hengl, 2018) available in GEE.

We calibrated the remaining MG-OPTRAM parameters (c_0, c_1, c_2) based on SMAP observations from 2015 to 2019 at 9-km resolutions. To that end, we used SMAP 9-km soil moisture data for the variable θ on the left-hand side of Eq. (4.10), and MODIS-derived 500-m reflectance data, resampled at 9 km, for the variables STR and NDVI on the right-hand side of Eq. (4.10). We used a least-squares regression to fit Eq. (4.10) to these variables to calibrate c_0, c_1, and c_2 for each 9-km pixel over the CV. We constrained the regression to ensure the estimated STR_{sm} in Eq. (4.9) remains within its physical bounds, i.e., between STR_d and STR_w.

Once MG-OPTRAM was calibrated for the entire CV, we used stand-alone MODIS optical data to map soil moisture over the CV using Eq. (4.10) (MG-OPTRAM). We also used Eq. (4.5) (original OPTRAM) to understand to what extent MG-OPTRAM can improve this approach. We validated the obtained soil moisture estimates over the period of 2000-2023 based on in-situ observations. For further comparisons, we used the original SMAP data as well as the S1-DPA dataset (Fan et al., 2025).

4. Results and Discussion

Figure 4.2 presents the NDVI-STR space derived from monthly-averaged MODIS data in the Central Valley from 2015 to 2019. Following Sadeghi et al. (2017), we fitted two lines (dry and wet edges) to the densest part of the data cloud based on a visual inspection. As seen, this analysis led to one set of model parameters ($i_d = 0$, $s_d = 2$, $i_w = 0.1$, $s_w = 12$) for the entire CV. This visual analysis was done by the author and could be obtained differently if done by another person. The user-dependent nature of this approach and its effects on the final OPTRAM results were thoroughly discussed in Sadeghi et al. (2023). We used this set of parameters for both OPTRAM and MG-OPTRAM.

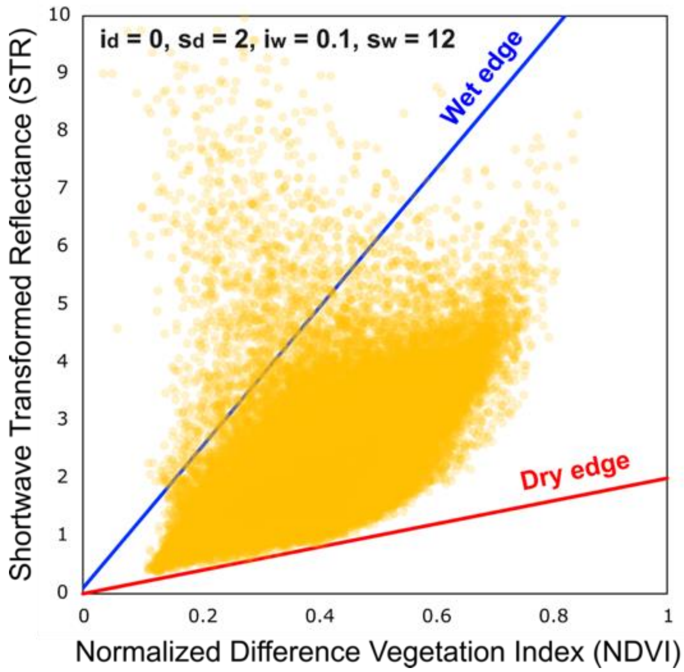

Figure 4.2. The NDVI-STR space derived from monthly averaged MODIS data in the Central Valley, 2015-2019.

We applied MG-OPTRAM in two different ways: (1) for reconstructing SMAP-like data for periods beyond SMAP's lifetime (2015-present), and (2) to downscale SMAP data from 9 km to 500 m spatial resolution. We discuss these two applications separately in the following sections.

4.1. Reconstructing SMAP-like Data using MG-OPTRAM

As a primary test of MG-OPTRAM performance, we compared its soil moisture estimates with original SMAP observations. To examine to what extent Eq. (4.10) could fit well SMAP observations, we mapped the calibration goodness of fit in terms of R^2 in Fig. 4.2 (left). As observed, a relatively high R^2 was obtained for most pixels over the CV with a mean $R^2 = 0.78$. This primarily shows the overall soundness of the MG-OPTRAM formulation, Eq. (4.10), as a physico-emprical model, and its consistency with SMAP satellite observations. Nonetheless, poor correlations are evident in a few pixels, especially near the California Delta. Due to the abundance of surface water in this area, this poor correlation is likely primarily because of SMAP's poor performance due to the so-called "waterbody contamination" (Chaubell et al., 2017; Yang et al, 2021) (see the Delta area in Fig. 4.5 as well).

Figure 4.3 (right) also shows the R^2 map beyond the calibration period (2020-2023), where SMAP data were not used to inform the model parameters. As seen, this map is generally similar to the calibration R^2 map (Fig. 4.3, left) showing relatively high R^2 in most pixels with a mean R^2 = 0.75 over the CV. This generally good agreement between Eq. (4.10) and SMAP indicates the overall validity of the model and its calibrated parameters beyond the calibration period. This result made us confident to extend the MG-OPTRAM for the entire MODIS era and use the calibrated Eq. (4.10) to obtain a long-term soil moisture dataset (2000-present).

To further visualize the temporal correlations between Eq. (4.10) and SMAP, we showed some sample time series in Fig. 4.4 presenting a variety of pixels over the CV. As observed, the newly proposed calibration strategy based on SMAP observations (MG-OPTRAM) could substantially increase the correlation on some occasions compared to the original OPTRAM approach based on Eq. (4.5). In addition, as expected, MG-OPTRAM showed much less bias (in terms of RMSE) than OPTRAM in most pixels. We also see some areas (e.g., Fig. 4.4a), where OPTRAM and MG-OPTRAM show nearly similar performance in terms of R^2 and RMSE. This is where the additional MG-OPTRAM parameters (c_0, c_1, c_2) were found to be negligible during calibration.

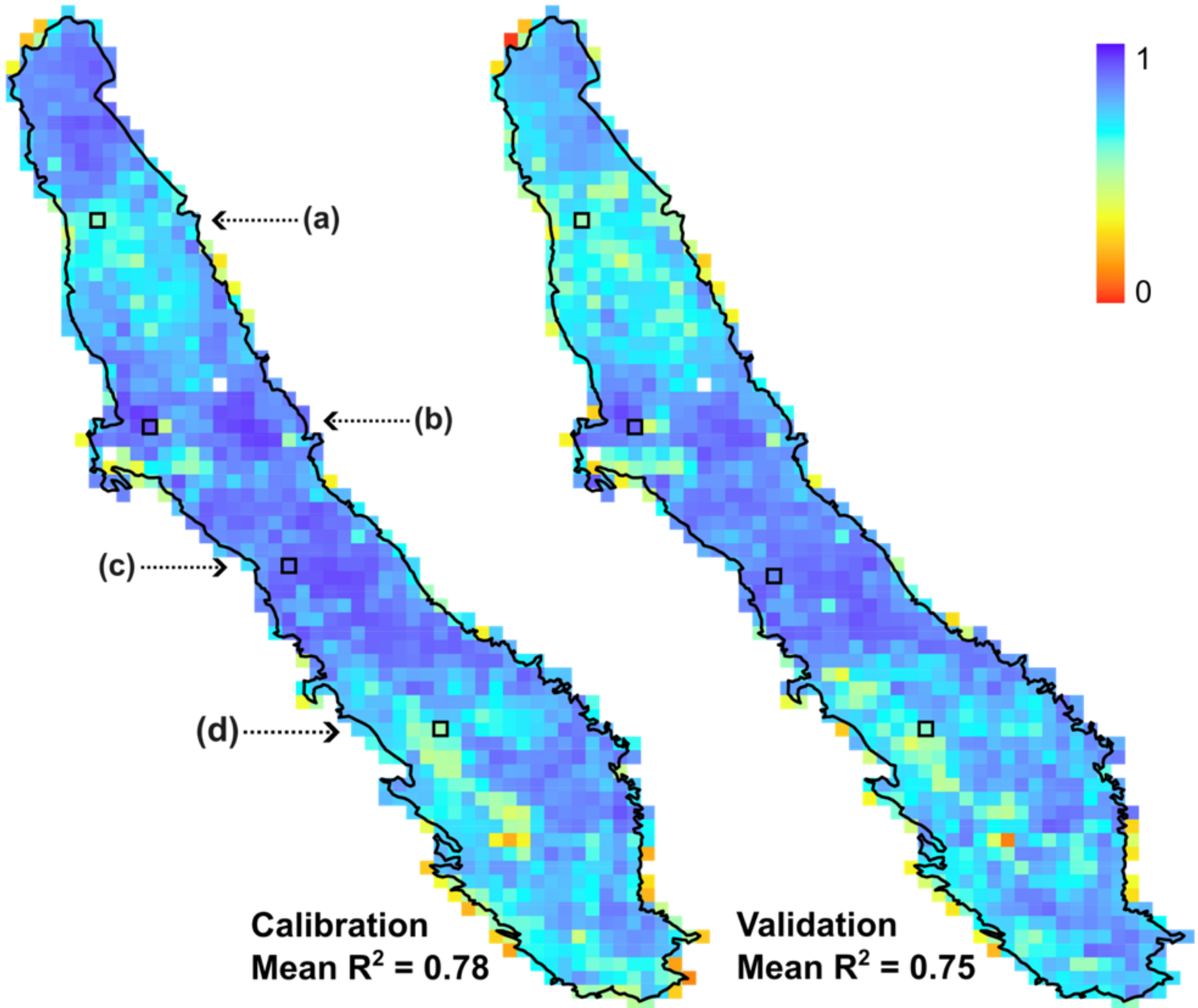

Figure 4.3. The R-squared (R^2) values derived from the calibration (2015-2019) and validation (2020-2023) data over the Central Valley, California. Black rectangles mark the locations of four sample points used to visualize soil moisture estimates during the calibration and validation periods in Figure 4.4.

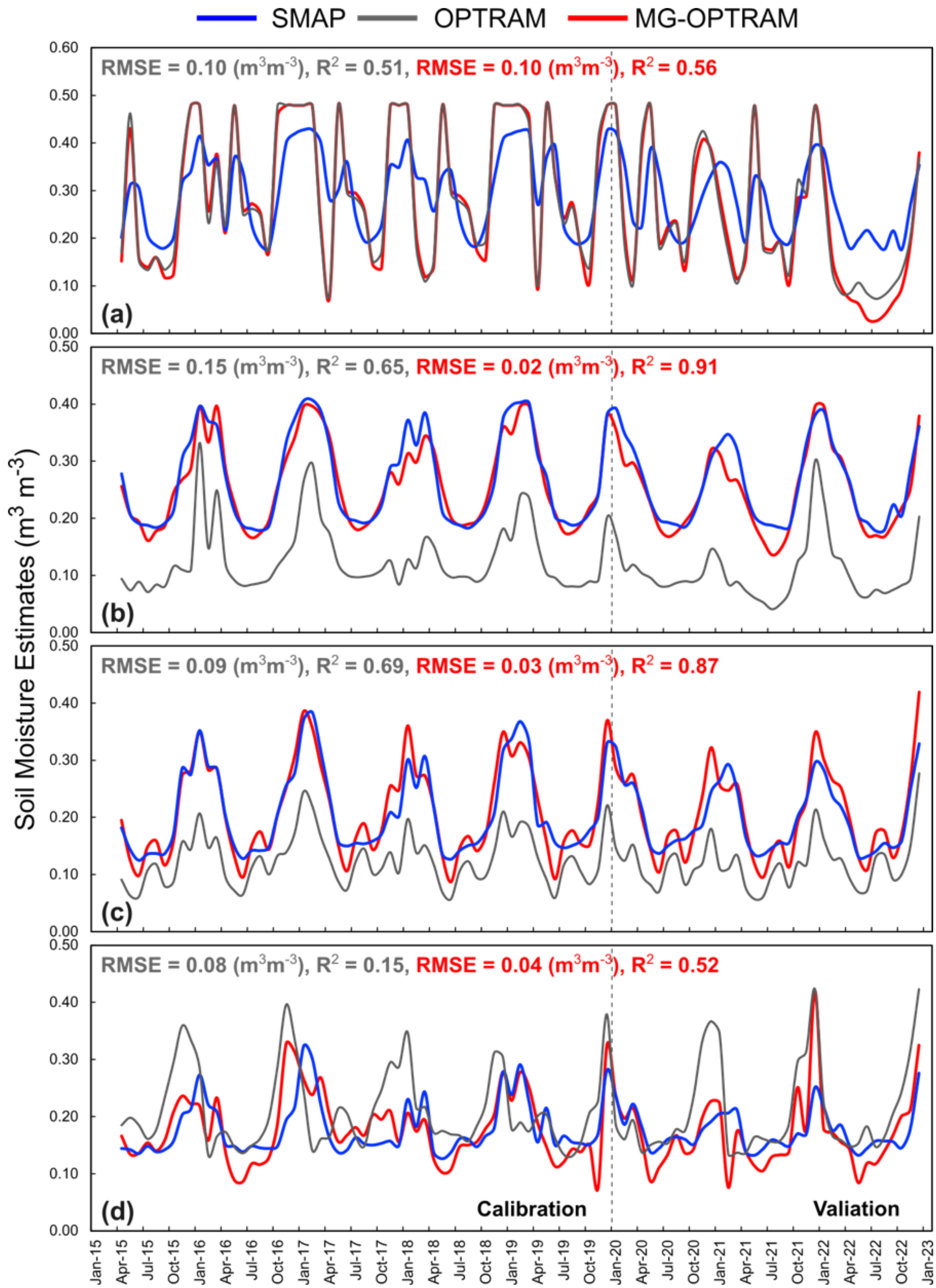

Figure 4.4. Soil moisture estimates by SMAP (reference), OPTRAM and MG-OPTRAM at a 9-km grid cell for the calibration (2015-2019) and validation periods (2020-2022) at four sample points in the Central Valley, California. Sample point locations are indicated in Figure 4.3.

Figures 4.3 and 4.4 showed generally good agreements between SMAP and MG-OPTRAM regarding the temporal changes of soil moisture (i.e., seasonality and inter-annual variabilities). To shed light on their agreements regarding spatial variability, Fig. 4.5 presents some sample maps of monthly-averaged soil moisture over the CV for various seasons in 2020. To better compare these maps, we resampled MG-OPTRAM's 500-m data at the SMAP spatial resolution (9 km). As expected from Fig. 4.3, the seasonal variations (e.g., wet conditions in January and dry conditions in July) are consistent in both datasets. In addition, the spatial distribution of soil moisture is generally similar between the two datasets. For example, the northern CV is generally wetter than the southern CV in both datasets, or the rice fields in Butte, Glenn, Colusa, Sutter and Yuba counties (see Fig. 4.1) are generally wetter than the rest of the CV. The latter is the case in warmer seasons (e.g., July), especially because of the flood irrigation of the rice fields in these seasons.

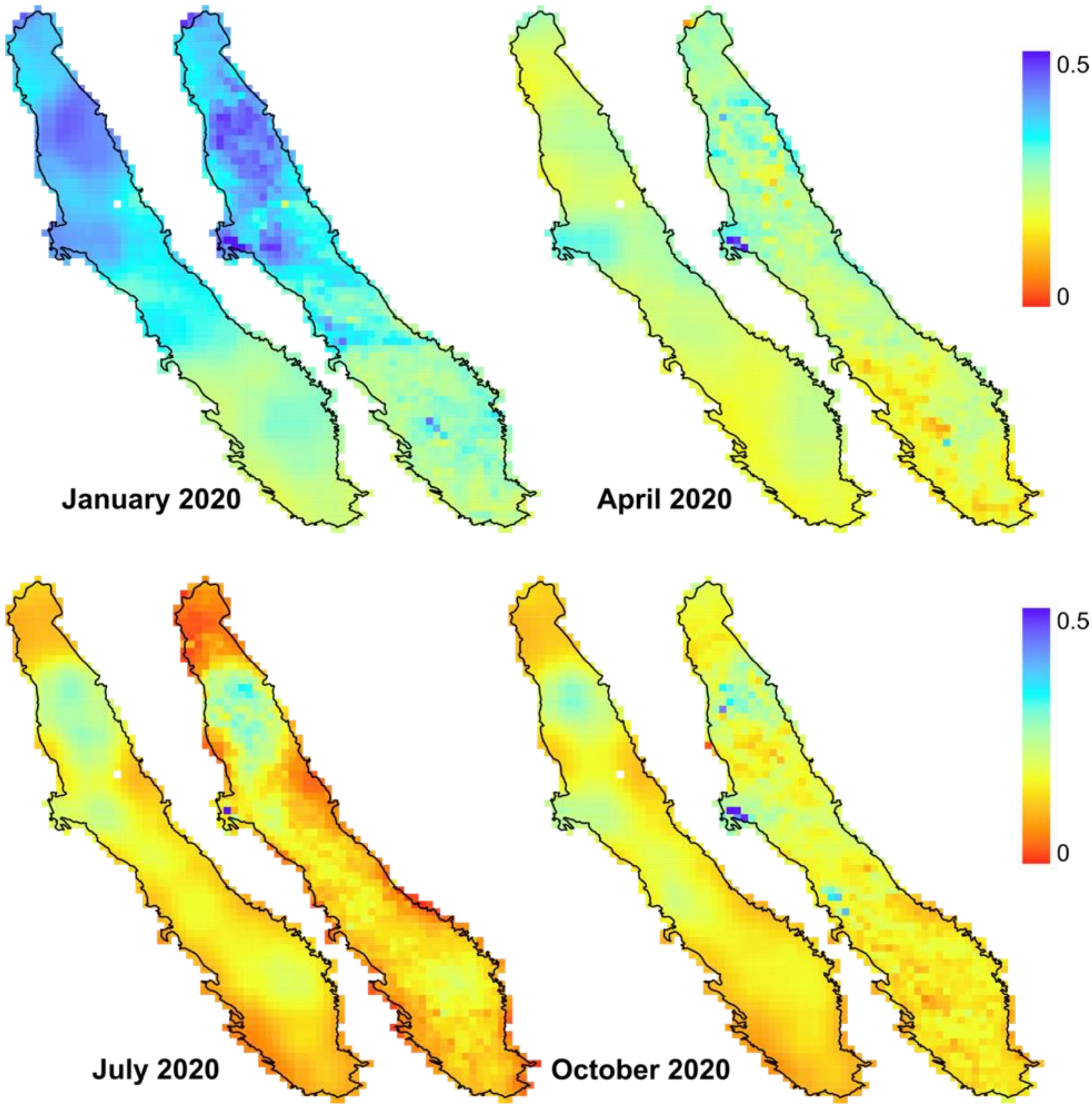

Figure 4.5. The spatial distribution of monthly soil moisture estimates (m^3 m^{-3}) by SMAP as a reference (left), and MG-OPTRAM at 9-km resolution (right), over the Central Valley, California in January, April, July, and October 2020.

To further evaluate the 9-km SMAP-like data reconstructed by MG-OPTRAM, we explored them at multiple in-situ stations across California as presented in Fig. 4.6. As expected from Fig. 4.3, showing generally high correlations between SMAP and MG-OPTRAM, we see generally good agreements between these two datasets in Fig. 4.6. In addition, MG-OPTRAM could successfully extrapolate SMAP from 2000 to 2015 merely based on MODIS optical observations. This overall success is evident by reasonable agreements between MG-OPTRAM and in-situ data from 2000 to 2015 and beyond. This agreement was made on both seasonality and interannual variability of soil moisture. While the former is evident in almost all sites, the latter can be seen in sites like WLS, HLD, LSN, PTV, ROD, TON, and VAR. In most of these sites, the error metrics of MG-OPTRAM are comparable but slightly degraded compared to those of SMAP.

In a few sites, however, MG-OPTRAM showed poor performance compared to in-situ data. Among them, the HBK (shrubland) and BI2 (corn) sites are notable. In HBK, we found that MG-OPTRAM suffers from highly noisy MODIS STR data, which could not be adequately isolated for soil moisture, STR_{sm}, using our newly proposed Eq. (4.9). This could be primarily due to our simplistic linear empirical model, Eq. (4.9), trying to estimate the non-soil-moisture variations of STR only from NDVI and the time of the year. From a physical standpoint (e.g., radiative transfer equation), STR variations in response to soil moisture, surface roughness, and canopy geometry can be much more complex and nonlinear. The same reason could lead to errors in Eq. (4.9) in the BI2 site, where the land surface properties could change more dynamically due to farming practice. In addition, the poor model performance here seems to be partly due to the relatively poor performance of SMAP itself, which was used to calibrate MG-OPTRAM.

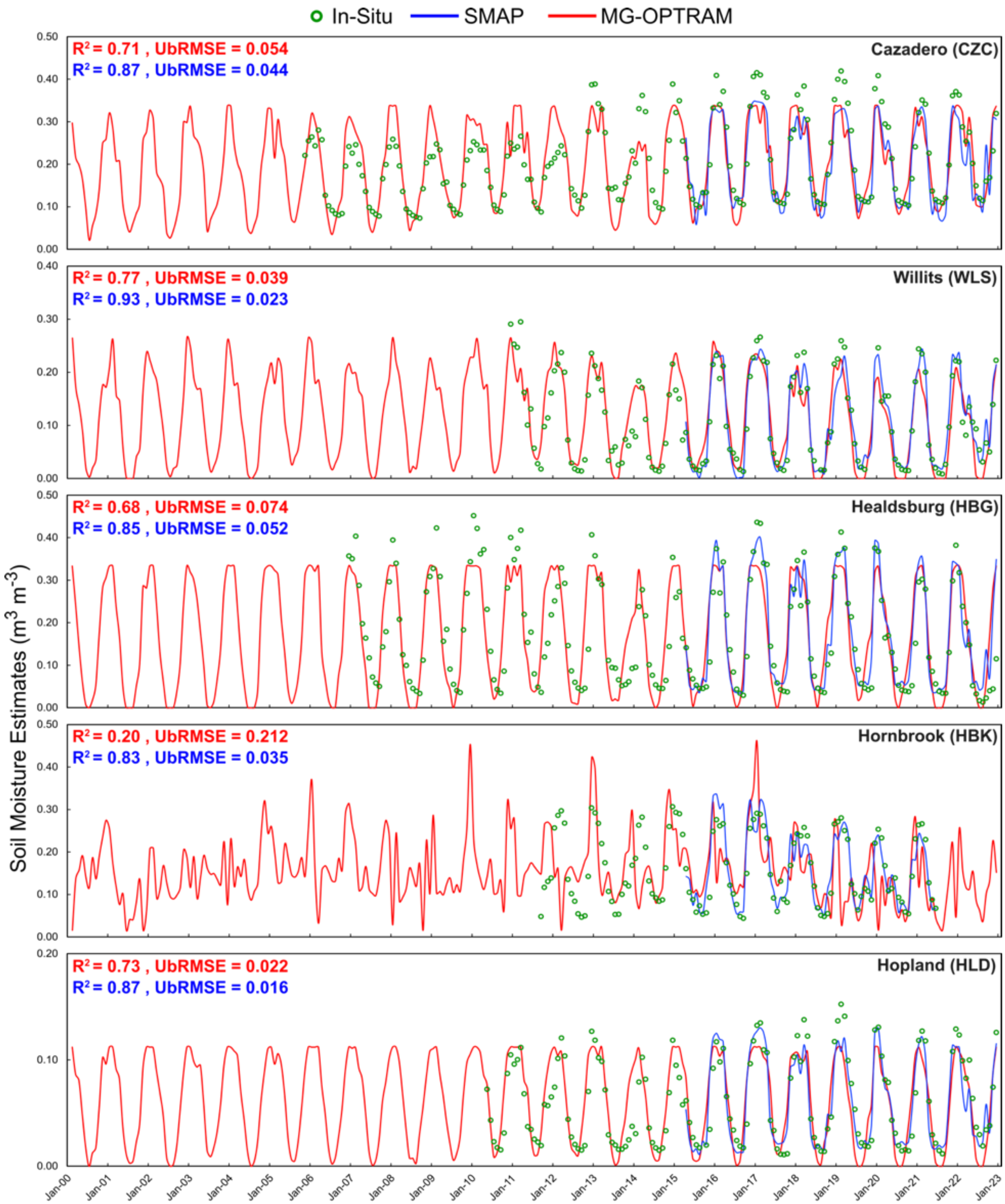

Figure 4.6. Remote sensing estimated soil moisture (SMAP, MG-OPTRAM at 9-km resolution) compared to in-situ soil moisture measurements from the NOAA and AmeriFlux Networks.

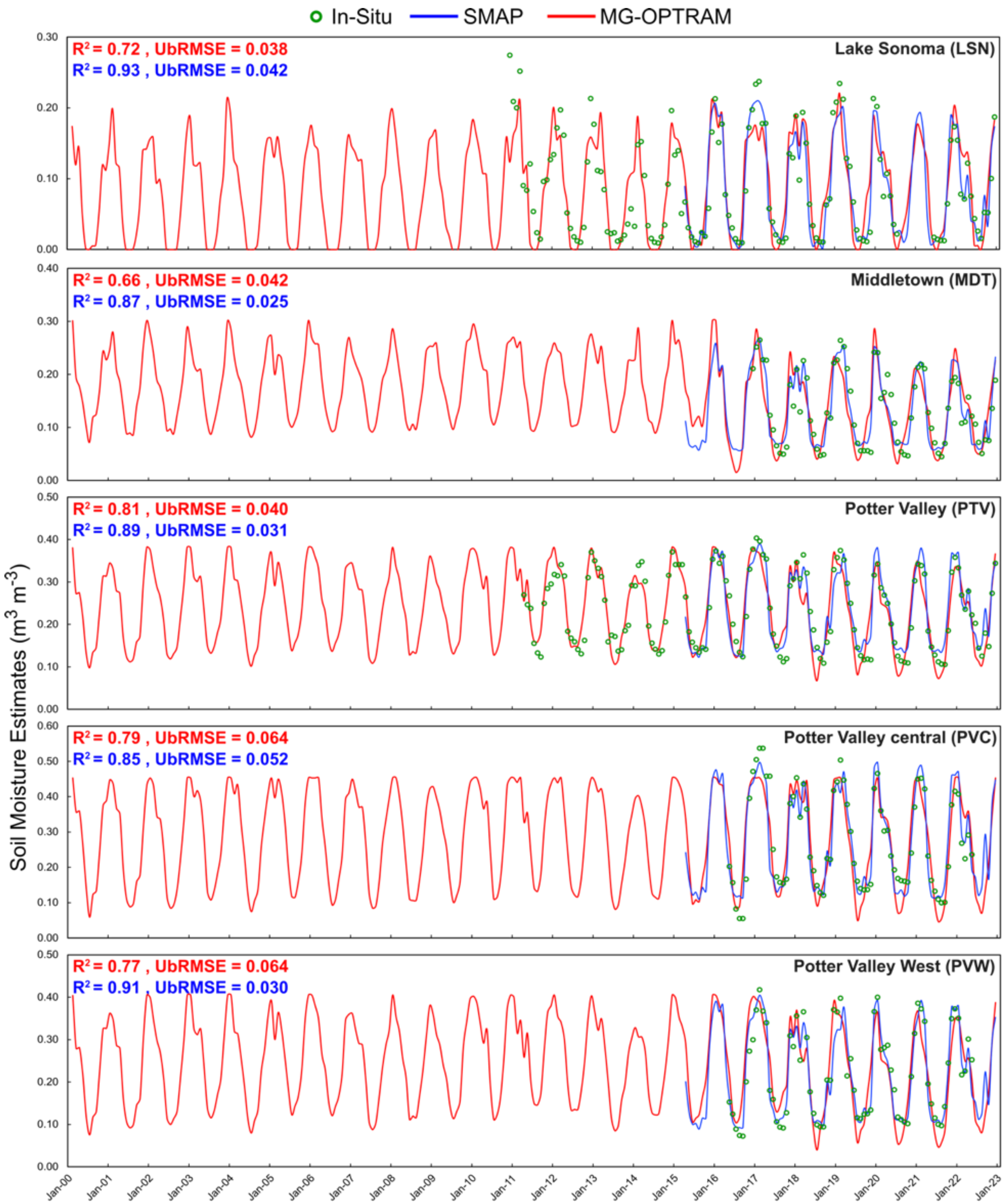

Figure 4.6 (continued). Remote sensing estimated soil moisture (SMAP, MG-OPTRAM at 9-km resolution) compared to in-situ soil moisture measurements from the NOAA and AmeriFlux Networks.

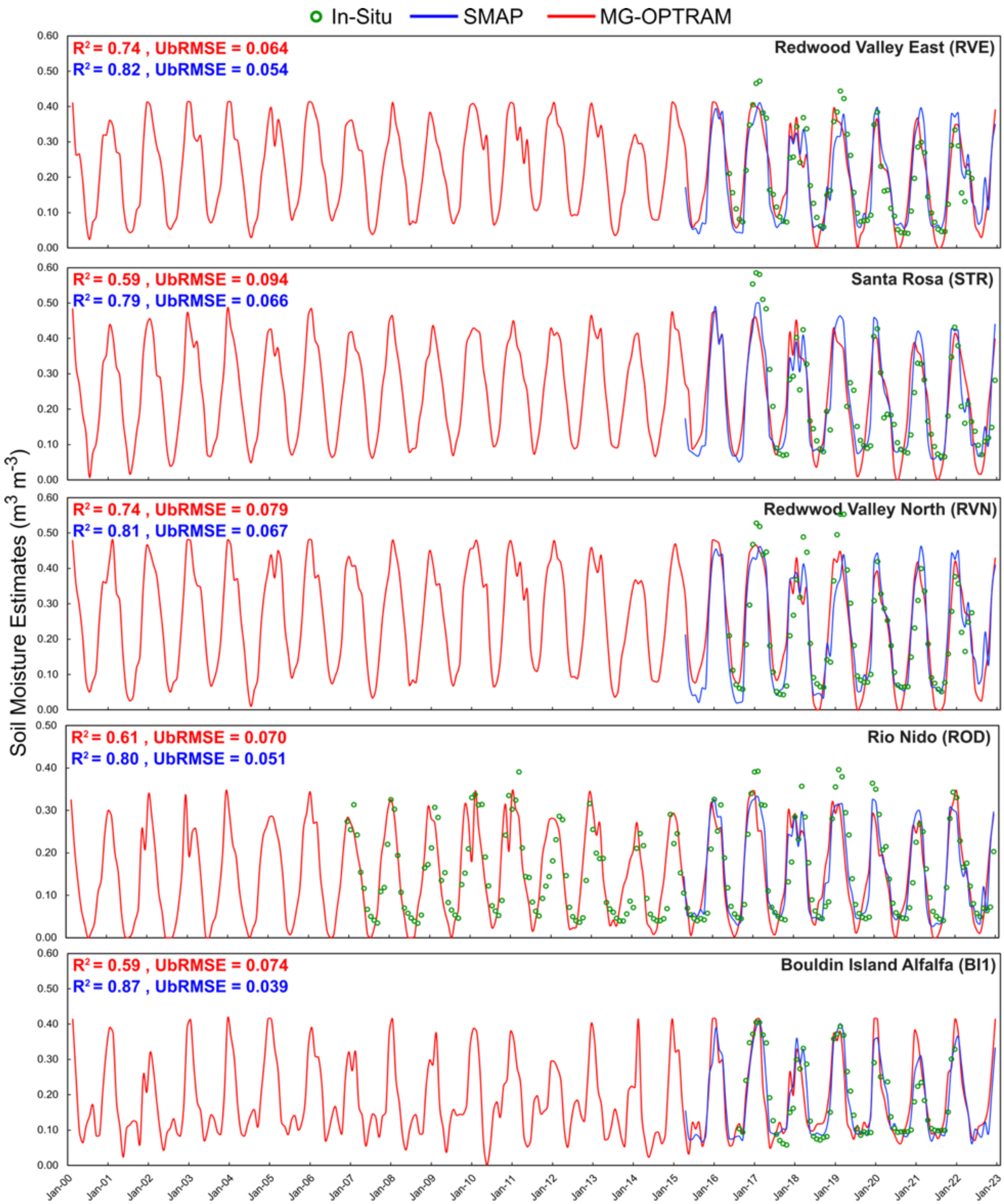

Figure 4.6 (continued). Remote sensing estimated soil moisture (SMAP, MG-OPTRAM at 9-km resolution) compared to in-situ soil moisture measurements from the NOAA and AmeriFlux Networks.

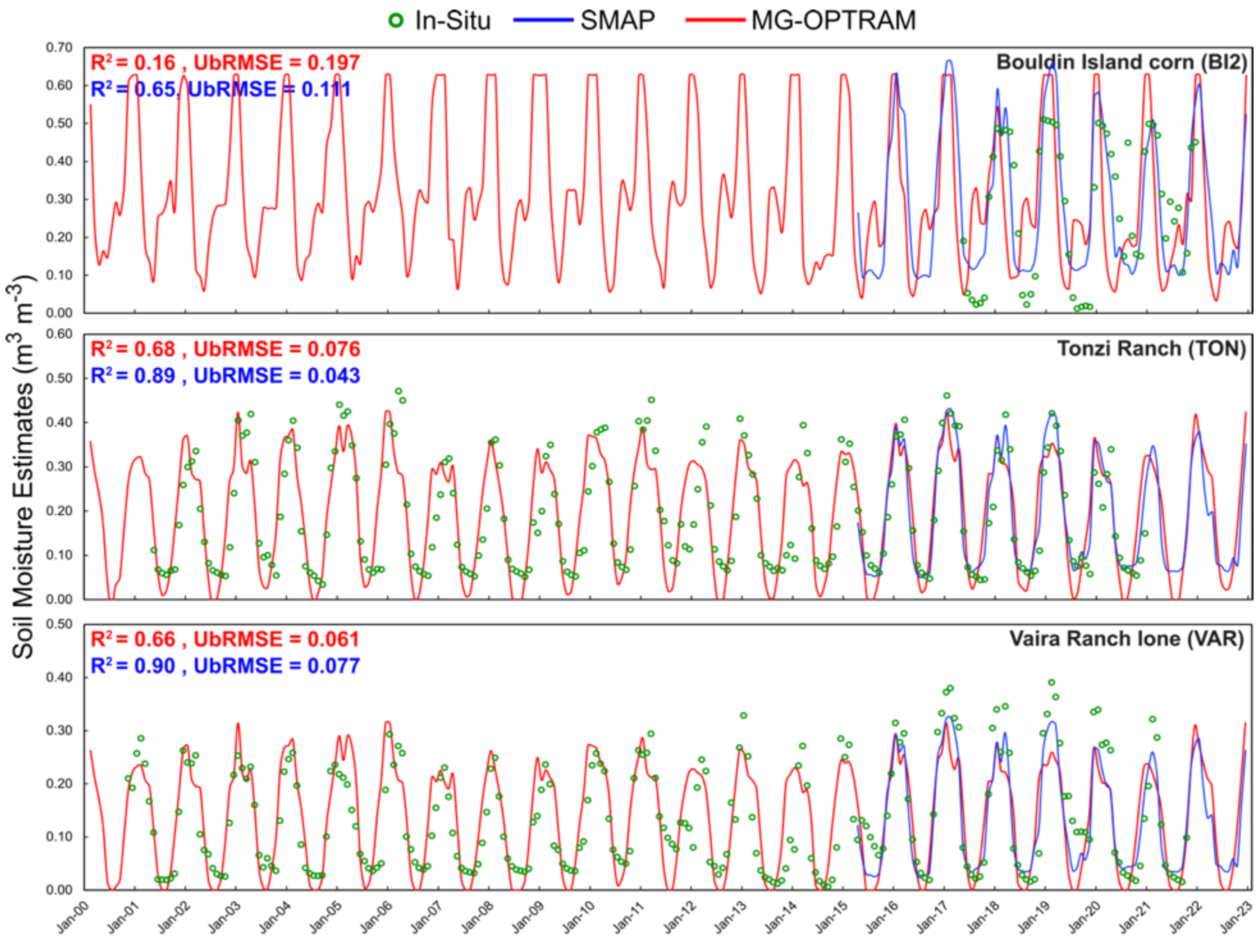

Figure 4.6 (continued). Remote sensing estimated soil moisture (SMAP, MG-OPTRAM at 9-km resolution) compared to in-situ soil moisture measurements from the NOAA and AmeriFlux Networks.

4.2. Downscaling SMAP Data using MG-OPTRAM

So far, we have discussed soil moisture data at the SMAP resolution (9 km). A key advantage of MG-OPTRAM at this scale is its ability to extend SMAP's 9-km data record back to 2000, offering a longer temporal coverage. Since a calibrated MG-OPTRAM relies solely on optical data inputs, it is also capable of generating soil moisture data at the spatial resolution of MODIS. This allows us to produce soil moisture estimates at a 500-m resolution, significantly finer than that of SMAP. In this section, we explore the validity and reliability of these high-resolution datasets.

Figure 4.7 presents some sample high-resolution MG-OPTRAM maps. For comparison, it also shows SMAP 9-km data as well as the S1-DPA 1-km data as reference. As observed, MG-OPTRAM retains the overall patterns of SMAP soil moisture in space and time such as the north-to-south trend and the seasonal lows and highs. In addition, it displays more detailed features, hidden in SMAP, such as river channels, lakes, and flood-irrigated rice fields in warm seasons. Most of these features are also captured by the S1-DPA dataset as another radar-based independent reference. The observed agreements between MG-OPTRAM and S1-DPA in many parts of the valley are another proof of the general validity of the spatial variabilities estimated by MG-OPTRAM.

It is worth noting that S1-DPA contains its errors when compared with in-situ data with an average ubRMSE of 0.077 m^3 m^{-3} as reported by Fan et al. (2025). Additionally, while OPTRAM is a simple model using only optical data to estimate soil moisture, S1-DPA incorporates various datasets besides the radar observations, including vegetation cover, snow cover, soil texture, and surface temperature.

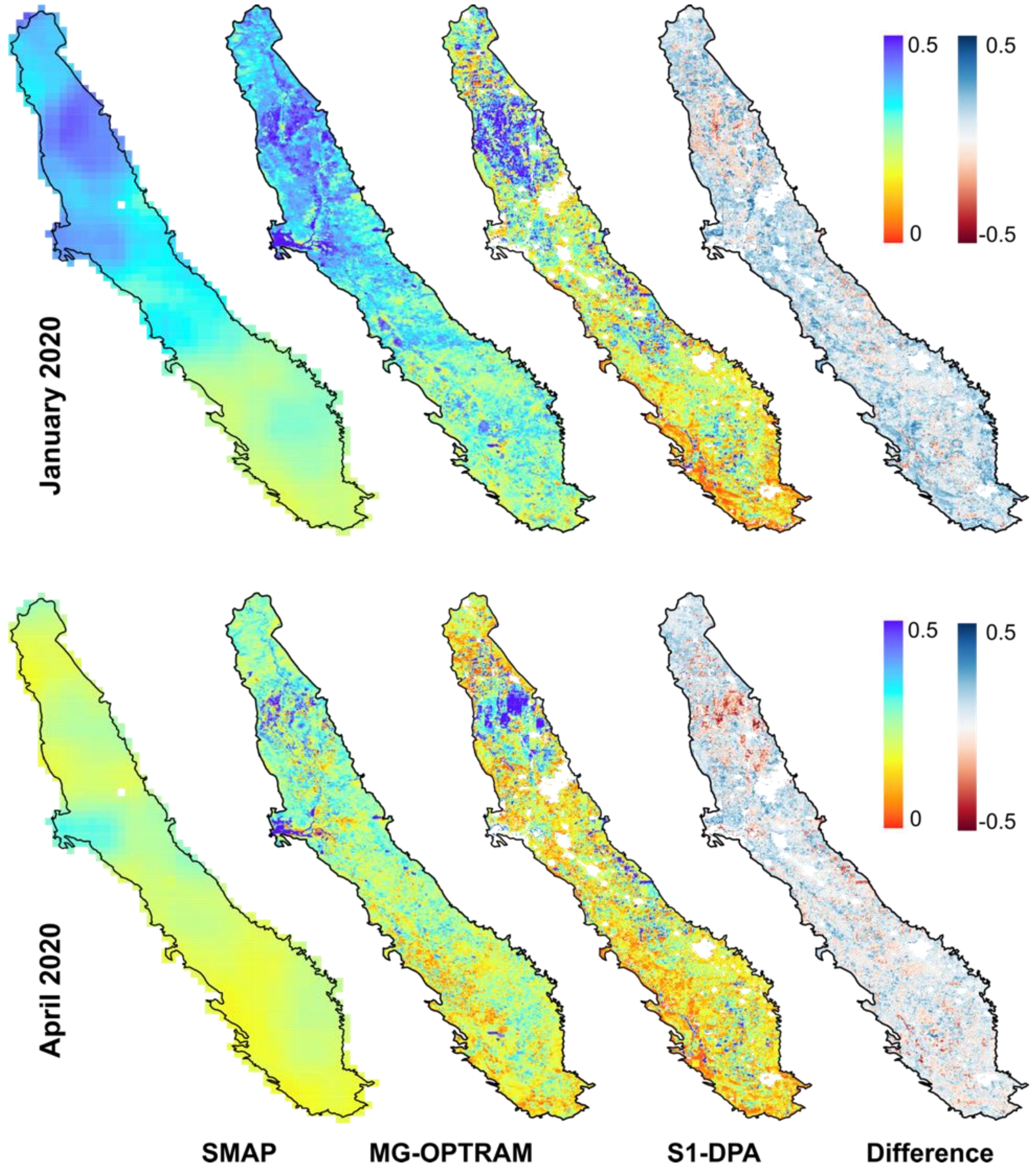

Figure 4.7. The spatial distribution of monthly soil moisture estimates (m^3 m^{-3}) by SMAP data, MG-OPTRAM at 500-m resolution, S1-DPA data at 1-km resolution and the difference in soil moisture estimates between MG-OPTRAM and S1-DPA, over the Central Valley, California in January, April, July, and October 2020.

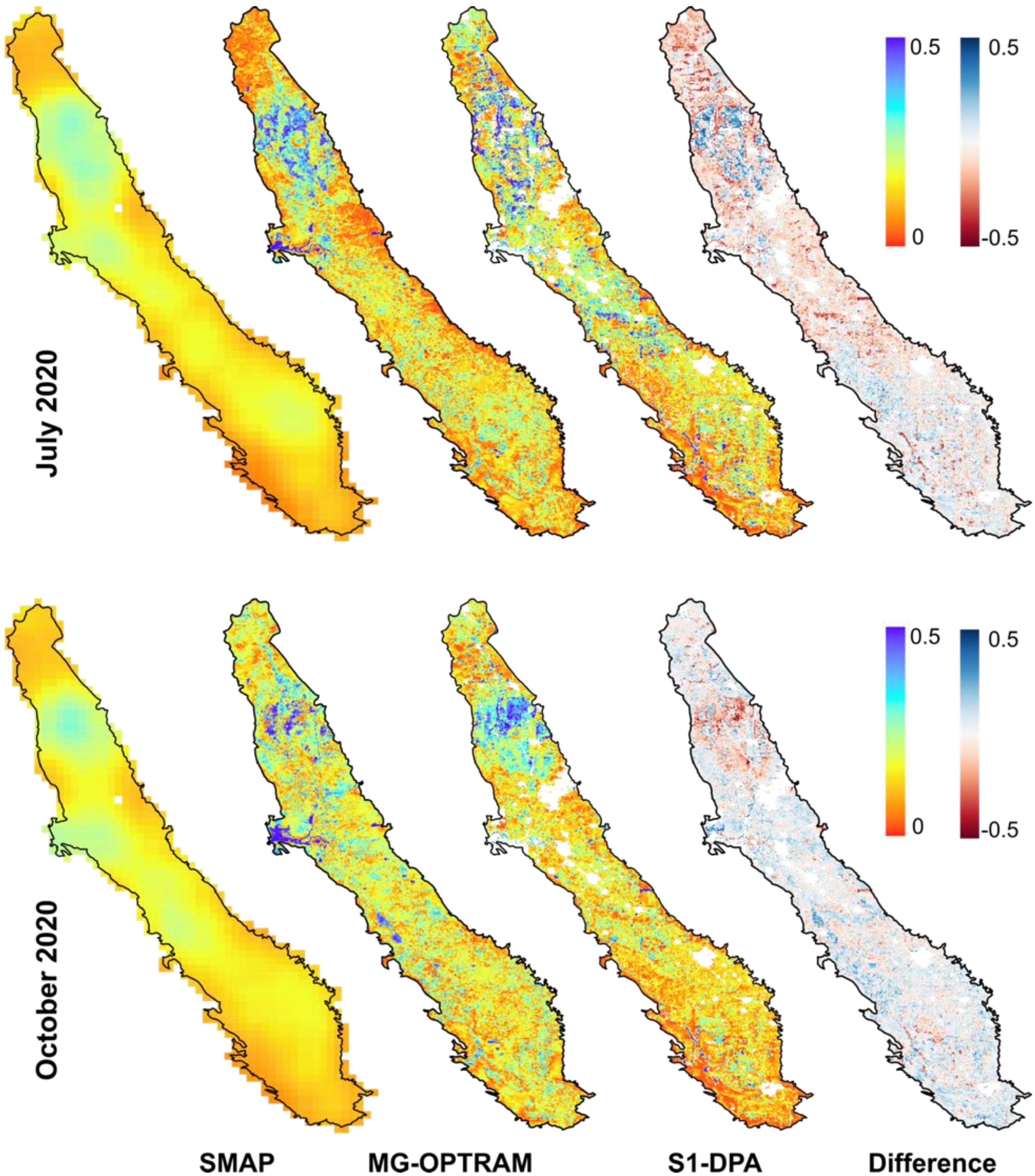

Figure 4.7 (Continued). The spatial distribution of monthly soil moisture estimates ($m^3\ m^{-3}$) by SMAP data, MG-OPTRAM at 500-m resolution, S1-DPA data at 1-km resolution and the difference in soil moisture estimates between MG-OPTRAM and S1-DPA, over the Central Valley, California in January, April, July, and October 2020.

Figure 4.8 zooms in on two regions in the CV, including the rice fields and the Delta. The water-body reference maps (Pekel et al., 2016) further prove that the spatial features captured by MG-OPTRAM are mostly representative of reality. MG-OPTRAM also shows good agreements with the true color image and landcover map capturing the landcover boundaries. In addition, this figure discloses the SMAP's true resolution (~ 36 km) which is well coarser than its sampling resolution (9 km). Therefore, MG-OPTRAM promises to close a large spatial gap in SMAP data.

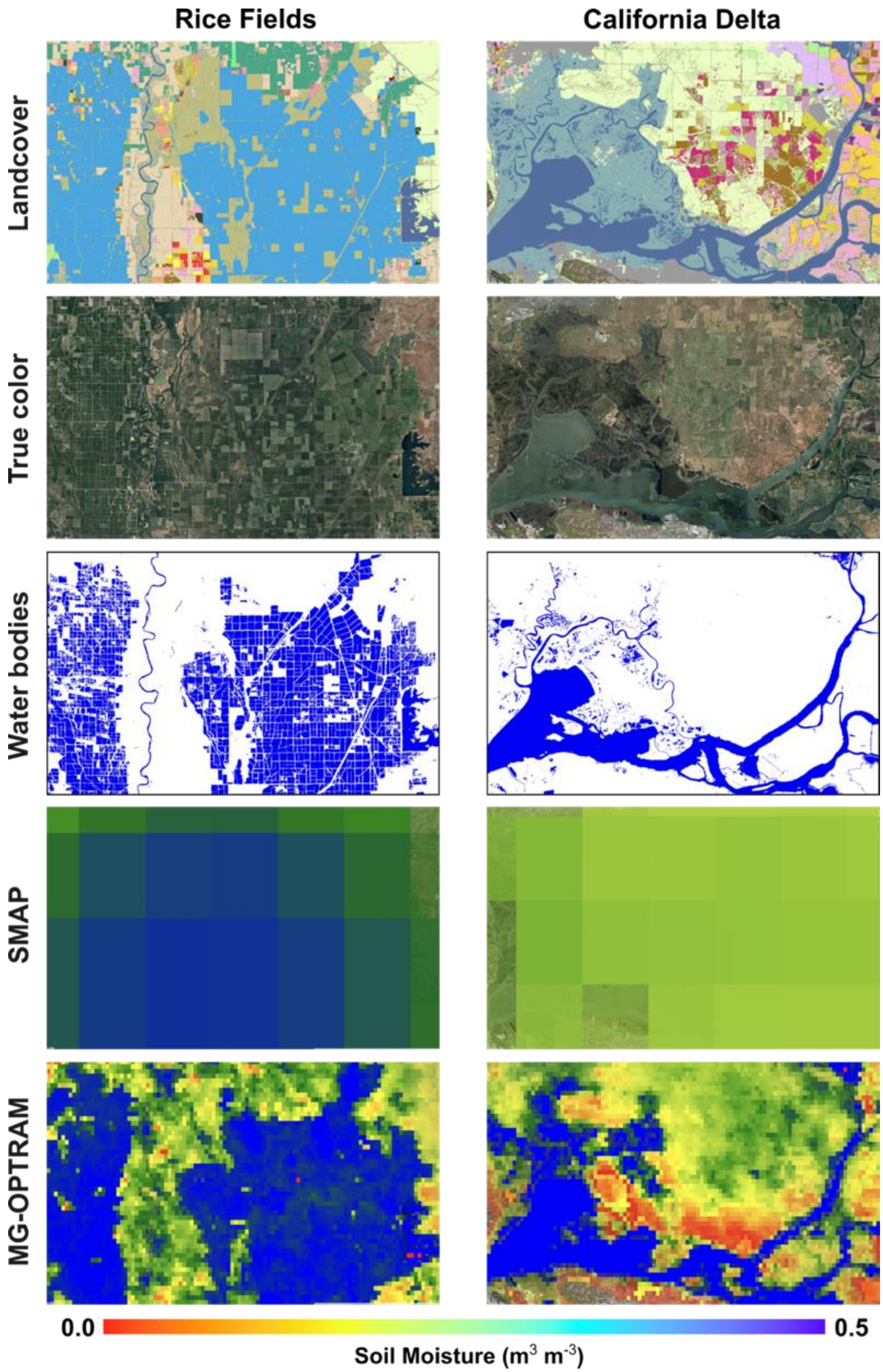

Figure 4.8. Landcover image (CDL), True-color image, surface water image (JRC), SMAP and MG-OPTRAM retrievals of surface soil moisture at 500-m resolution over the rice fields of Butte and Glenn counties and the California Delta (May 2020).

We also examined to what extent the high-resolution MG-OPTRAM is valid for the temporal dynamics of soil moisture in the CV and beyond. To that end, Fig. 4.9 compares soil moisture estimates by OPTRAM and MG-OPTRAM with in-situ observations for various stations of the NOAA and AmeriFlux networks. This figure clearly indicates that MG-OPTRAM, Eq. (4.10), outperforms OPTRAM, Eq. (4.5), in all sites. This is because OPTRAM is a special case of MG-OPTRAM, and we would not expect OPTRAM to outperform MG-OPTRAM. In most sites, the difference between these two models is significant reflecting the value of the new modifications of OPTRAM as well as the incorporation of SMAP to inform the new model inputs.

Despite the higher performance of MG-OPTRAM than OPTRAM, the error metrics indicate that 500-m MG-OPTRAM data shows more deviations from in-situ data compared to those of 9-km data. This indicates that the downscaling process brought some more uncertainties into the MG-OPTRAM in terms of the temporal changes. These uncertainties can be potentially explained first by the fact that MG-OPTRAM parameters were calibrated at the 9-km scale, and the same parameters were used at the 500-m scale. The assumption that the fitting parameters c_0, c_1, and c_2 are invariant within each 9-km pixel could be violated due to strong sub-pixel heterogeneities occurring in reality. Another main source of these uncertainties could be the more complex dynamics of the light reflection processes at higher resolutions, leading to more errors of our simplistic linear empirical model in Eq. (4.9) to capture the soil-moisture-related changes of STR over time.

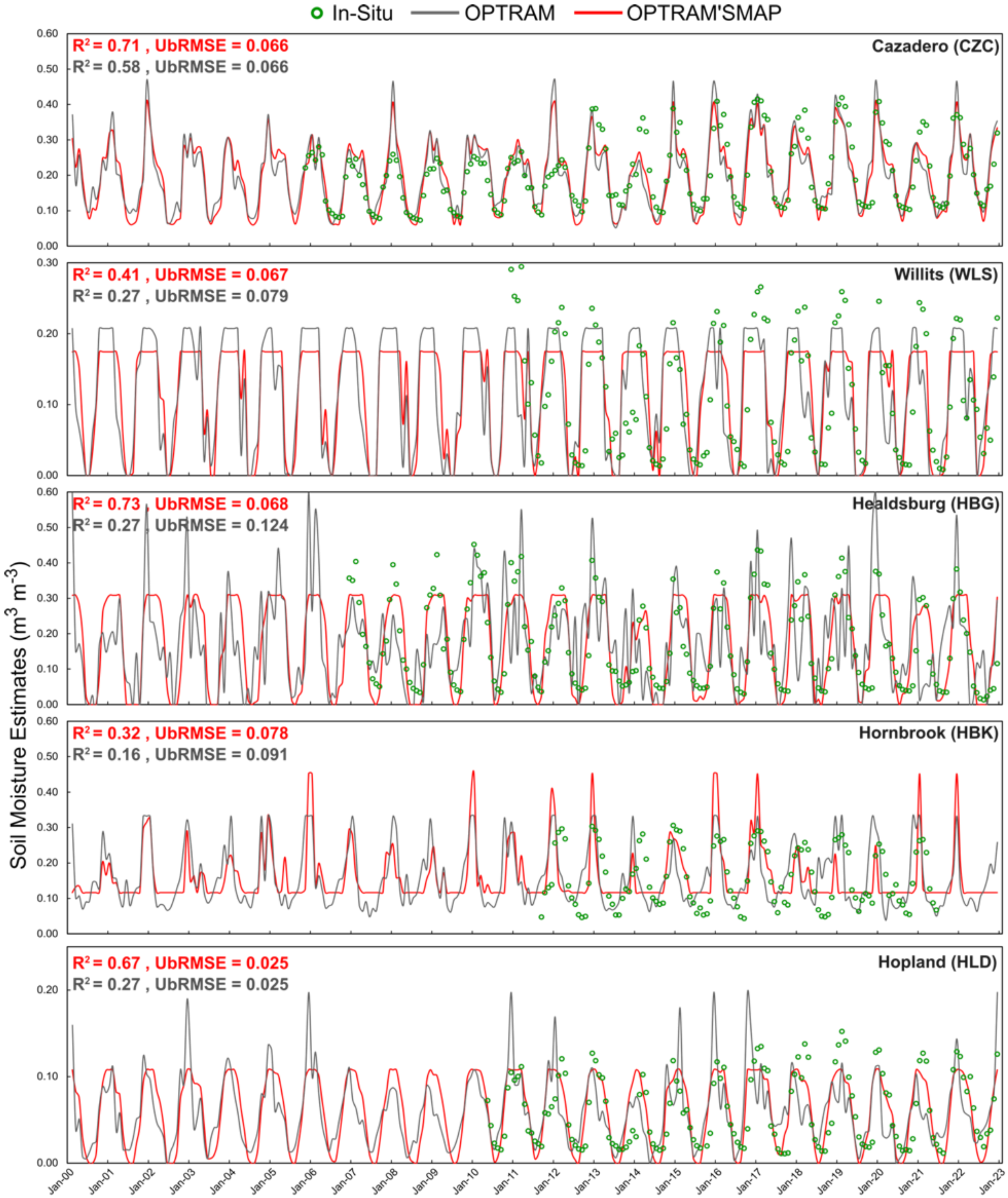

Figure 4.9. Remote sensing estimated soil moisture (OPTRAM, MG-OPTRAM at 500-m resolution) compared to in-situ soil moisture measurements from the NOAA and AmeriFlux Networks.

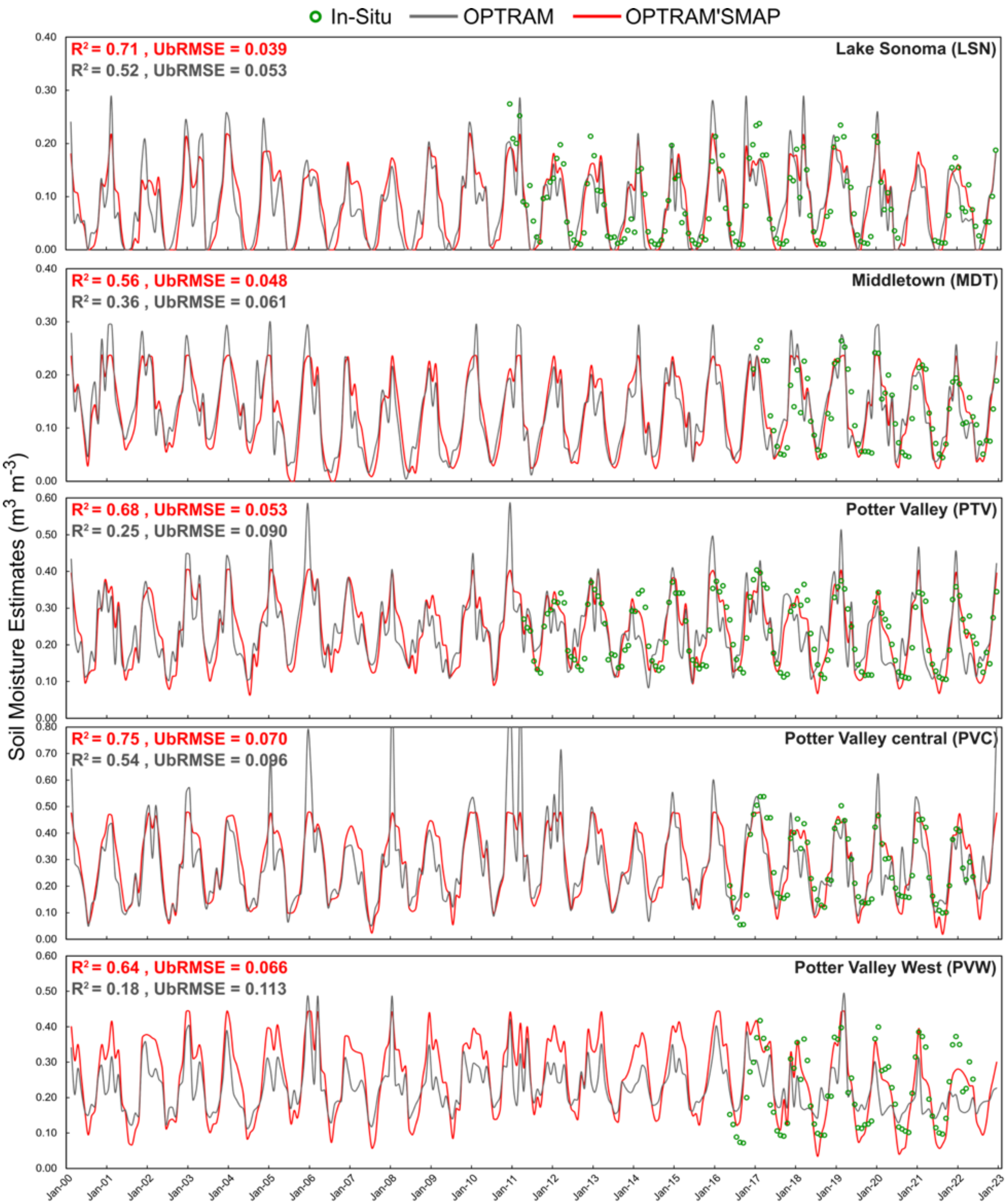

Figure 4.10 (Continued). Remote sensing estimated soil moisture (OPTRAM, MG-OPTRAM at 500-m resolution) compared to in-situ soil moisture measurements from the NOAA and AmeriFlux Networks.

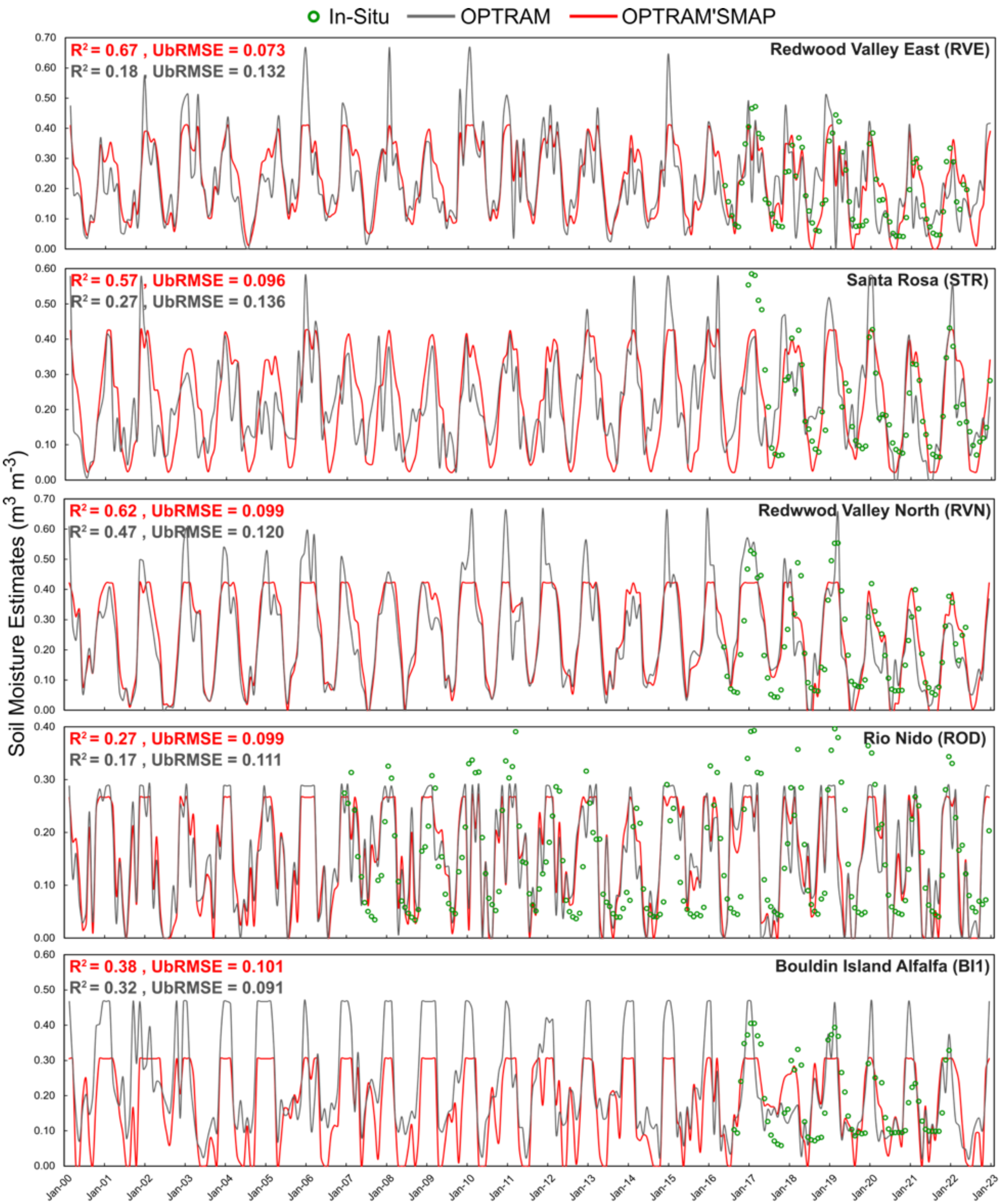

Figure 4.11 (Continued). Remote sensing estimated soil moisture (OPTRAM, MG-OPTRAM at 500-m resolution) compared to in-situ soil moisture measurements from the NOAA and AmeriFlux Networks.

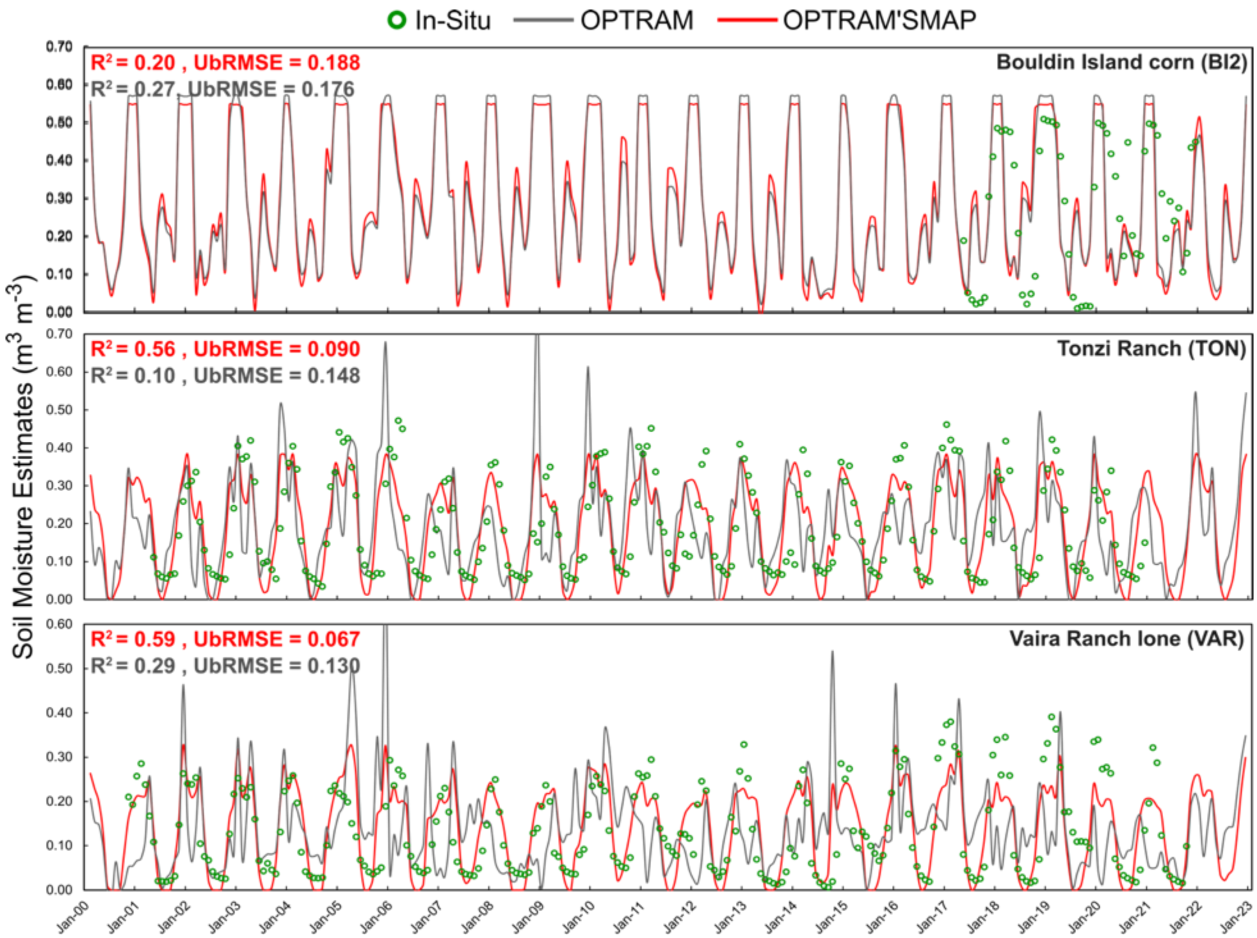

Figure 4.12 (Continued). Remote sensing estimated soil moisture (OPTRAM, MG-OPTRAM at 500-m resolution) compared to in-situ soil moisture measurements from the NOAA and AmeriFlux Networks.

5. Conclusions

This chapter addressed the third objective of this dissertation by developing the Microwave-Guided OPTRAM (MG-OPTRAM) to enhance the Optical TRApezoid Model (OPTRAM) for estimating soil moisture from optical satellite data (STR and NDVI). MG-OPTRAM introduces two key advancements: (1) it uses the soil-moisture-related component of STR instead of total STR to better isolate the soil moisture signal, and (2) it incorporates SMAP observations to calibrate newly introduced model parameters at the pixel level. As a result, MG-OPTRAM enables both (1) the reconstruction of SMAP-like soil moisture data over a longer period (2000–present) than the SMAP mission itself (2015–present), and (2) the downscaling of SMAP data to a finer 500-m resolution using MODIS observations.

The SMAP-like soil moisture estimates from MG-OPTRAM at 9-km resolution showed promising agreement with both SMAP and in-situ data. However, the downscaled 500-m products exhibited higher uncertainties in some cases. These discrepancies highlight the model's current limitations in capturing the complex interactions between soil moisture and surface reflectance at finer spatial scales. Consequently, the coarser-resolution MG-OPTRAM estimates appear to be more robust than their high-resolution counterparts.

Further research is needed to advance the OPTRAM framework. In particular, it is essential to better understand how soil moisture and other environmental variables influence STR to separate moisture-induced changes from other sources of variability. We believe that developing more physically realistic models than the simplified Eq. (4.9) proposed in this study could lead to more accurate and reliable versions of OPTRAM, especially at high spatial resolutions.

Chapter 5 - Conclusion and Recommendations

Soil moisture is a critical environmental variable influencing water, carbon, and energy dynamics at the surface-atmosphere interface (Robinson et al., 2008; De Queiroz et al., 2020). Advances in satellite remote sensing have enabled consistent and spatially distributed soil moisture estimations over large areas, addressing limitations of traditional techniques such as the gravimetric method (Ahmed et al., 2011; Huete, 2004).

Remote sensing approaches for soil moisture estimation utilize various parts of the electromagnetic spectrum, including microwave backscatter (Njoku & Entekhabi, 1996), thermal infrared emission (Hassan-Esfahani et al., 2015) and soil optical reflectance (Tian & Philpot, 2015; Babaeian et al., 2016; Sadeghi et al., 2017). Each method presents unique advantages and limitations, depending on the environmental setting and intended application (Zhang & Zhou, 2016; L. Wang & Qu, 2009).

Microwave-based approaches offer reliable estimates but their coarse spatial resolution (25 to 40 km), limits their ability in small-scale agricultural or hydrological applications. Thermal methods, while physically robust, require a computationally demanding process of individual parameterization/calibration for each observation date (Sadeghi et al., 2017; Mallick et al., 2009), and are restricted to satellites with thermal bands. It excludes platforms like Sentinel-2 with high spatiotemporal resolution and multiple spectral bands but lacking a thermal band.

To overcome these limitations, the Optical Trapezoid Model (OPTRAM) is proposed as a physically based model that estimates surface soil moisture using optical satellite data. OPTRAM relies on a recently established physical relationship between soil moisture and shortwave infrared transformed reflectance (STR). Unlike methods relying on Land Surface Temperature (LST), OPTRAM uses STR, which is influenced solely by surface properties and not by the ambient atmospheric conditions (Sadeghi et al., 2017). This makes OPTRAM suitable for application across a wide range of optical satellites and requires only a one-time calibration for a given location.

OPTRAM assumes a linear correlation between soil and vegetation water contents and anticipates that the Normalized Difference Vegetation Index (NDVI) and STR would form a trapezoid data cloud, with drier pixels located at a lower position and wetter pixels located at a higher position within this data cloud. By analyzing the densest part of the cloud, OPTRAM fits two lines, referred to as the dry and wet edges, and assigns soil moisture values to each pixel based on its proximity to these edges (Sadeghi et al., 2015) (see Fig. 1.2).

Despite its strengths, OPTRAM faces challenges in parameter calibration, particularly in defining the wet edge in areas with high moisture content and in applying a single set of parameters across heterogeneous landscapes. This dissertation addressed these limitations by proposing and evaluating three methodological advancements designed to improve the accuracy, and consistency of OPTRAM-derived soil moisture estimates.

In Chapter 1, we reviewed remote sensing approaches for near-surface soil moisture estimation, comparing their respective advantages and drawbacks. Among them, optical reflectance methods and specifically OPTRAM emerged as a promising alternative due to their high spatial resolution, satellite versatility, and single-time parameterization. We also defined the theoretical background of OPTRAM model and discussed its limitations.

In Chapter 2, we addressed the first limitation of OPTRAM: the challenge of determining wet edge parameters in wet regions, where the upper portion of the STR data cloud is scattered due to the presence of oversaturated pixels and water bodies. Users often interpret the densest part of the data cloud differently, leading to inconsistencies in wet edge parameterization and consequently, variability in the final soil moisture estimates. To tackle this issue, we developed a new OPTRAM variant which accounts for oversaturation and is capable of mapping soil moisture, oversaturated pixels and water bodies and evaluating its potential in reducing sensitivity to wet edge uncertainties and minimizing user dependency in OPTRAM-derived soil moisture estimates.

Unlike the original OPTRAM, referred to as OPTRAM-1, which filters out water bodies and forces moisture content to the saturated point, the new OPTRAM variant, OPTRAM-2, allows the model outputs to exceed soil porosity, in cases where there is a pond of water on the soil surface. In such scenarios, the model output represents not only the moisture content in the surface soil layer, but also the optically detectable component of the surface water on top of the soil, as illustrated in Figure 2.1. To assess user dependency, we designed an experiment simulating four scenarios, each has distinct wet edge parameters and generates soil moisture maps using both OPTRAM-1 and OPTRAM-2.

To evaluate the proposed method, we applied this approach to Landsat 8 imagery across the Central Valley (CV), California. The results showed the limited ability of OPTRAM-1 to map water bodies and oversaturated pixels even with minor adjustments to the model formulation by retaining pixels with negative NDVI values, as confirmed through comparison with a reference surface water map. In contrast, in all the scenarios that we employed OPTRAM-2, we were able to reasonably capture oversaturated pixels and permanent water bodies. Moreover, soil moisture estimates generated by different wet edge scenarios using OPTRAM-2 showed stronger and more consistent linear correlations, indicating the new variant is less sensitive to variations in wet edge parameterization than OPTRAM-1.

In Chapter 3, we addressed another limitation of OPTRAM, its reliance on a single set of parameters across heterogeneous landscapes. This regional calibration approach introduces bias, often reflecting the soil moisture characteristics of the predominant landcover type that forms the majority of the NDVI-STR data cloud. To overcome this limitation, we developed a landcover-specific calibrated OPTRAM (OPTRAM-LS) that incorporates landcover information into OPTRAM parametrization. We then compared its performance to a region-wide calibrated OPTRAM (OPTRAM-CV) for generating high spatial resolution soil moisture maps.

While OPTRAM-CV applies a single set of parameters across the entire study area, OPTRAM-LS calibrates parameters separately for different landcover types, accounting for their unique spectral reflectance characteristics, and corresponding STR and NDVI values. We tested this approach using Sentinel-2 surface reflectance data to map soil moisture across the Central Valley (CV), California. Landcover information was obtained from the Cropland Data Layer (CDL) dataset. To evaluate model performance, we used in situ soil moisture data from the AmeriFlux and NOAA networks. Given the limited availability of in-situ data observations in California, we also used the SMAP- HydroBlocks (SMAP-HB) dataset, a well-validated high-resolution soil moisture dataset, for further validation.

The results showed that OPTRAM-LS could significantly improve soil moisture estimation accuracy compared to OPTRAM-CV by reducing bias and lowering the RMSE. Furthermore, OPTRAM-LS shows higher correlation (in terms of R^2) with both SMAP-HB and in-situ observations, in the majority of in-situ sites, confirming the advantage of land cover-specific calibration. There were some in-situ stations in which OPTRAM-CV calibration yielded slightly better performance. These mixed results suggest that although land cover-specific calibration is an important step forward, it does not fully account for the spatial heterogeneity within individual land cover types. This highlights the potential value of more localized calibration strategies, including sub-land cover or pixel-level approaches, for further improvement.

Another major finding of this chapter highlights the importance of using additional datasets, such as microwave observations from SMAP, in OPTRAM framework to not only calibrate but also to isolate soil moisture signals from confounding variables in STR reflectance. These findings form the final chapter of this dissertation.

In Chapter 4, we focused on integrating microwave and optical observations to develop a Microwave-Guided OPTRAM (MG-OPTRAM) framework, aiming to enhance the accuracy of OPTRAM-derived soil moisture estimates. This approach builds on the fact that STR observations are affected not only by soil moisture, but also by other variables such as land/canopy dynamics and clouds and shadows. MG-OPTRAM addresses this by isolating the soil-moisture-related component of STR, thereby reducing noise from unrelated surface and atmospheric conditions.

The model incorporates SMAP observations as microwave data for calibrating newly introduced model parameters at the SMAP pixel level (9 km) over 2015-2019 and uses MODIS data for NDVI and STR inputs. We validated MG-OPTRAM against SMAP over 2019-2021 and after confirming that the model estimates soil moisture accurately, we applied MG-OPTRAM in two different ways. First, to reconstruct SMAP-like soil moisture data from 2000 to present, extending beyond SMAP's operational period (2000–present); and second to downscale SMAP data from 9 km to 500 m spatial resolution using MODIS optical observations. We used in situ soil moisture data from the AmeriFlux and NOAA networks in California, along with a radar-based Sentinel-1 soil moisture product (S1-DPA) for model validation.

Results indicated that MG-OPTRAM's 9-km soil moisture estimates were in strong agreement with both SMAP and in-situ data. It effectively captured both temporal variability (i.e., seasonality and inter-annual changes) and spatial patterns, such as the wetter condition in north CV relative to the south and the distinct saturation of rice fields during the floor irrigation in May.

At the downscaled 500-m resolution, MG-OPTRAM retains the overall patterns seen in SMAP (e.g., north-to-south trend and seasonal cycles) while showing detailed features such as river channels and lakes, hidden in SMAP. Most of these features are also captured by the S1-DPA dataset, supporting the spatial accuracy of MG-OPTRAM outputs.

When compared against in situ observations, MG-OPTRAM consistently outperforms the OPTRAM; however, higher uncertainties were observed in the 500-m product in some cases compared to 9-km resolution data. These discrepancies underscore the challenges of capturing fine-scale soil moisture dynamics using optical reflectance alone. As such, the coarser-resolution (9-km) MG-OPTRAM outputs currently demonstrate greater robustness and reliability than their high-resolution (500-m) counterparts. Overall, MG-OPTRAM successfully overcomes the limitations of OPTRAM and SMAP by fusing microwave and optical data.

In conclusion, all contributions through the chapters of this dissertation significantly advance the OPTRAM approach and ultimately develope a model, MG-OPTRAM, that reduces sensitivity to model parameters, decreases uncertainties in OPTRAM, and increases soil moisture estimation accuracy through integrating microwave data and calibration at the pixel level. This novel model not only enhances OPTRAM's soil moisture estimation but also addresses key SMAP limitations, such as coarse spatial resolution and relatively short temporal coverage, with data available since 2015. By adopting the enhanced OPTRAM formulation (from Chapter 2) and reducing calibration areas from region-wide (original OPTRAM) to land cover-specific (Chapter 3) and then to SMAP pixel level, Microwave-Guided OPTRAM represents the most evolved form of the model, encompassing all the potentials of the previous chapters as well.

The dissertation demonstrates that MG-OPTRAM, proposed in the last chapter, meets our ultimate goal which was to develop a high spatial resolution and accurate soil moisture dataset over a long period. Based on the findings of each chapter, the following recommendations are offered for future research and application:

I. Use Case Differentiation for OPTRAM Variants

While OPTRAM-2, introduced in Chapter 2, significantly improved the model's capacity to identify oversaturated pixels and surface water bodies, the original OPTRAM remains suitable when the primary objective is mapping only soil moisture. In such cases, we recommend a minor yet impactful modification to the original formulation, specifically adopting Equation (2.3) instead of Equation (2.2) as presented in Chapter 2. This adjustment improves the delineation of water bodies without compromising soil moisture estimation. Throughout the remainder of the dissertation, this modified version (Equation 2.3) is used whenever referring to the original OPTRAM.

II. Integrating Additional Predictors into OPTRAM

The higher SMAP-HB accuracy against in-situ data proved in chapter 3 suggests further research to increase the OPTRAM performance by accepting other independent variables in this model, such as precipitation or microwave satellite soil moisture. Future research should explore methods to integrate such variables into OPTRAM's semi-analytical formulation while maintaining its conceptual simplicity. In addition, more specific OPTRAM calibration strategies, for example, for individual soil textures, can be studied to further improve its accuracy.

III. Advancing MG-OPTRAM and STR Interpretation

Although MG-OPTRAM framework presented in Chapter 4, outperformed OPTRAM in estimating soil moisture when compared against multiple validation datasets (SMAP, in situ observations and Sentinel-1), Further research is needed to advance the model framework. In particular, it is essential to better understand how soil moisture and other environmental variables influence STR to separate moisture-induced changes from other sources of variability. We believe that developing more physically realistic models than the simplified equation proposed in this study could lead to more accurate and reliable versions of OPTRAM, especially at high spatial resolutions.

IV. Advancing OPTRAM Calibration Using SAR Data

Given the demonstrated potential of the Sentinel-1 DPA dataset, used as an independent satellite-based reference in the final chapter, in accurately capturing soil moisture dynamics and physical features such as lakes, rivers, and oversaturated pixels in rice fields, future research should explore the use of Synthetic Aperture Radar (SAR) data, such as Sentinel-1 imagery, for calibrating OPTRAM instead of relying solely on SMAP data. SAR offers finer spatial resolution at the meter scale and benefits from all-weather, day-and-night observation capabilities (Fan et al., 2024). Combining optical and SAR remote sensing data could provide advantages including fine spatial resolution, wide coverage, extended temporal records, and multi-temporal observations, potentially improving OPTRAM's robustness and applicability.

References

Acharya, U., Daigh, A. L., & Oduor, P. G. (2022). Soil Moisture Mapping with Moisture-Related Indices, OPTRAM, and an Integrated Random Forest-OPTRAM Algorithm from Landsat 8 Images. Remote Sensing, 14(15), 3801.

Ahmed, A., Zhang, Y. and Nichols, S., 2011. Review and evaluation of remote sensing methods for soil-moisture estimation. SPIE reviews, 2(1), p.028001.

Ambrosone, M., Matese, A., Di Gennaro, S.F., Gioli, B., Tudoroiu, M., Genesio, L., Miglietta, F., Baronti, S., Maienza, A., Ungaro, F. and Toscano, P., 2020. Retrieving soil moisture in rainfed and irrigated fields using Sentinel-2 observations and a modified OPTRAM approach. International journal of applied earth observation and geoinformation, 89, p.102113

Babaeian, E., Homaee, M., Montzka, C., Vereecken, H., Norouzi, A. A., & van Genuchten, M. Th. (2016). Soil moisture prediction of bare soil profiles using diffuse spectral reflectance information and vadose zone flow modeling. Remote Sensing of Environment, 187, 218–229. https://doi.org/10.1016/j.rse.2016.10.029

Babaeian, E., Sidike, P., Newcomb, M. S., Maimaitijiang, M., White, S. A., Demieville, J., ... & Tuller, M. (2019). A new optical remote sensing technique for high-resolution mapping of soil moisture. Frontiers in big Data, 2, 37.

Boryan, C., Yang, Z., Mueller, R. and Craig, M., 2011. Monitoring US agriculture: the US department of agriculture, national agricultural statistics service, cropland data layer program. Geocarto International, 26(5), pp.341-358.

Burdun, I., Bechtold, M., Sagris, V., Komisarenko, V., De Lannoy, G., & Mander, Ü. (2020). A comparison of three trapezoid models using optical and thermal satellite imagery for water table depth monitoring in Estonian bogs. Remote Sensing, 12(12), 1980.

Burdun, I., Bechtold, M., Aurela, M., De Lannoy, G., Desai, A.R., Humphreys, E., Kareksela, S., Komisarenko, V., Liimatainen, M., Marttila, H. and Minkkinen, K., 2023. Hidden becomes clear: Optical remote sensing of vegetation reveals water table dynamics in northern peatlands. Remote Sensing of Environment, 296, p.113736.

Carlson, T., 2007. An overview of the" triangle method" for estimating surface evapotranspiration and soil moisture from satellite imagery. Sensors, 7(8), pp.1612-1629.

Carlson, T.N., Gillies, R.R. and Perry, E.M., 1994. A method to make use of thermal infrared temperature and NDVI measurements to infer surface soil water content and fractional vegetation cover. Remote sensing reviews, 9(1-2), pp.161-173.

Chaubell, J., Yueh, S., Chan, S. and Peng, J., 2017. SMAP: Water Contamination Correction, Presented at SMAP Cal/Val Workshop # 8, NASA, 20-22 June 2017, Amherst, MA.

Available at: https://smap.jpl.nasa.gov/events/50/smap-calval-workshop-8-amherst-ma/ [Accessed 1 April 2025]

Chen, M., Zhang, Y., Yao, Y., Lu, J., Pu, X., Hu, T., & Wang, P. (2020). Evaluation of the OPTRAM Model to retrieve soil moisture in the Sanjiang Plain of Northeast China. Earth and Space Science, 7(6), e2020EA001108.

Colliander, A., Fisher, J. B., Halverson, G., Merlin, O., Misra, S., Bindlish, R., ... & Yueh, S. (2017). Spatial downscaling of SMAP soil moisture using MODIS land surface temperature and NDVI during SMAPVEX15. IEEE Geoscience and Remote Sensing Letters, 14(11), 2107-2111.

de Queiroz, M.G., da Silva, T.G.F., Zolnier, S., Jardim, A.M.D.R.F., de Souza, C.A.A., Júnior, G.D.N.A., de Morais, J.E.F. and de Souza, L.S.B., 2020. Spatial and temporal dynamics of soil moisture for surfaces with a change in land use in the semi-arid region of Brazil. Catena, 188, p.104457.

Earth Resources Observation and Science (EROS) Center. (2020). Landsat 8-9 Operational Land Imager / Thermal Infrared Sensor Level-2, Collection 2 [dataset]. U.S. Geological Survey. https://doi.org/10.5066/P9OGBGM6

Entekhabi, D., Njoku, E.G., O'neill, P.E., Kellogg, K.H., Crow, W.T., Edelstein, W.N., Entin, J.K., Goodman, S.D., Jackson, T.J., Johnson, J. and Kimball, J., 2010. The soil moisture active passive (SMAP) mission. Proceedings of the IEEE, 98(5), pp.704-716.

Entekhabi, D., Yueh, S., O'Neill, P.E., Kellogg, K.H., Allen, A., Bindlish, R., Brown, M., Chan, S., Colliander, A., Crow, W.T. and Das, N., 2014. SMAP Handbook–Soil Moisture Active Passive: Mapping Soil Moisture and Freeze/Thaw from Space.

Fan, J., Chen, D., Zou, C., Zhen, Q., Du, Y., Jiang, D., Liu, S. and Zan, M., 2024. Monitoring soil moisture in cotton fields with synthetic aperture radar and optical data in arid and semi-arid regions. Journal of Applied Remote Sensing, 18(3), pp.034501-034501.

Fan, D., Zhao, T., Jiang, X., García-García, A., Schmidt, T., Samaniego, L., ... & Peng, J. (2025). A Sentinel-1 SAR-based global 1-km resolution soil moisture data product: Algorithm and preliminary assessment. Remote Sensing of Environment, 318, 114579.

Fang, B., Lakshmi, V., Bindlish, R., & Jackson, T. J. (2018). Downscaling of SMAP soil moisture using land surface temperature and vegetation data. Vadose Zone Journal, 17(1), 1-15.

Goulden, M., 2018. AmeriFlux AmeriFlux US-CZ3 Sierra Critical Zone, Sierra Transect, Sierran Mixed Conifer, P301. Lawrence Berkeley National Laboratory (LBNL), Berkeley, CA (United States). AmeriFlux; UC Irvine.

Hassanpour, R., Zarehaghi, D., Neyshabouri, M. R., Feizizadeh, B., & Rahmati, M. (2020). Modification on optical trapezoid model for accurate estimation of soil moisture content in a maize growing field. Journal of Applied Remote Sensing, 14(3), 034519-034519.

Hengl, T., 2018. Soil bulk density (fine earth) 10 x kg/m-cubic at 6 standard depths (0, 10, 30, 60, 100 and 200 cm) at 250 m resolution. https://doi.org/10.5281/zenodo.2525665.

Hosseini, A.S., Asadi, D., Mohammadzadeh, S. and Ghalandari, S., 2023. Exploring spatial and temporal dynamics of soil moisture using SMAP, Khorasan Razavi, Iran. Asian Journal of Social Science and Management Technology, 5(4), pp.193-203.

Huete, A.R., 2004. Remote sensing for environmental monitoring. Environmental monitoring and characterization, pp.183-206.

Jensen, D., Reager, J.T., Zajic, B., Rousseau, N., Rodell, M. and Hinkley, E., 2018. The sensitivity of US wildfire occurrence to pre-season soil moisture conditions across ecosystems. Environmental Research Letters, 13(1), p.014021.

Jensen, J.R., 2009. Remote sensing of the environment: An earth resource perspective 2/e. Pearson Education India.

Longo-Minnolo, G., Consoli, S., Vanella, D., Ramírez-Cuesta, J. M., Greimeister-Pfeil, I., Neuwirth, M., & Vuolo, F. (2022). A stand-alone remote sensing approach based on the use of the optical trapezoid model for detecting the irrigated areas. Agricultural Water Management, 274, 107975.

Ma, C., Johansen, K., & McCabe, M. F. (2022). Combining Sentinel-2 data with an optical-trapezoid approach to infer within-field soil moisture variability and monitor agricultural production stages. Agricultural Water Management, 274, 107942.

Madelon, R., Rodríguez-Fernández, N. J., van der Schalie, R., Scanlon, T., Al Bitar, A., Kerr, Y. H., ... & Dorigo, W. (2022). Toward the Removal of Model Dependency in Soil Moisture Climate Data Records by Using an L-Band Scaling Reference. IEEE Journal of Selected Topics in Applied Earth Observations and Remote Sensing, 15, 831-848.

Mallick, K., Bhattacharya, B.K. and Patel, N.K., 2009. Estimating volumetric surface moisture content for cropped soils using a soil wetness index based on surface temperature and NDVI. Agricultural and Forest Meteorology, 149(8), pp.1327-1342.

Mananze, S., Pôças, I., & Cunha, M. (2019). Agricultural drought monitoring based on soil moisture derived from the optical trapezoid model in Mozambique. Journal of Applied Remote Sensing, 13(2), 024519-024519.

Mohamadzadeh, N. and Ahmadisharaf, A., 2024. Classification algorithms for remotely sensed images. In Remote Sensing of Soil and Land Surface Processes (pp. 357-368). Elsevier.

Mohamadzadeh, N., Sadeghi, M., Vergopolan, N., Liang, L., Bandara, U., Altare, C. and Caldas, M.M., 2025. Landcover-specific calibration of the optical trapezoid model (OPTRAM) for soil moisture monitoring in the Central Valley, California. Frontiers in Remote Sensing, 6, p.1519420. https://doi.org/10.3389/frsen.2025.1519420

Mohseni, F., Ahrari, A., Haunert, J. H., & Montzka, C. (2024). The synergies of SMAP enhanced and MODIS products in a random forest regression for estimating 1 km soil moisture over Africa using Google Earth Engine. Big Earth Data, 8(1), 33-57.

Mokhtari, A., Sadeghi, M., Afrasiabian, Y. and Yu, K., 2023. OPTRAM-ET: A novel approach to remote sensing of actual evapotranspiration applied to Sentinel-2 and Landsat-8 observations. Remote Sensing of Environment, 286, p.113443.

Moran, M.S., Clarke, T.R., Inoue, Y. and Vidal, A., 1994. Estimating crop water deficit using the relation between surface-air temperature and spectral vegetation index. Remote sensing of environment, 49(3), pp.246-263.

Nemani, R., Pierce, L., Running, S. and Goward, S., 1993. Developing satellite-derived estimates of surface moisture status. Journal of Applied Meteorology and Climatology, 32(3), pp.548-557.

NOAA., 2024. About: NOAA Physical Sciences Laboratory. https://psl.noaa.gov/about/

Norouzi, S., Sadeghi, M., Liaghat, A., Tuller, M., Jones, S. B., & Ebrahimian, H. (2021). Information depth of NIR/SWIR soil reflectance spectroscopy. Remote Sensing of Environment, 256, 112315.

Ochsner, T.E., Cosh, M.H., Cuenca, R.H., Dorigo, W.A., Draper, C.S., Hagimoto, Y., Kerr, Y.H., Larson, K.M., Njoku, E.G., Small, E.E. and Zreda, M., 2013. State of the art in large-scale soil moisture monitoring. Soil Science Society of America Journal, 77(6), pp.1888-1919.

Özelkan, E. (2020). Water body detection analysis using NDWI indices derived from landsat-8 OLI. Polish Journal of Environmental Studies, 29(2), 1759-1769.

Pandey, R., Sarup, J., Matin, S. and Goswami, S.B., 2024. The Optical Trapezoid Model (OPTRAM)-based soil moisture estimation using Landsat 8 data. Journal of Spatial Science, 69(1), pp.137-147.

Pekel, J.F., Cottam, A., Gorelick, N. and Belward, A.S., 2016. High-resolution mapping of global surface water and its long-term changes. Nature, 540(7633), pp.418-422

Robinson, D.A., Campbell, C.S., Hopmans, J.W., Hornbuckle, B.K., Jones, S.B., Knight, R., Ogden, F., Selker, J. and Wendroth, O., 2008. Soil moisture measurement for ecological and hydrological watershed-scale observatories: A review. Vadose zone journal, 7(1), pp.358-389.

Sadeghi, M., Babaeian, E., Ebtehaj, A. M., Jones, S. B., & Tuller, M. (2018). Remote sensing of environmental variables and fluxes. Handbook of Environmental Engineering, 249-302.

Sadeghi, M., Babaeian, E., Tuller, M., & Jones, S. B. (2017). The optical trapezoid model: A novel approach to remote sensing of soil moisture applied to Sentinel-2 and Landsat-8 observations. Remote sensing of environment, 198, 52-68.

Sadeghi, M., Jones, S. B., & Philpot, W. D. (2015). A linear physically-based model for remote sensing of soil moisture using short wave infrared bands. Remote Sensing of Environment, 164, 66-76.

Sadeghi, M., Mohamadzadeh, N., Liang, L., Bandara, U., Caldas, M.M. and Hatch, T., 2023. A new variant of the optical trapezoid model (OPTRAM) for remote sensing of soil moisture and water bodies. Science of Remote Sensing, 8, p.100105.

Shu, B., Chen, Y., Zhang, K.X., Dehghanifarsani, L. and Amani-Beni, M., 2024. Urban engineering insights: Spatiotemporal analysis of land surface temperature and land use in urban landscape. Alexandria Engineering Journal, 92, pp.273-282.

Sleeter, B.M., 2008. Late 20th century land change in the Central California Valley Ecoregion.

Soulard, C.E. and Wilson, T.S., 2015. Recent land-use/land-cover change in the Central California Valley. Journal of Land Use Science, 10(1), pp.59-80.

Vergopolan, N., Chaney, N.W., Beck, H.E., Pan, M., Sheffield, J., Chan, S. and Wood, E.F., 2020. Combining hyper-resolution land surface modeling with SMAP brightness temperatures to obtain 30-m soil moisture estimates. Remote Sensing of Environment, 242, p.111740.

Vergopolan, N., Chaney, N.W., Pan, M., Sheffield, J., Beck, H.E., Ferguson, C.R., Torres-Rojas, L., Sadri, S. and Wood, E.F., 2021. SMAP-HydroBlocks, a 30-m satellite-based soil moisture dataset for the conterminous US. Scientific data, 8(1), p.264.

Vermote, E. (2021). MODIS/Terra Surface Reflectance 8-Day L3 Global 500m SIN Grid V061 [Data set]. NASA EOSDIS Land Processes Distributed Active Archive Center. Accessed 2025-02-21 from https://doi.org/10.5067/MODIS/MOD09A1.061.

Wang, A., Lettenmaier, D.P. and Sheffield, J., 2011. Soil moisture drought in China, 1950–2006. Journal of Climate, 24(13), pp.3257-3271.

Wang, Q. and Atkinson, P.M., 2018. Spatio-temporal fusion for daily Sentinel-2 images. Remote Sensing of Environment, 204, pp.31-42.

Wang, Y., Yang, J., Chen, Y., Fang, G., Duan, W., Li, Y. and De Maeyer, P., 2019. Quantifying the effects of climate and vegetation on soil moisture in an arid area, China. Water, 11(4), p.767.

Wen, F., Zhao, W., Wang, Q., & Sánchez, N. (2019). A value-consistent method for downscaling SMAP passive soil moisture with MODIS products using self-adaptive window. IEEE Transactions on Geoscience and Remote Sensing, 58(2), 913-924.

Xue, J. and Su, B., 2017. Significant remote sensing vegetation indices: A review of developments and applications. Journal of sensors, 2017(1), p.1353691.

Yang, Q., Zhao, T., Shi, J., Peng, Z. and Ye, C., 2021. A simulation-based approach for removing the effect of water contamination on SMAP soil moisture retrieval over the Qinghai-Tibet Plateau. Remote Sensing Letters, 12(8), pp.757-767

Zhang, D. and Zhou, G., 2016. Estimation of soil moisture from optical and thermal remote sensing: A review. Sensors, 16(8), p.1308.

Zhao, W., Sánchez, N., Lu, H., & Li, A. (2018). A spatial downscaling approach for the SMAP passive surface soil moisture product using random forest regression. Journal of hydrology, 563, 1009-1024.

Zhong, Y., Wei, Z., Miao, L., Wang, Y., Walker, J. P., & Colliander, A. (2024). Downscaling passive microwave soil moisture estimates using stand-alone optical remote sensing data. IEEE Transactions on Geoscience and Remote Sensing.